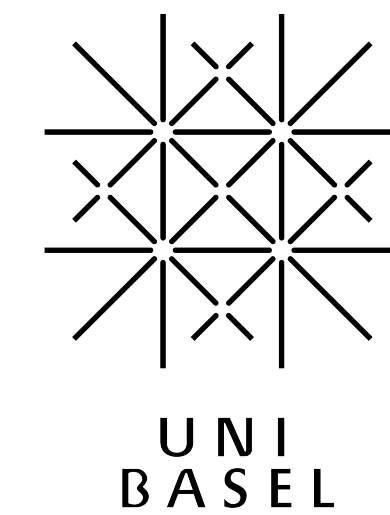


Texture transition in experimentally deformed quartzite [EGU2017-6966]

Rüdiger Kilian₁, Renée Heilbronner_{1,2}

(1) Department of Geosciences, University Basel, Basel, Switzerland
 (2) Department of Geology, Tromsø University, Tromsø, Norway



Quartz CPO interpretation:

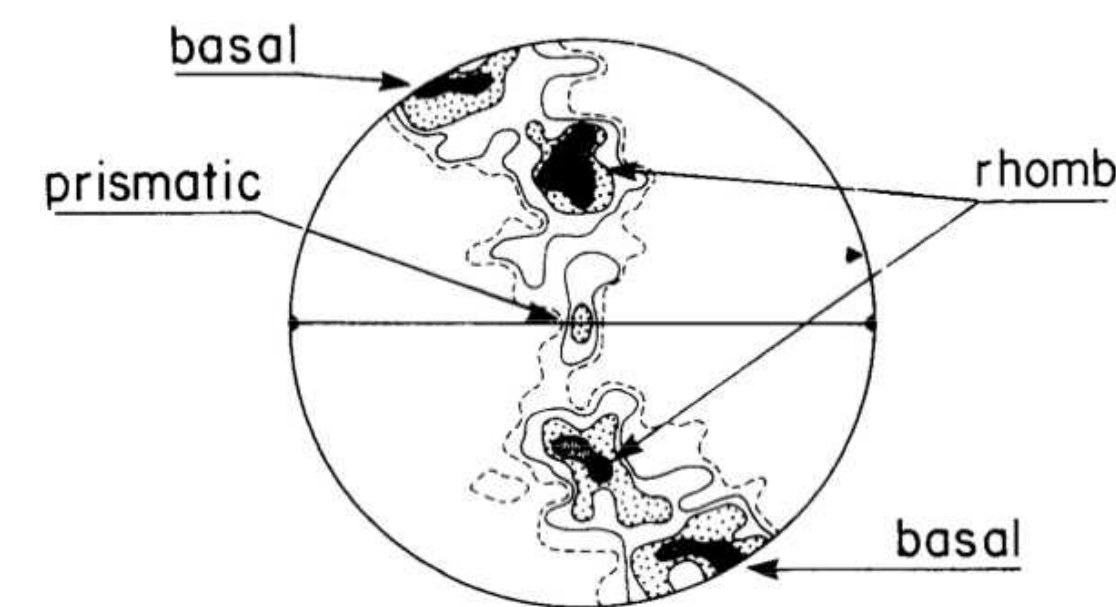
a) maxima in pole figure -> activity of specific slip system

b) slip systems have temperature dependency

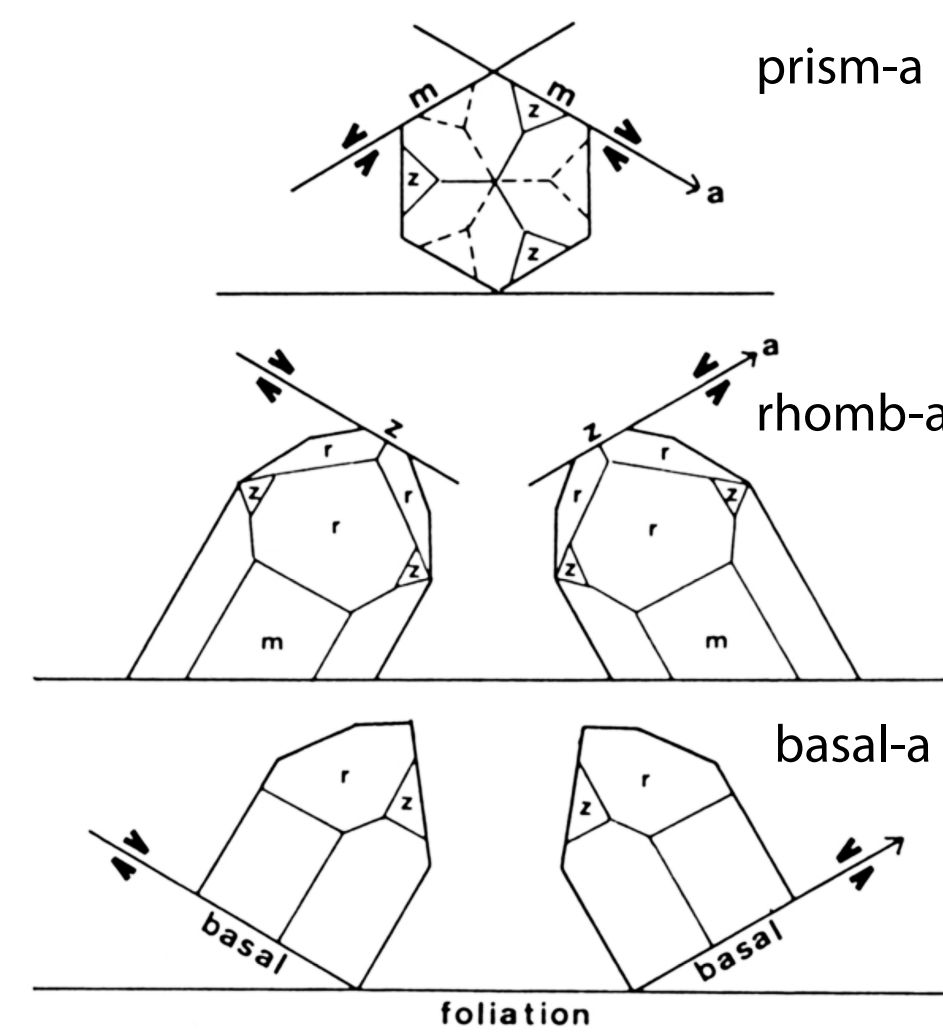
and/or

c) dependency on recrystallization process (experimental regimes ≠ blg, sgr, gbm)

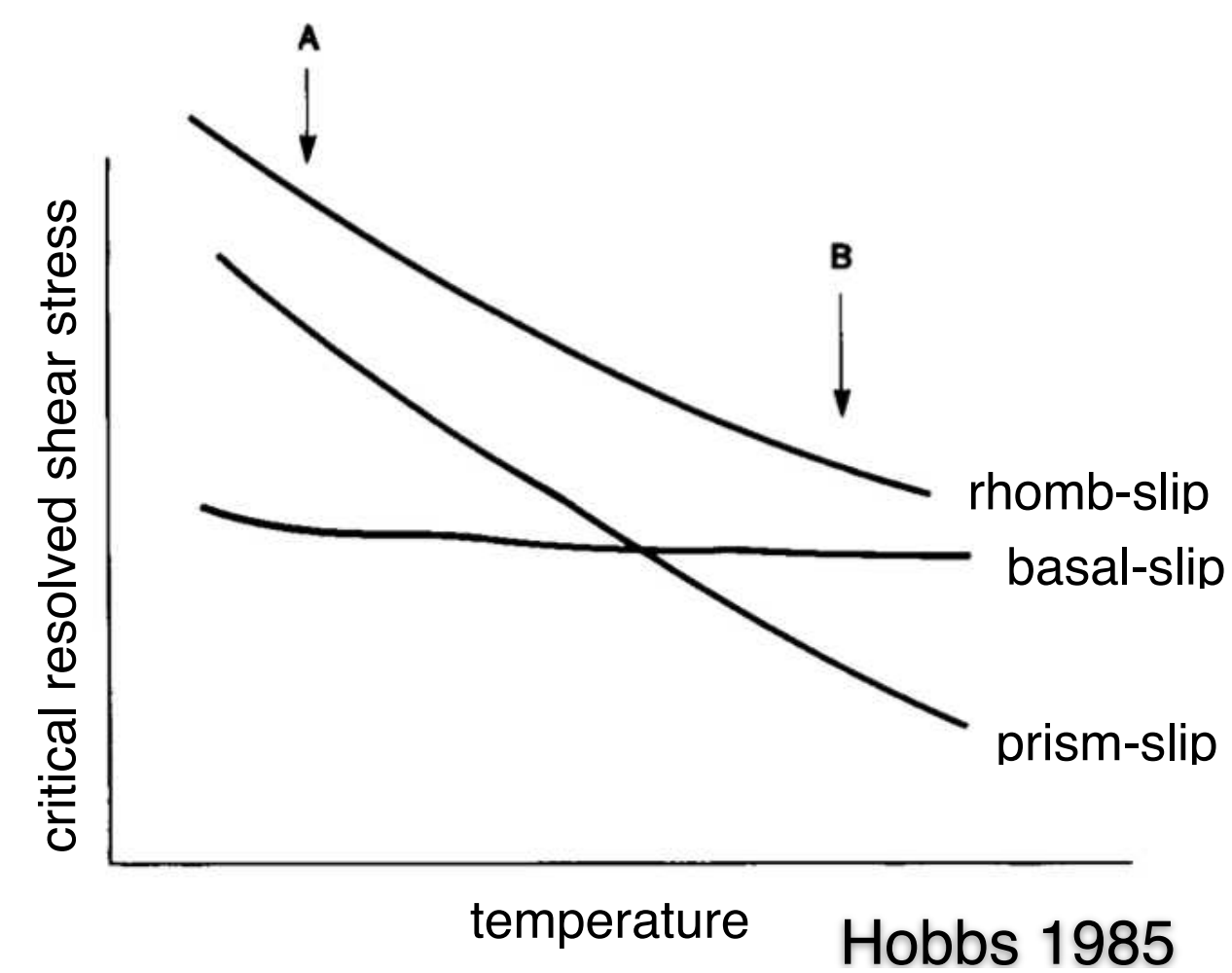
--> temptation to use as an indicator of metamorphic grade/temperature



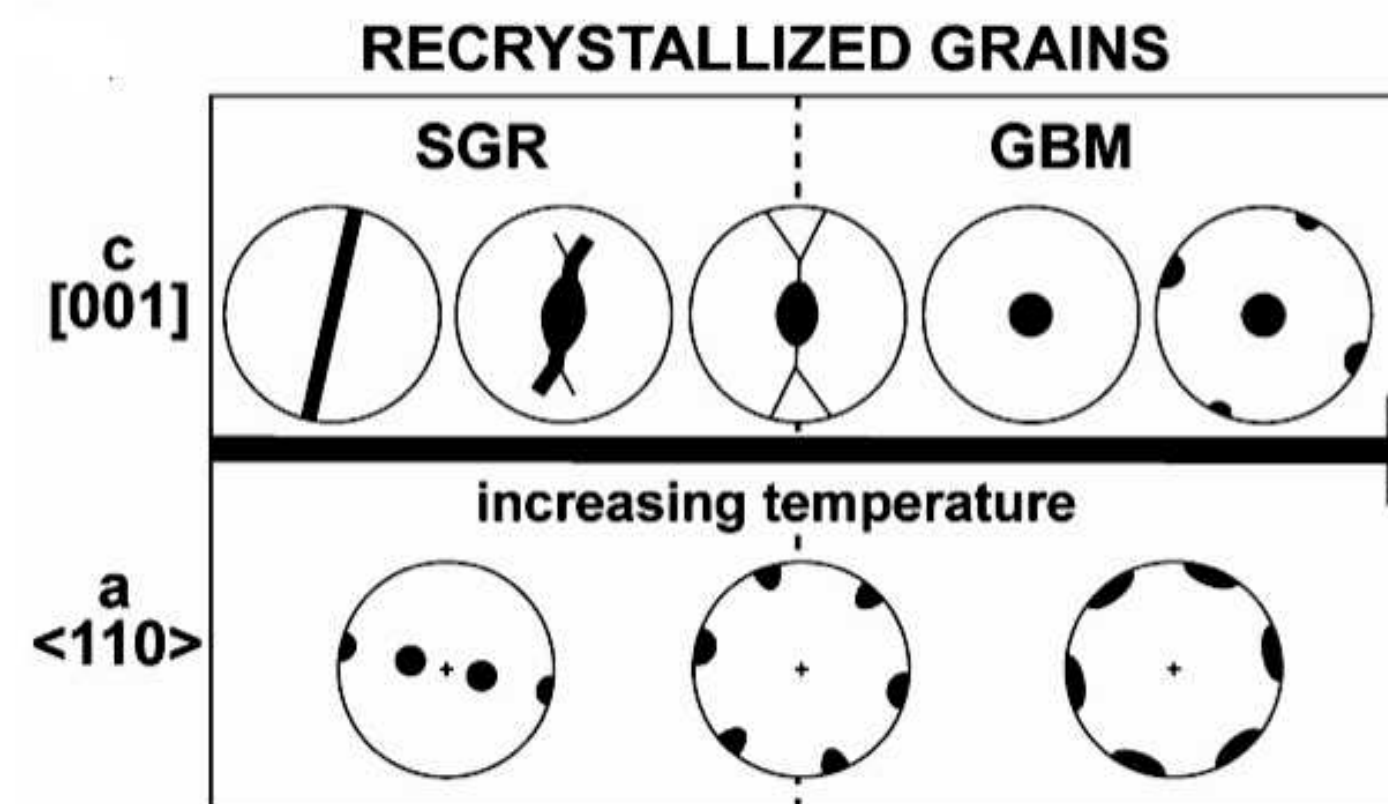
Bouchez & Pecher, 1981



Schmid & Casey, 1986

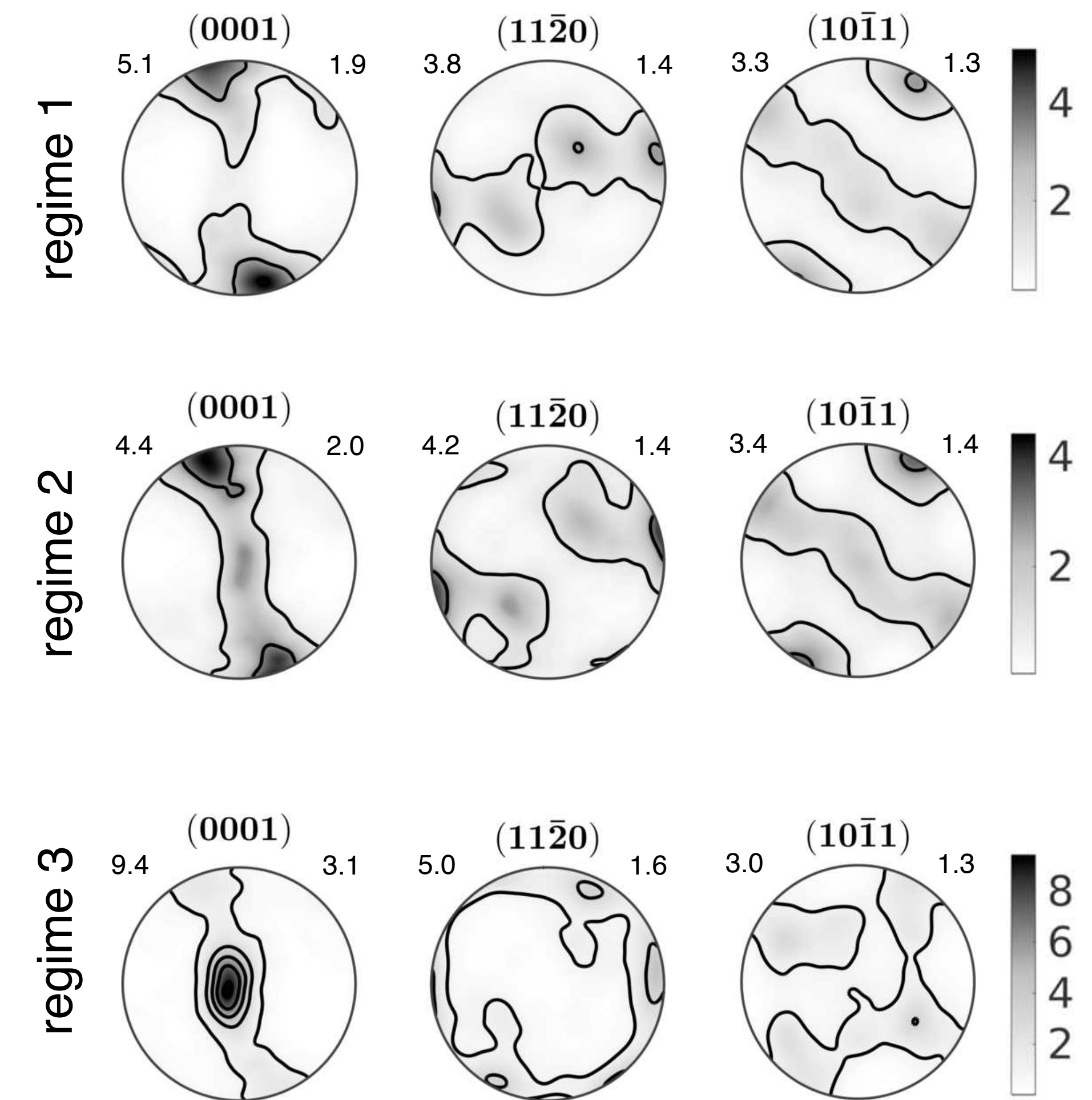


Hobbs 1985



Stipp et al. 2002

This study:



EBSD derived pole figures of experiments from Heilbronner & Tullis, 2002/6

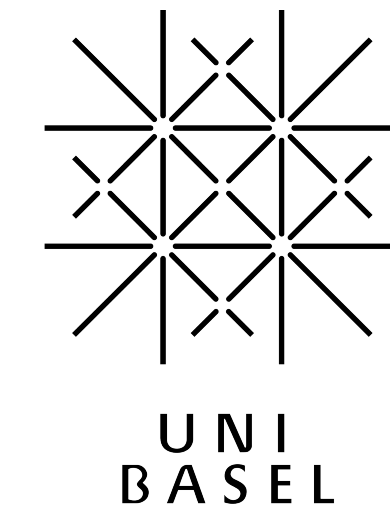
toc

<< >>

Texture transition in experimentally deformed quartzite [EGU2017-6966]

Rüdiger Kilian₁, Renée Heilbronner_{1,2}

(1) Department of Geosciences, University Basel, Basel, Switzerland
 (2) Department of Geology, Tromsø University, Tromsø, Norway



This study:

1) different texture forming processes:

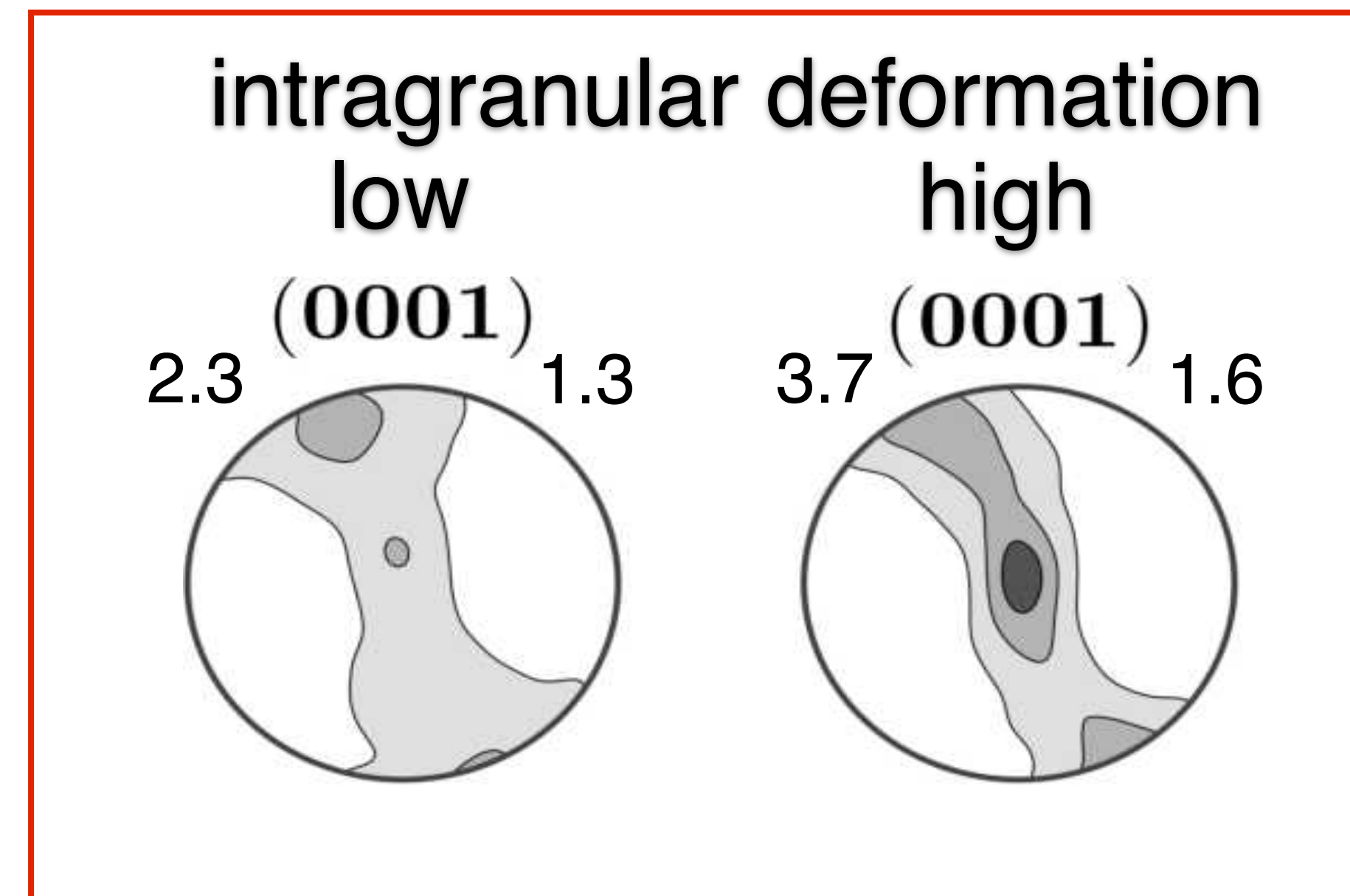
high stress -> oriented growth of “basal” grains

low stress -> dislocation glide and strain dependent CPO

2) no temperature dependency

Implications:

- CPO is strain dependent
- “basal” grains ≠ basal-a glide
- quartz CPO ≠ thermometer

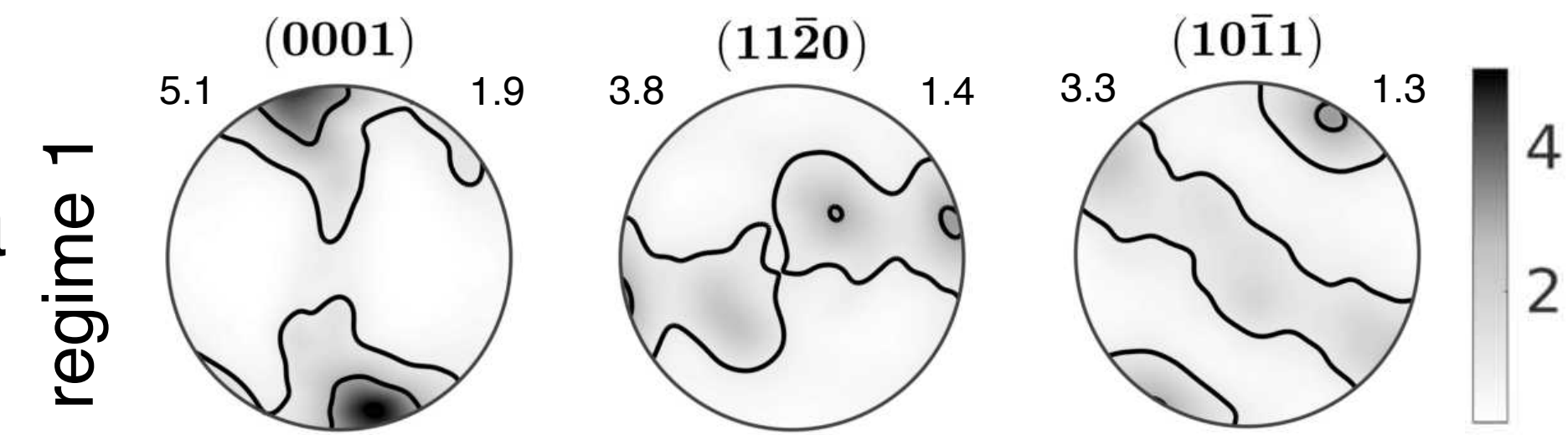


This study:



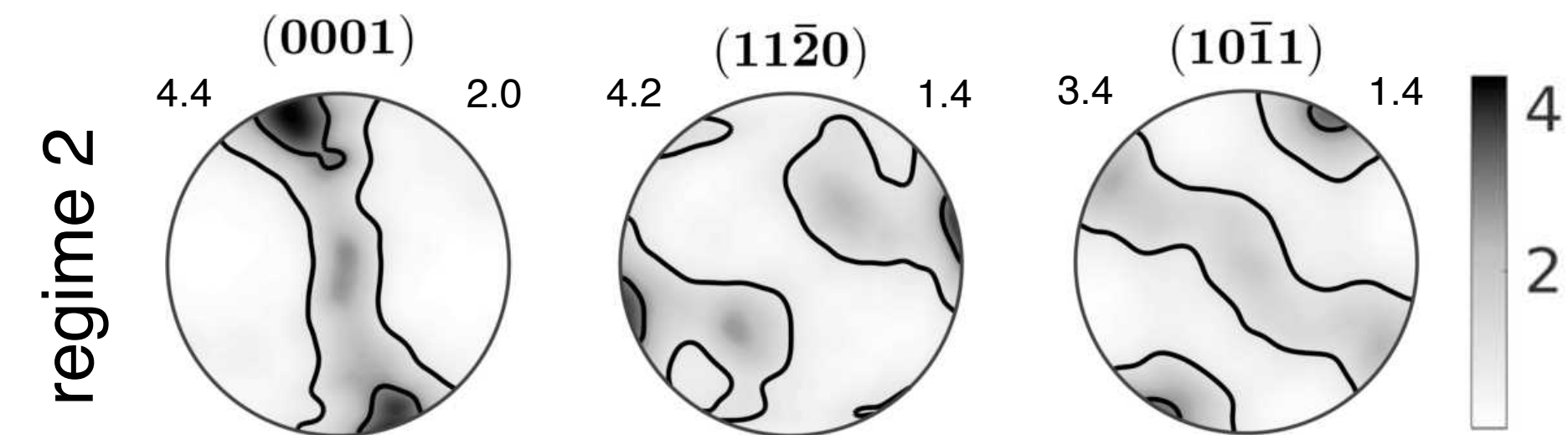
850 °C

$\tau = 650-315$ MPa



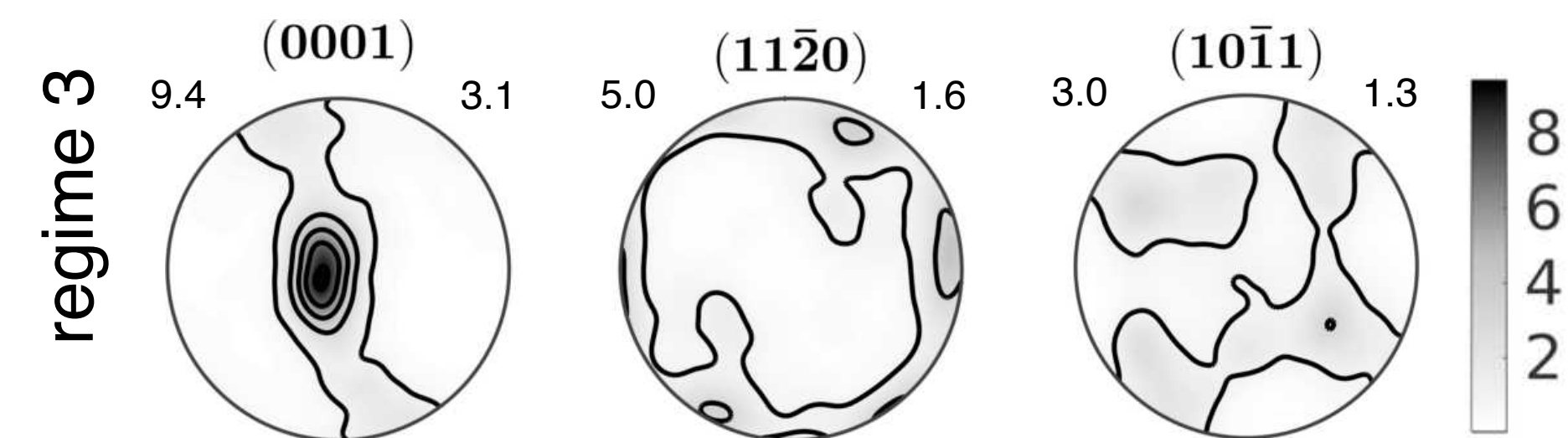
875 °C

$\tau = 201$ MPa



915 °C

$\tau = 103$ MPa



all at $3 \cdot 10^{-5}$ s⁻¹

and

$\Gamma_{\text{effective}}=3.3$

EBSD derived pole figures of experiments from Heilbronner & Tullis, 2002/6

toc

<<

>>

Texture transition in experimentally deformed quartzite [EGU2017-6966]

Rüdiger Kilian₁, Renée Heilbronner_{1,2}

(1) Department of Geosciences, University Basel, Basel, Switzerland

(2) Department of Geology, Tromsø University, Tromsø, Norway

0) Shortest version

1) Experiments

2) Orientation mapping

3) Textures

4) Texture and grain shape:
lengthening and alignment (1) (2*) (3)

4) Texture and grain size (1*) (2)

5) Polefigures of grain properties

6) Texture and intragranular deformation intensity (1) (2) (3) (4*)

7) Quantitative texture strength

8) $\langle a \rangle$ - transparency (1*) (2)

9) Misorientation analysis (1*) (2*) (3*) (4) (5)

10) Schmid factor analysis

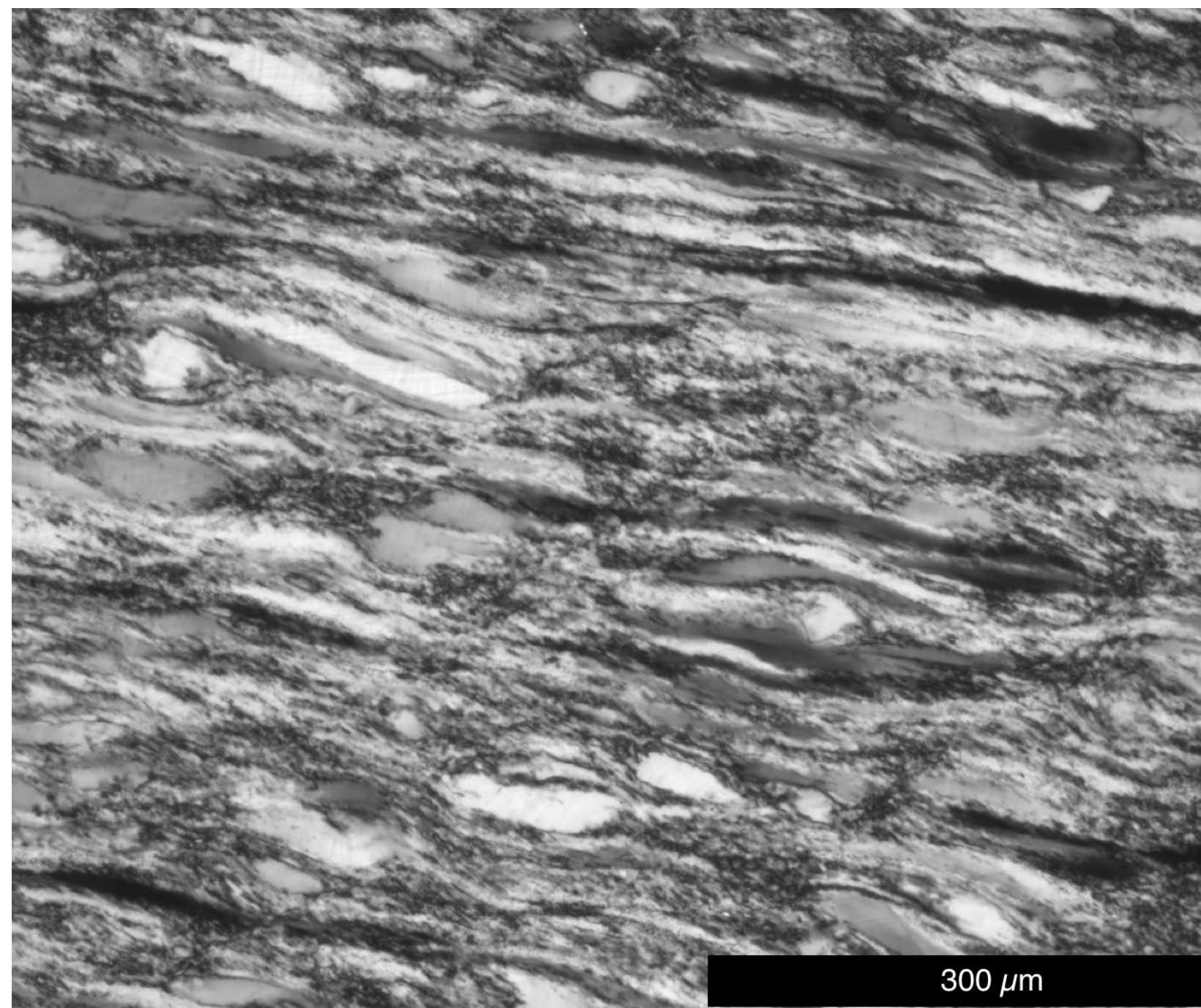
Summary & conclusion:

A1) gKAM definition

A2) noise filtering

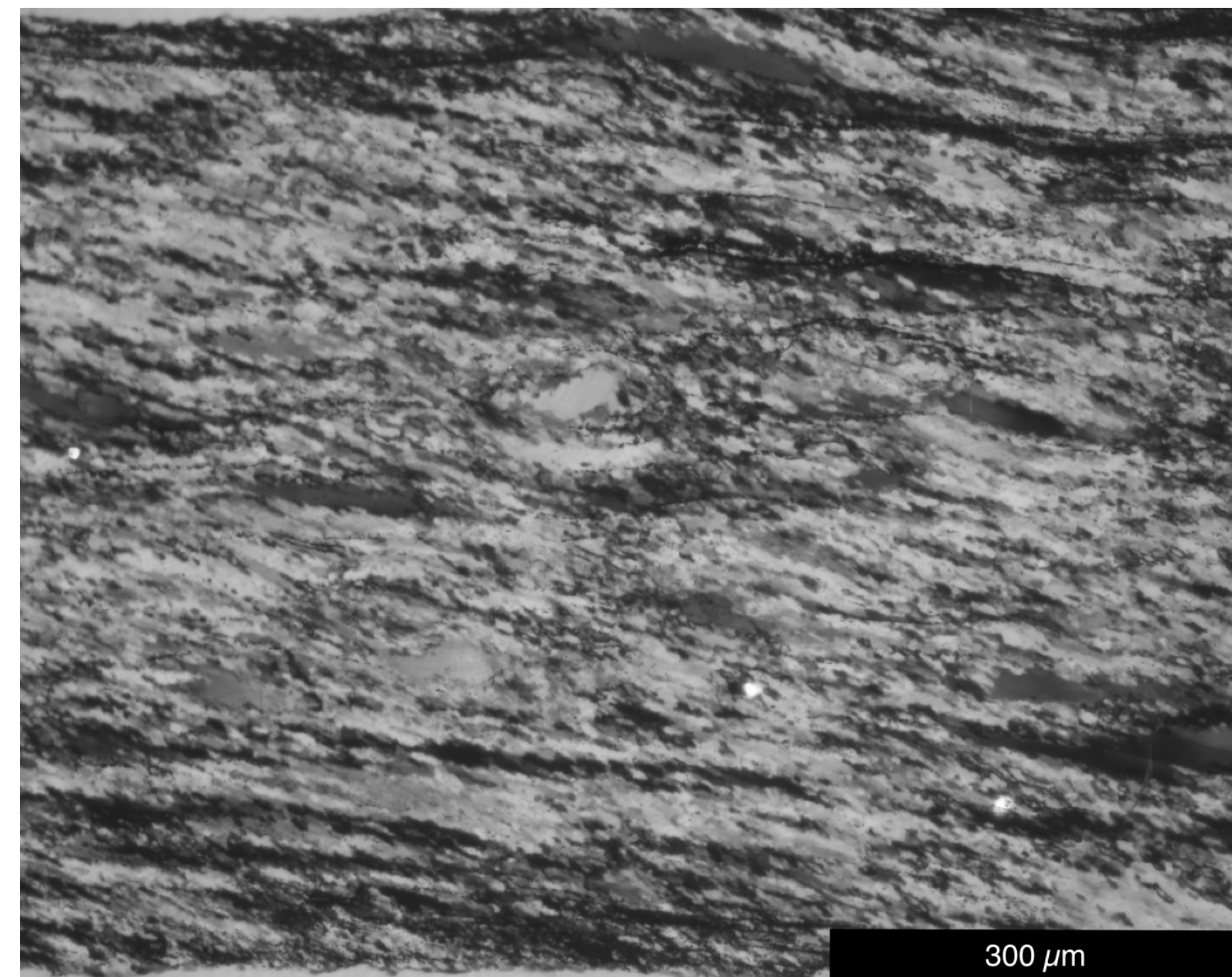
Re-accessing experiments by Heilbronner & Tullis, 2002/06

regime 1



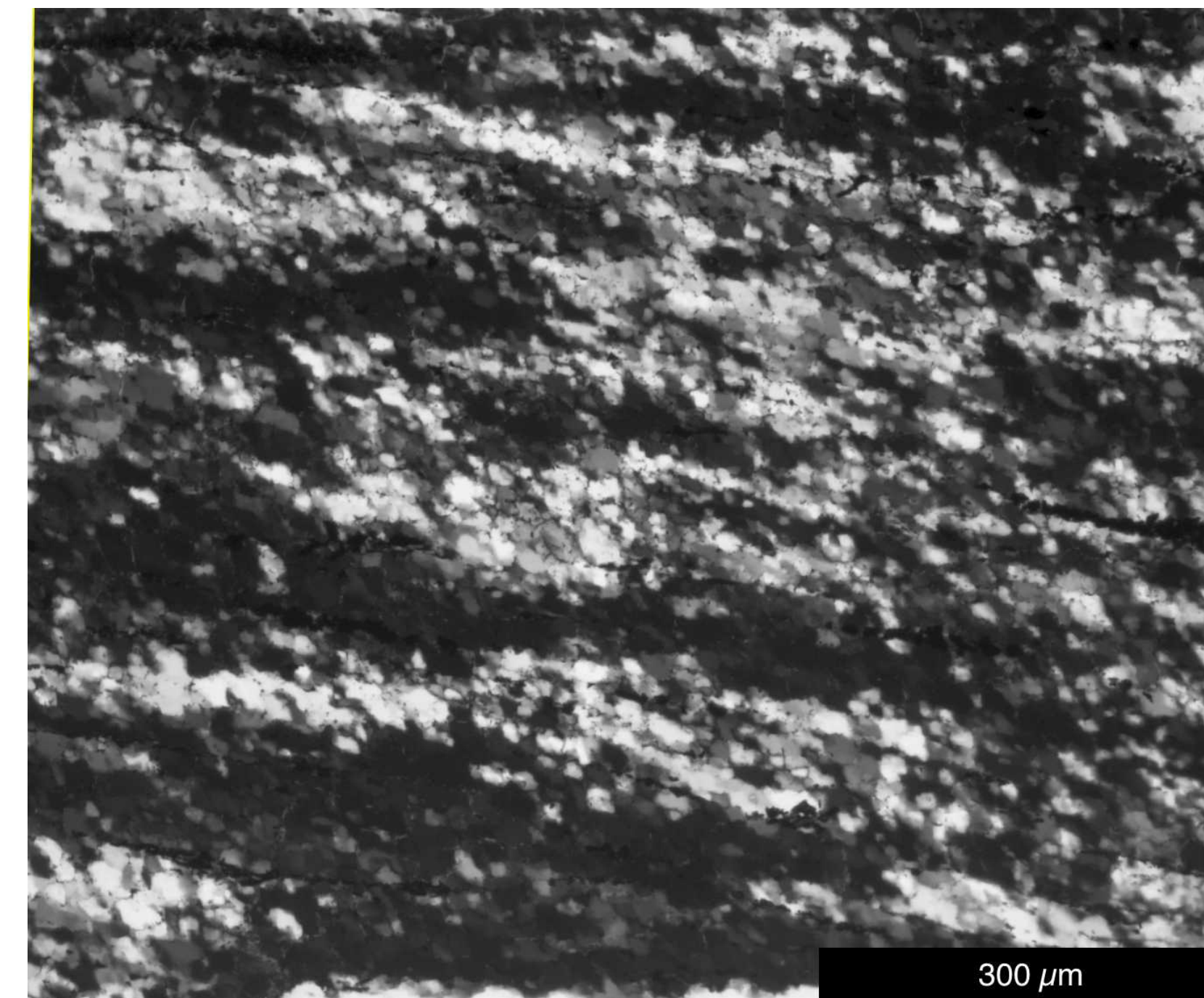
w1092: 850 °C / "as-is" / $3 \cdot 10^{-5} \text{ s}^{-1}$
 $\Gamma_{\text{effective}}=3.3^*$; 39% vert. shortening*
 $\tau = 650\text{-}315 \text{ MPa}$

regime 2

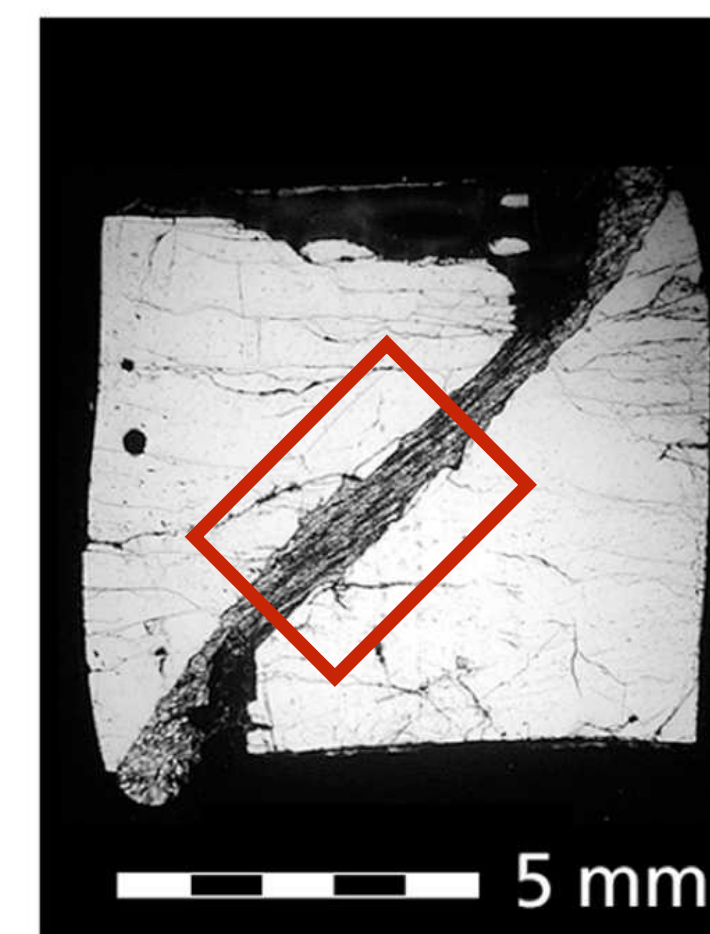


w946: 875 °C / 0.17 wt% H₂O / $3 \cdot 10^{-5} \text{ s}^{-1}$
 $\Gamma_{\text{effective}}= 3.3$; 48% vert. shortening
 $\tau = 201 \text{ MPa}$

regime 3



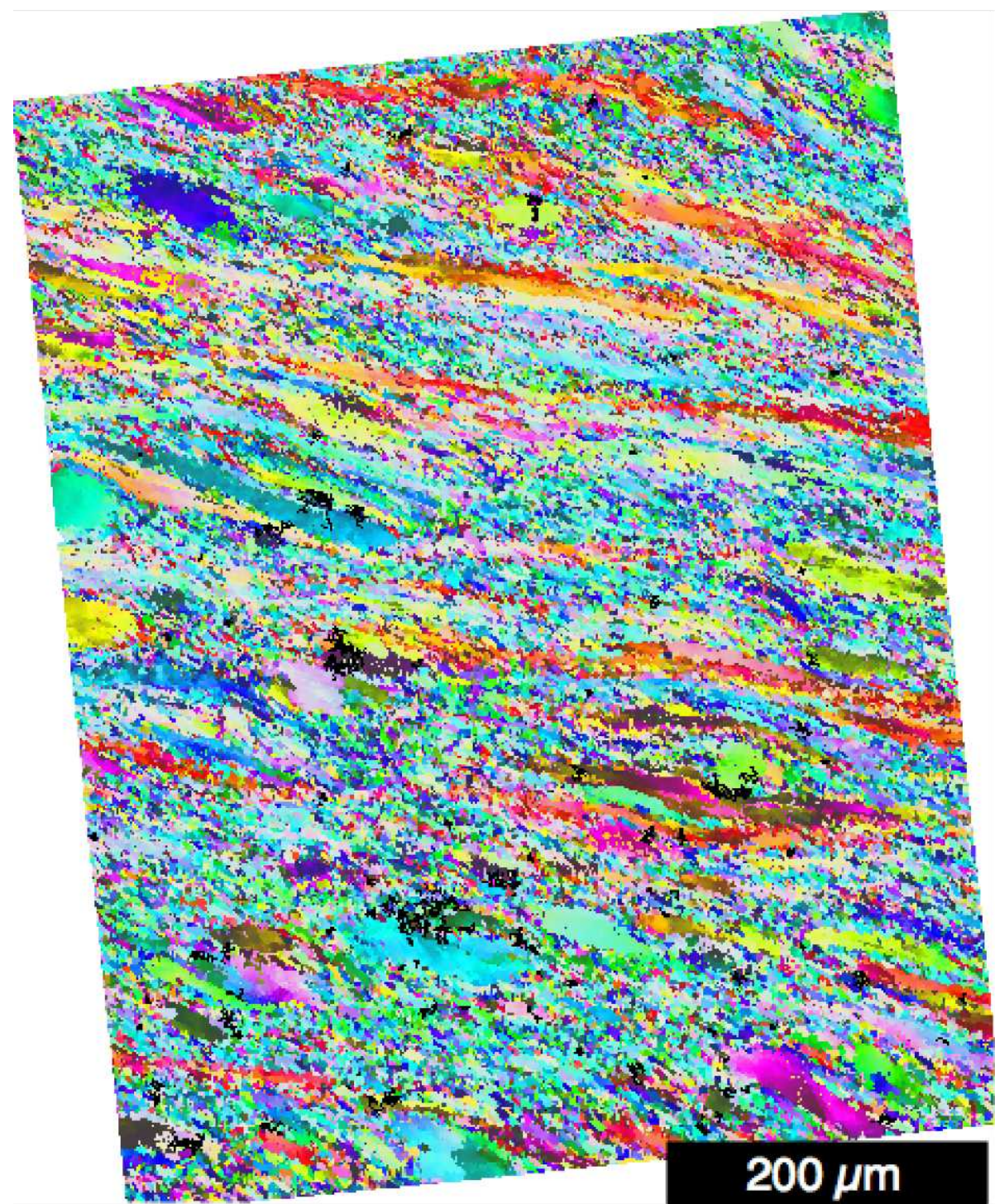
w935: 915 °C / 0.17 wt% H₂O / $3 \cdot 10^{-5} \text{ s}^{-1}$
 $\Gamma_{\text{effective}}=3.0$; 46% vert. shortening
 $\tau = 103 \text{ MPa}$



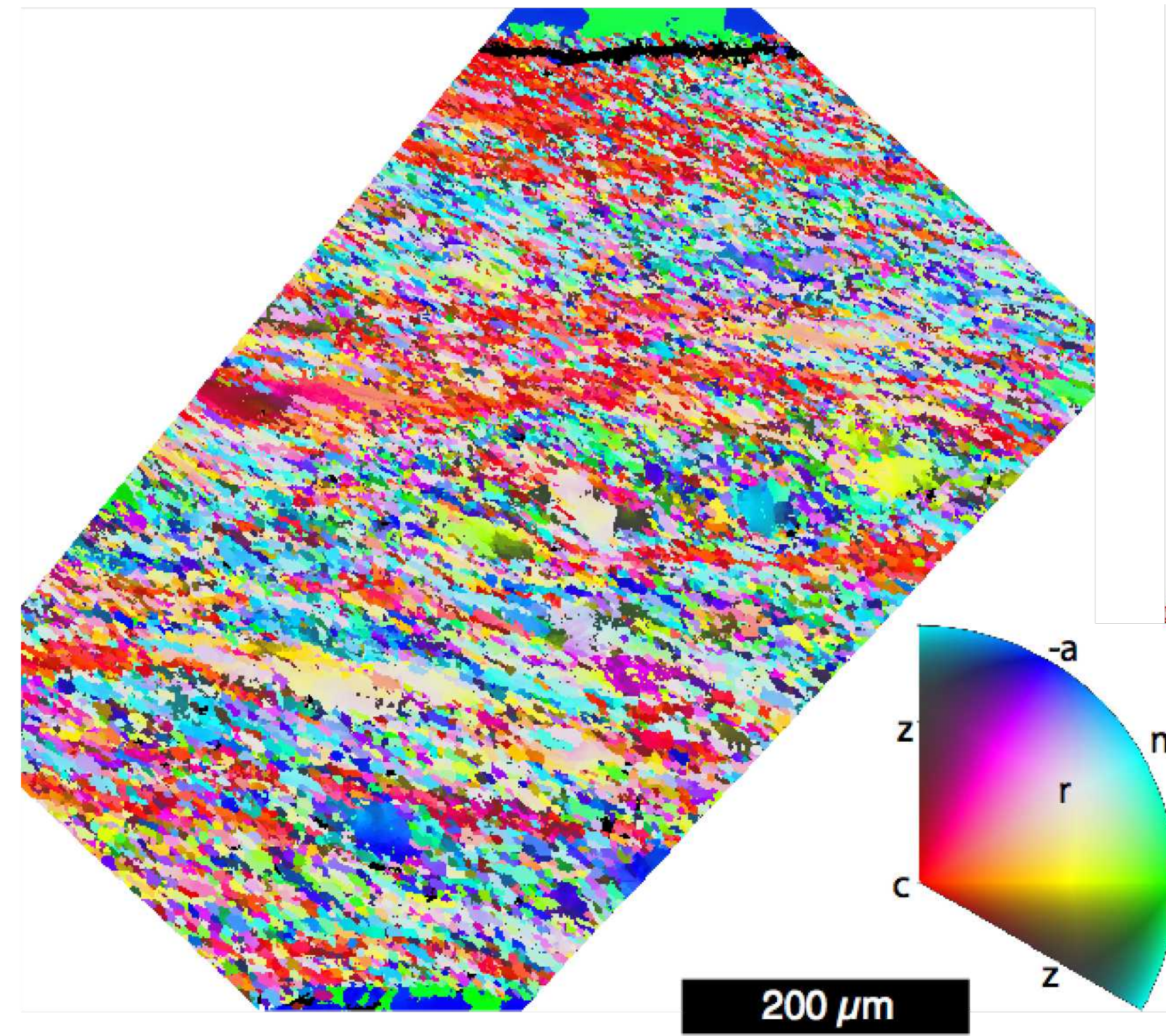
-> all experiments in very small temperature range (65°C)

*vertical shortening as $\Delta t/t_0$ (or $1-1/k$)
 and $\Gamma_{\text{effective}} = \tan(\psi)/k$ where ψ is the finite shear angle

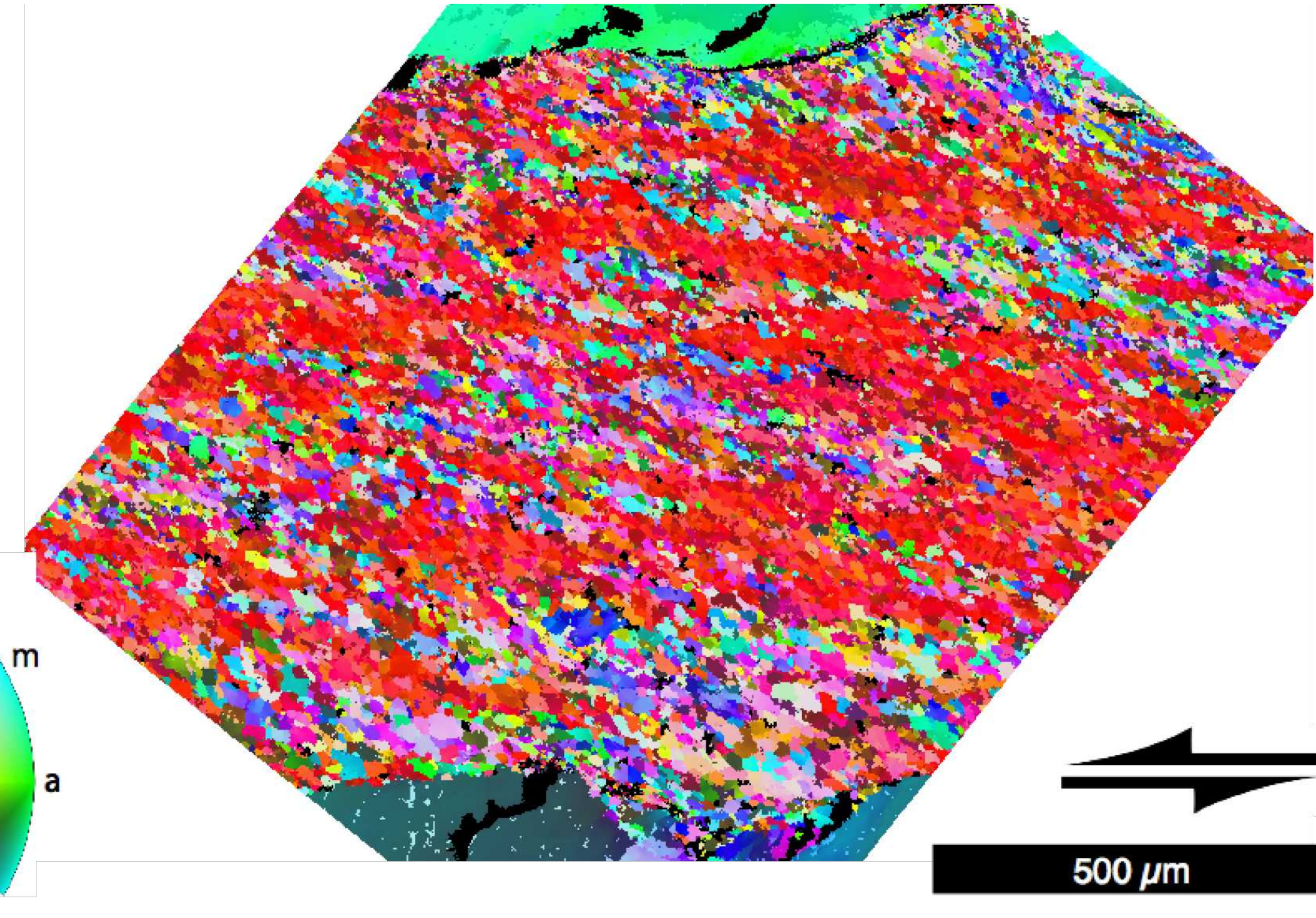
regime 1



regime 2



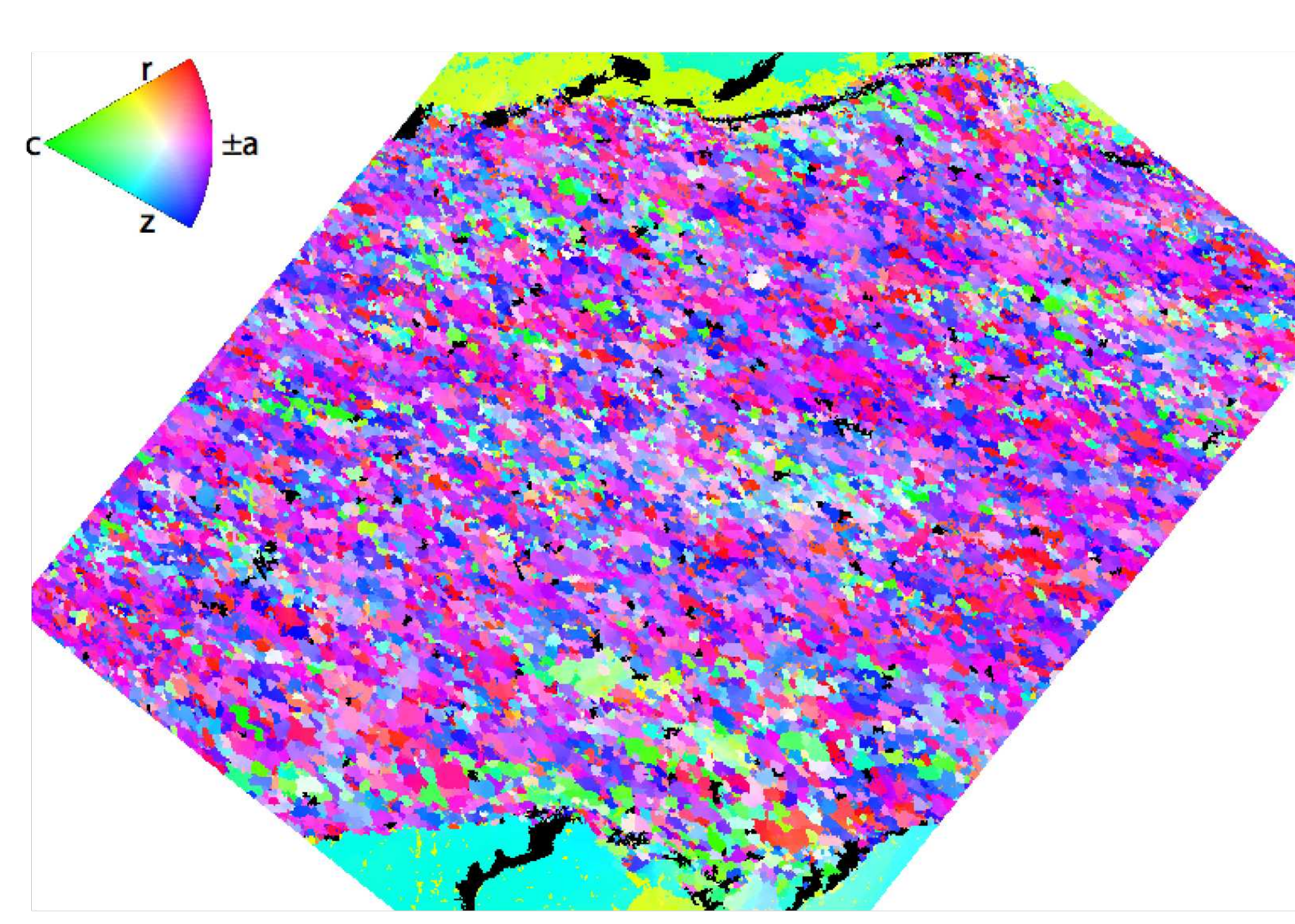
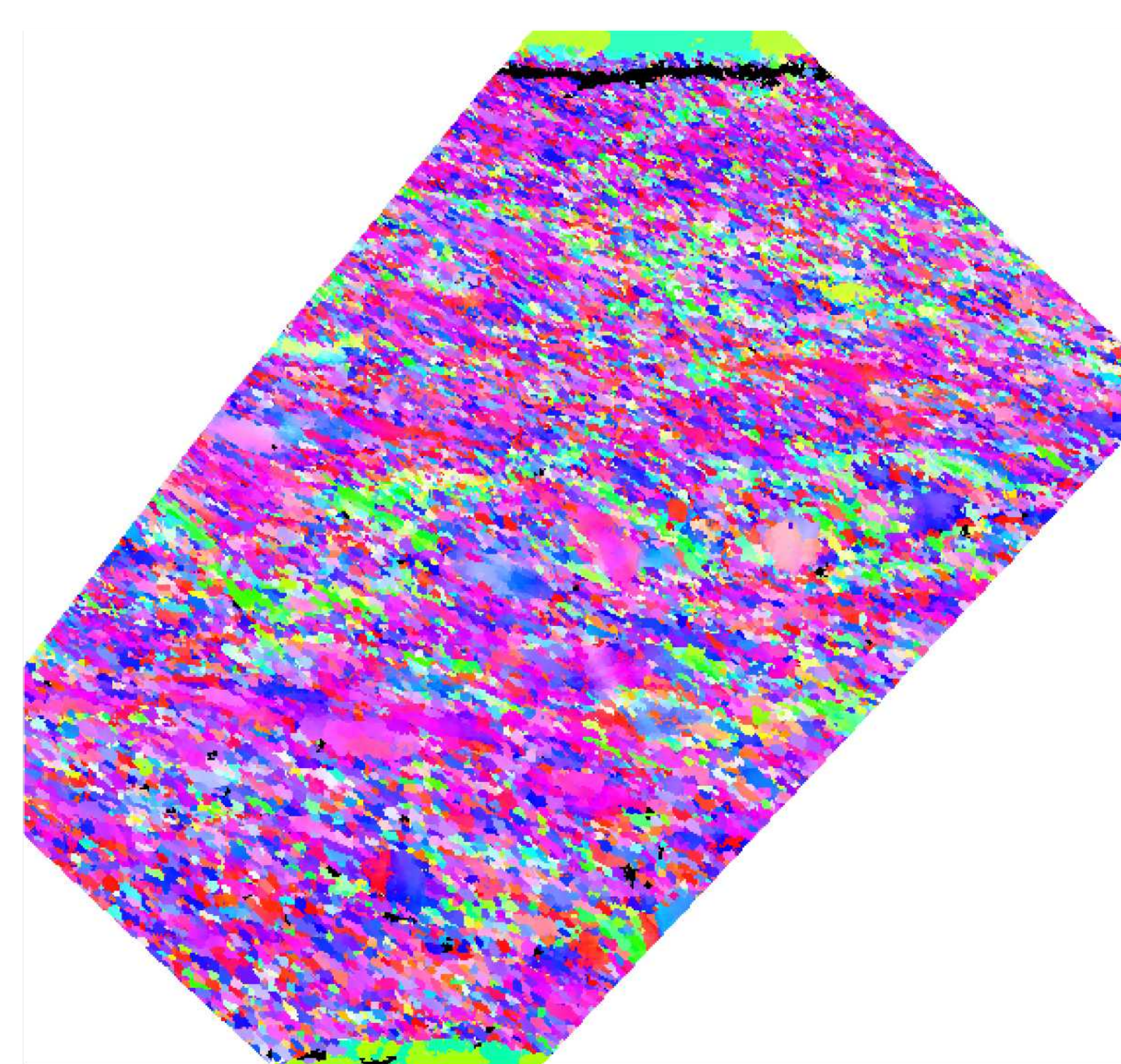
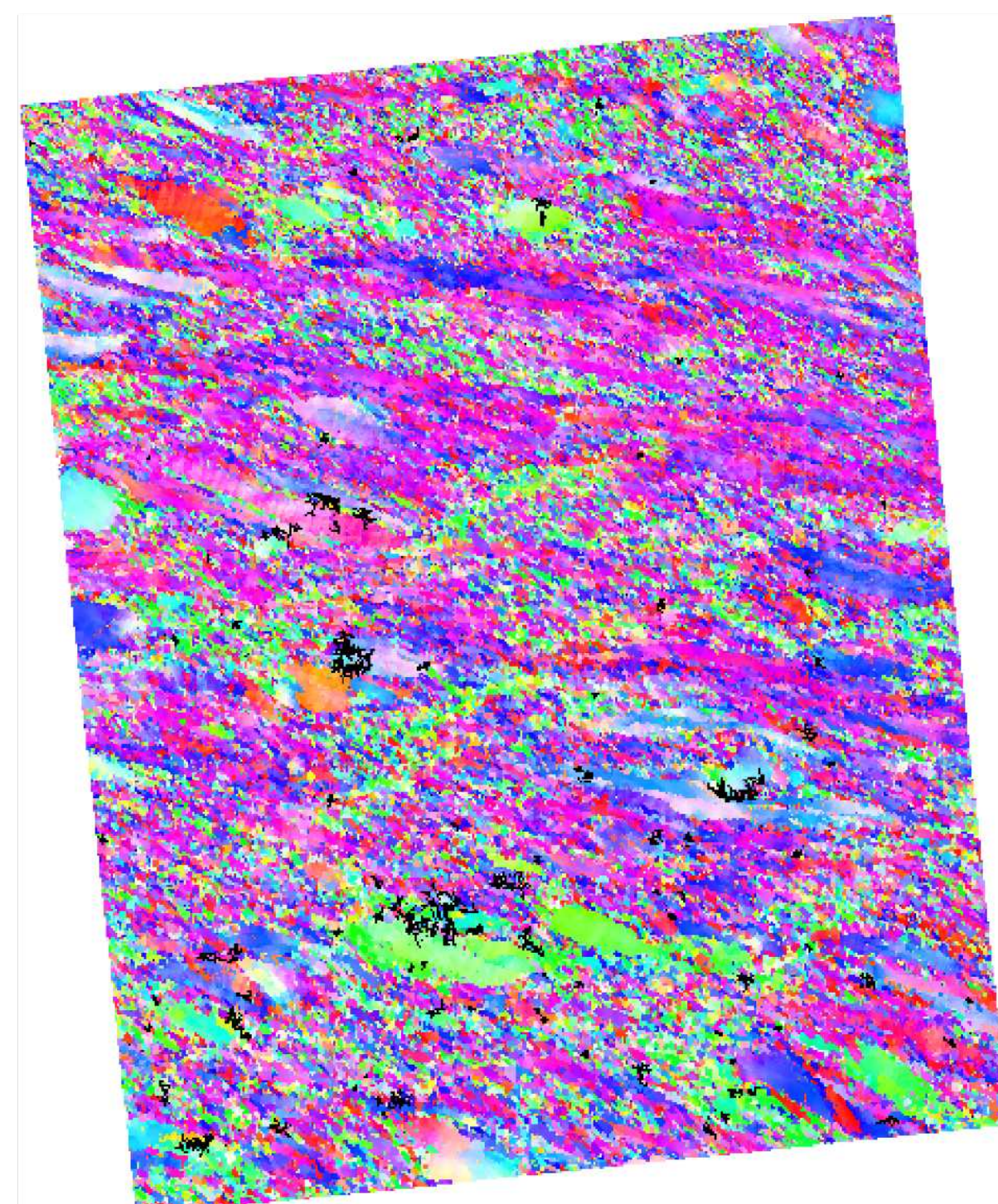
regime 3



Inverse polefigure colorcoding using the inferred vorticity axis (or specimen z direction or strain Y-direction) as a reference. Color key for purely rotational point group. For regime 2,3 samples, parts of the quartz forcing blocks are visible at the top and bottom.

reference direction perpendicular thin section plane (= specimen z)

-> increasing fraction of 'Y-grains'



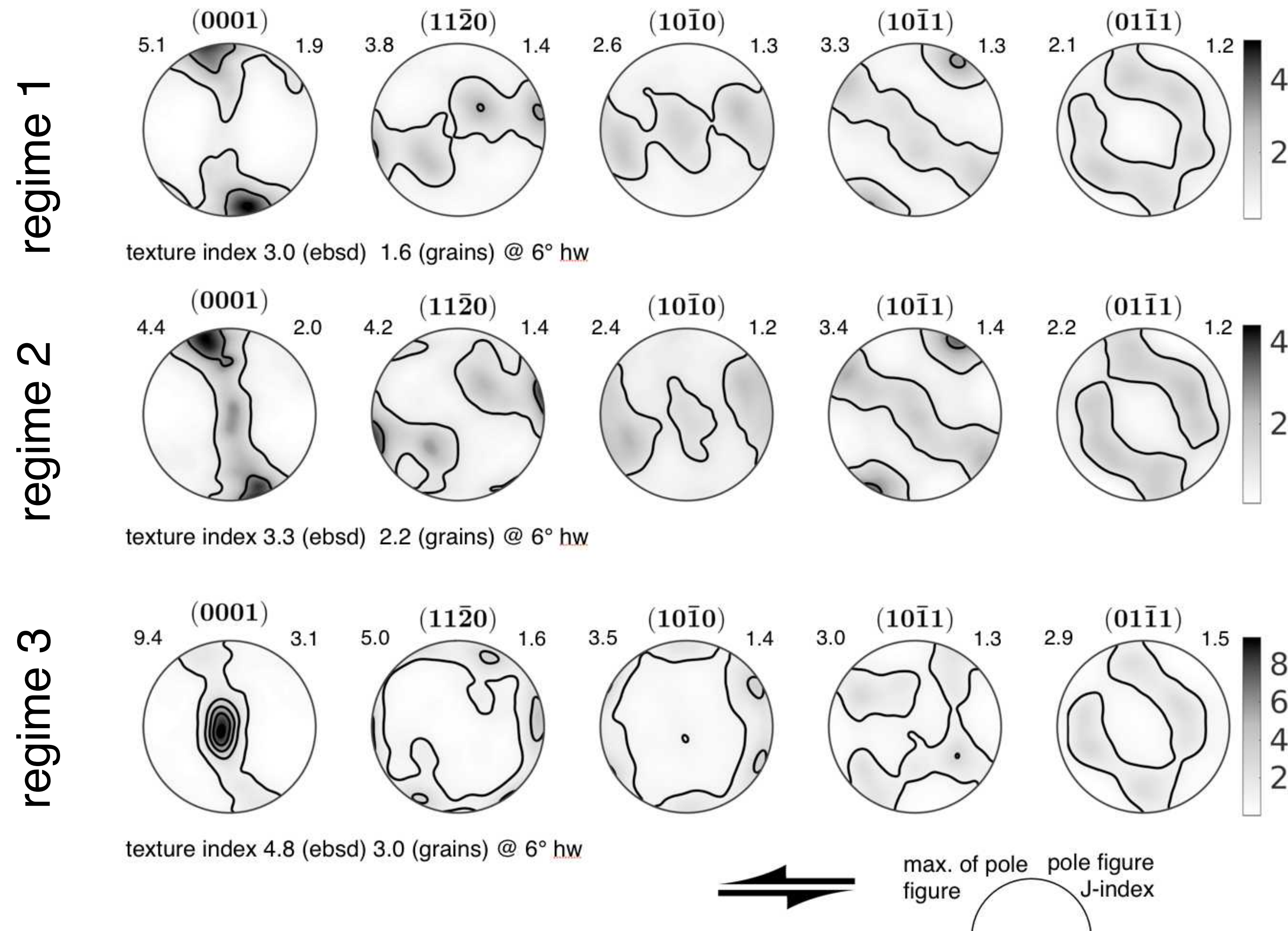
Inverse polefigure color coding using the ISA as a reference direction and a color key for Laue point group symmetry.

-> dominant alignment of <a>
-> decrease shear bands with c-grains

reference direction (ISA2-45°) ——— -8°
shear zone boundary (szb)

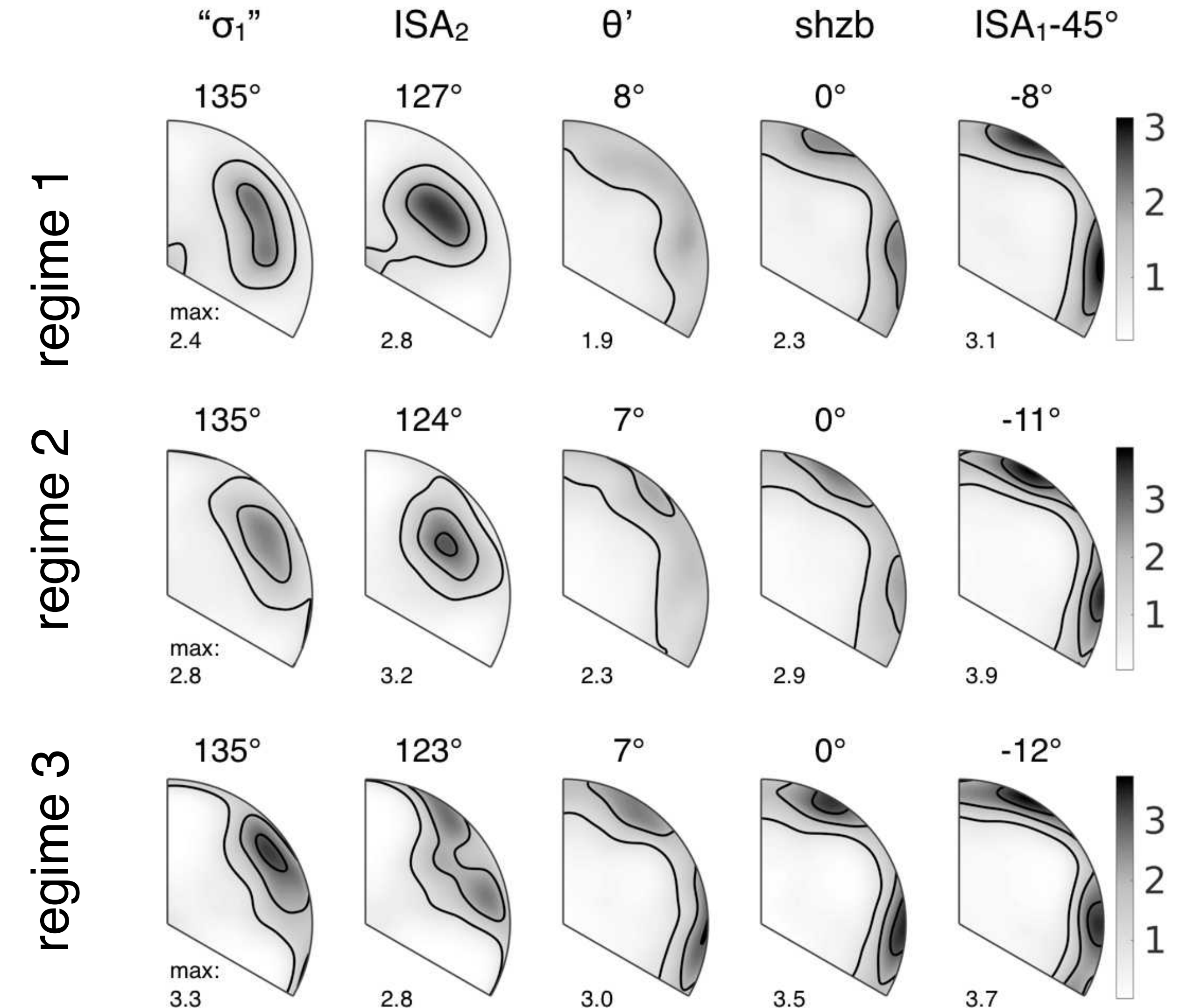
ref. direction ——— -10°

ref. direction ——— -11°

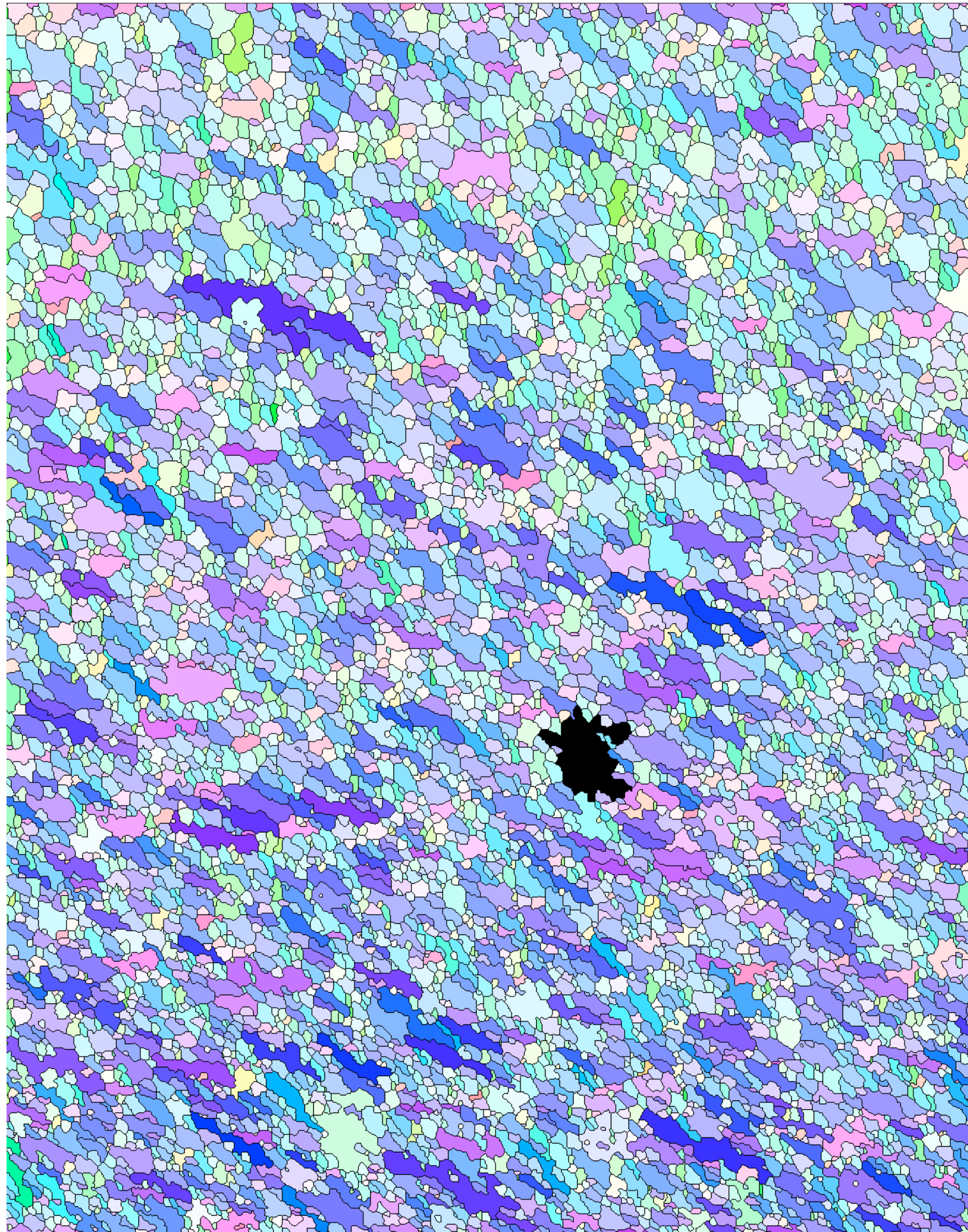


Pole figures from ebsd mappings of sample. Pole figures oriented with the shear zone boundary (forcing blocks). Contour intervals at 2 times uniform density.

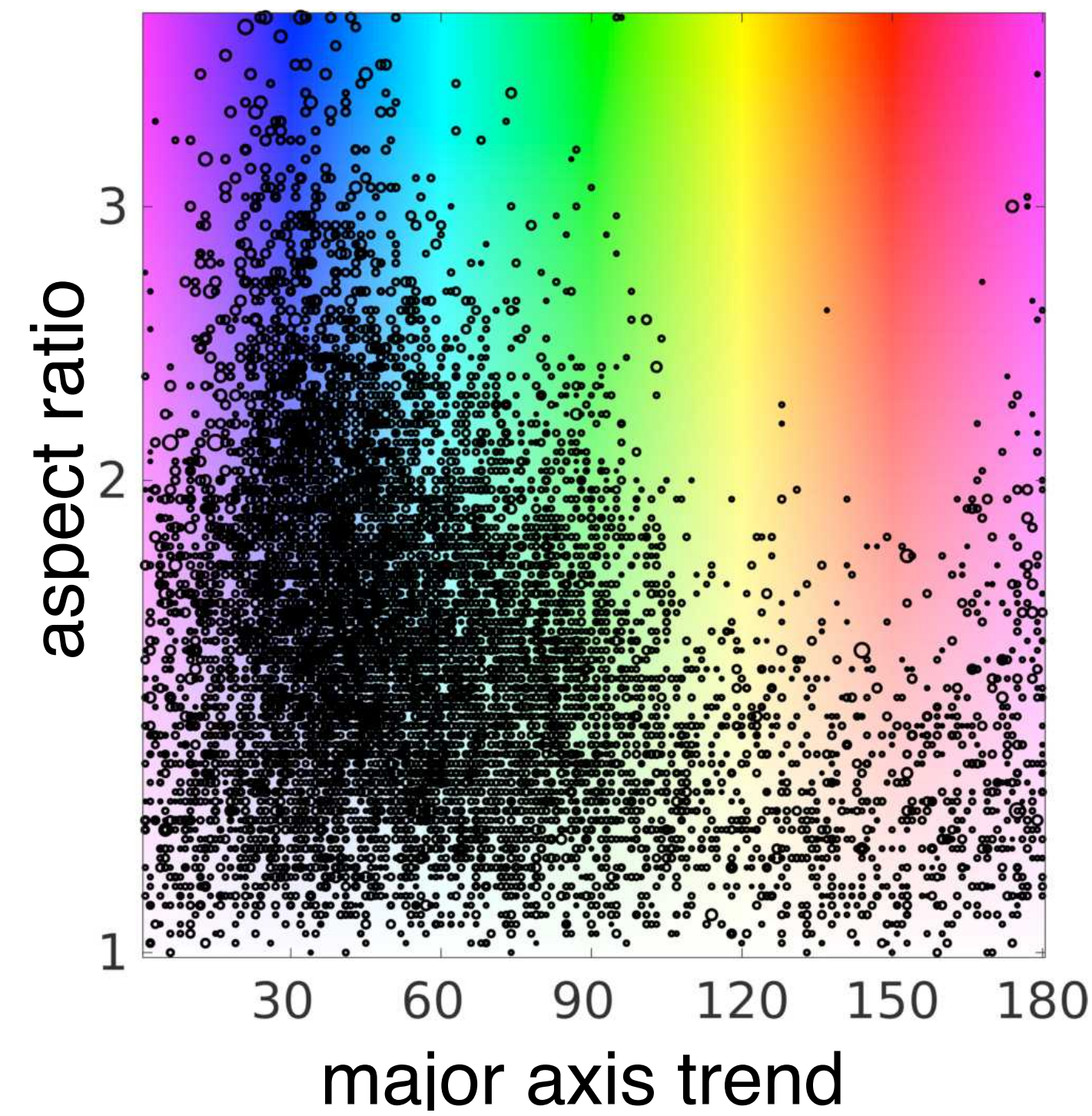
- > (c-axis) texture transition from regime 1 to regime 3
- > <a> alignment parallel to plane of highest shear stress (ISA₁-45°)
- > for regime 1 +2 (high stress experiments), pole to {r} || ISA₂



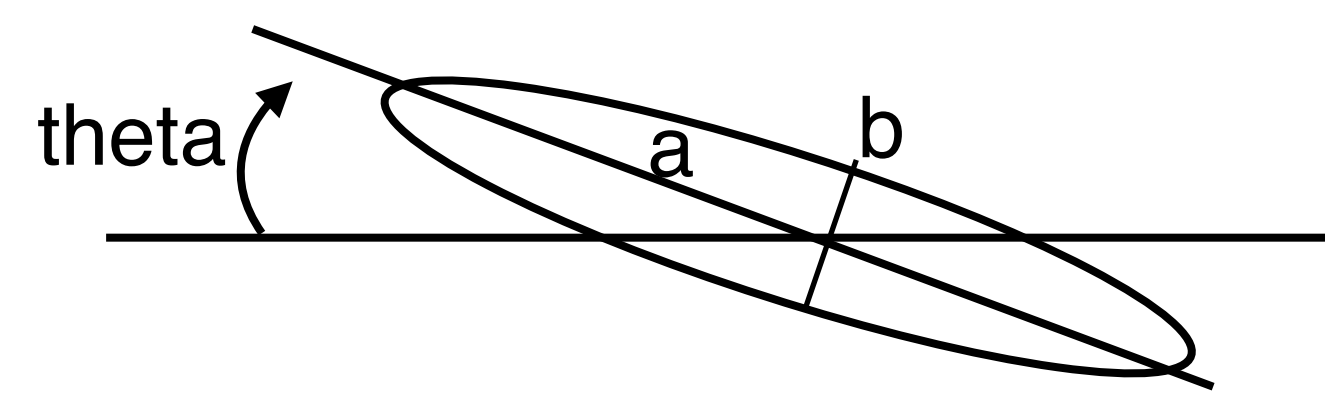
Inverse pole figures for selected reference directions: inferred loading direction ("σ₁"), instantaneous shortening axis (ISA₂), major axis direction of the ellipsoid (θ') obtained from sample strain, shear zone boundary (shzb), parallel to the forcing blocks in the experiments, and the plane 45° away from the instantaneous stretching axis (ISA₁). Contour intervals at 2 times uniform density.



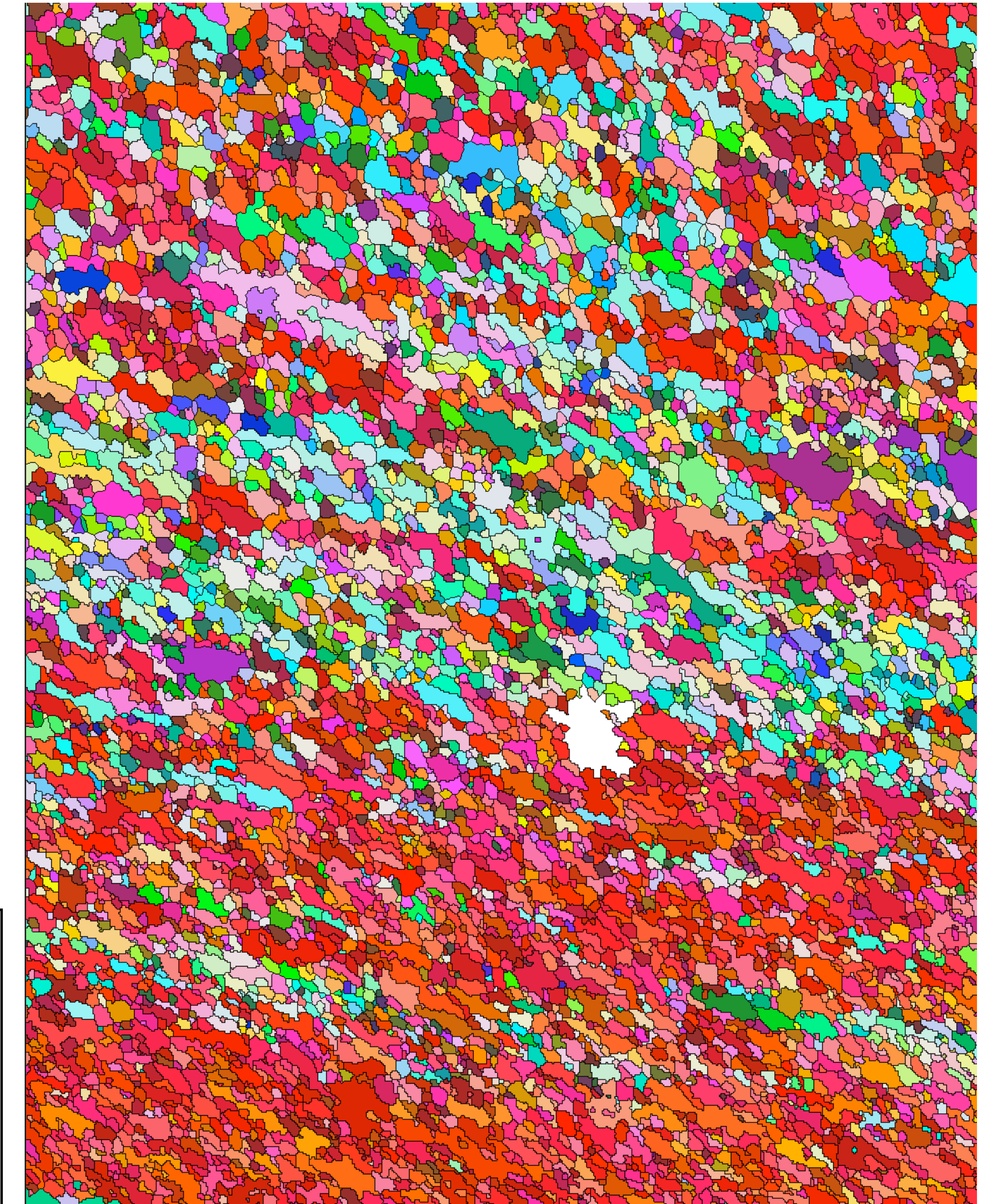
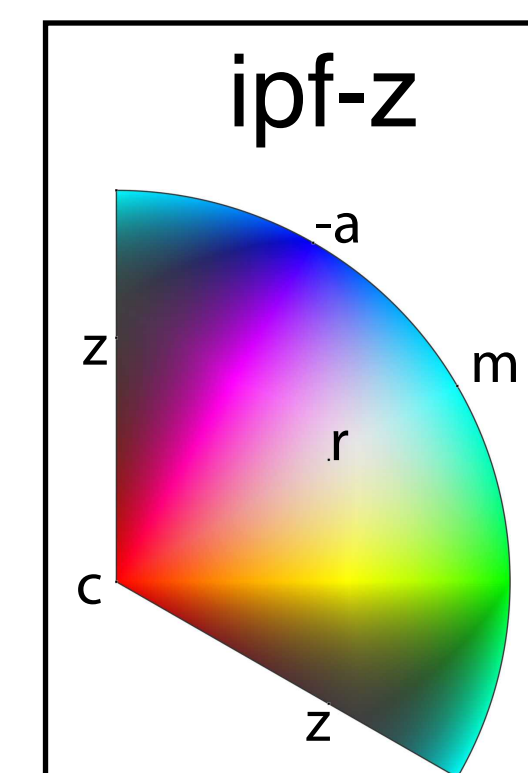
Grain property map: Color coding using hue for the trend of the grain major axis and log(intensity) for the aspect ratio.



Colorkey for grain property with values shown within a 180 (major axis trend) by 100 (aspect ratio) matrix. Size of points scaled by equivalent area diameter. All aspect ratios > 4 are attributed to the largest aspect ratio class.



100 μm



Corresponding area showing modal grain orientation with ipf-color coding with respect to the section normal.

-> grain shape and texture domains correlate?

- grain shape relation (2)

regime 1

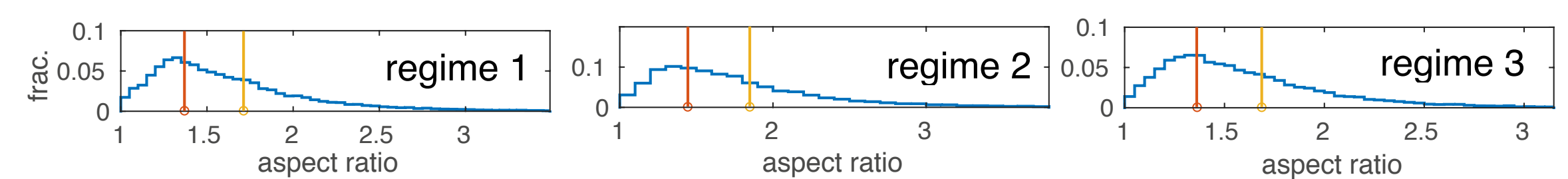
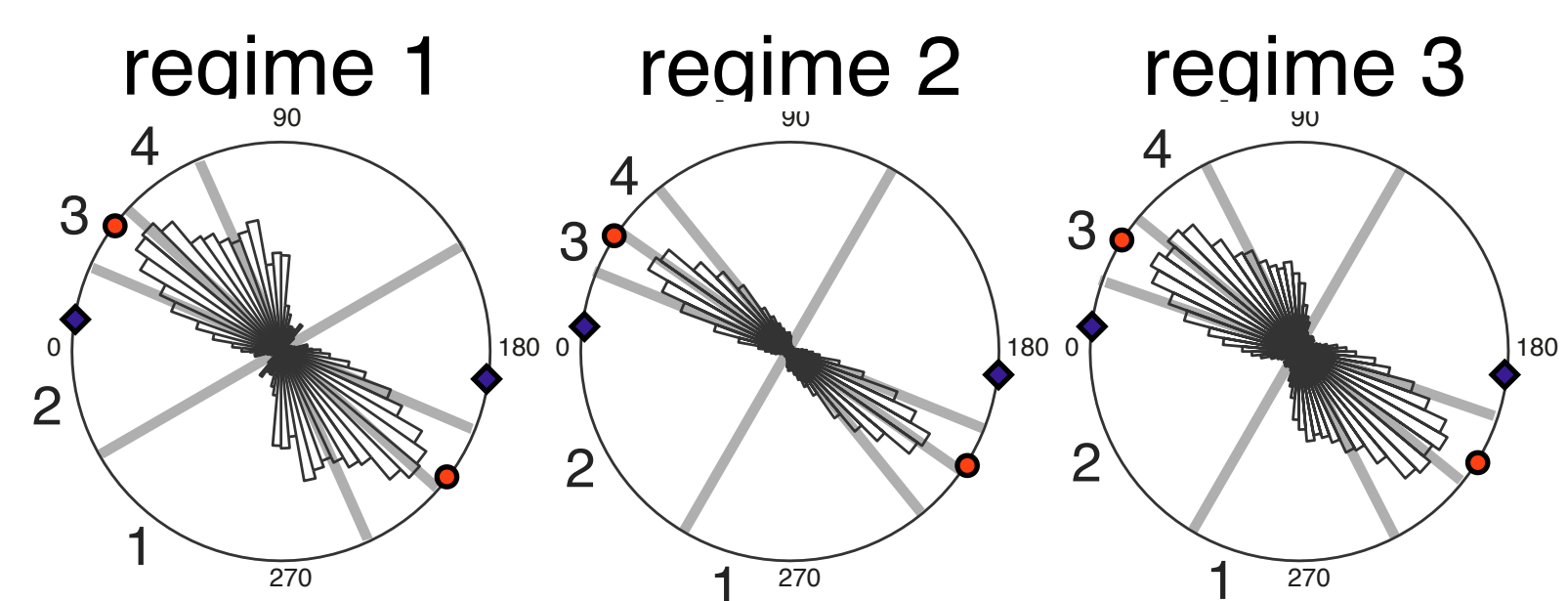
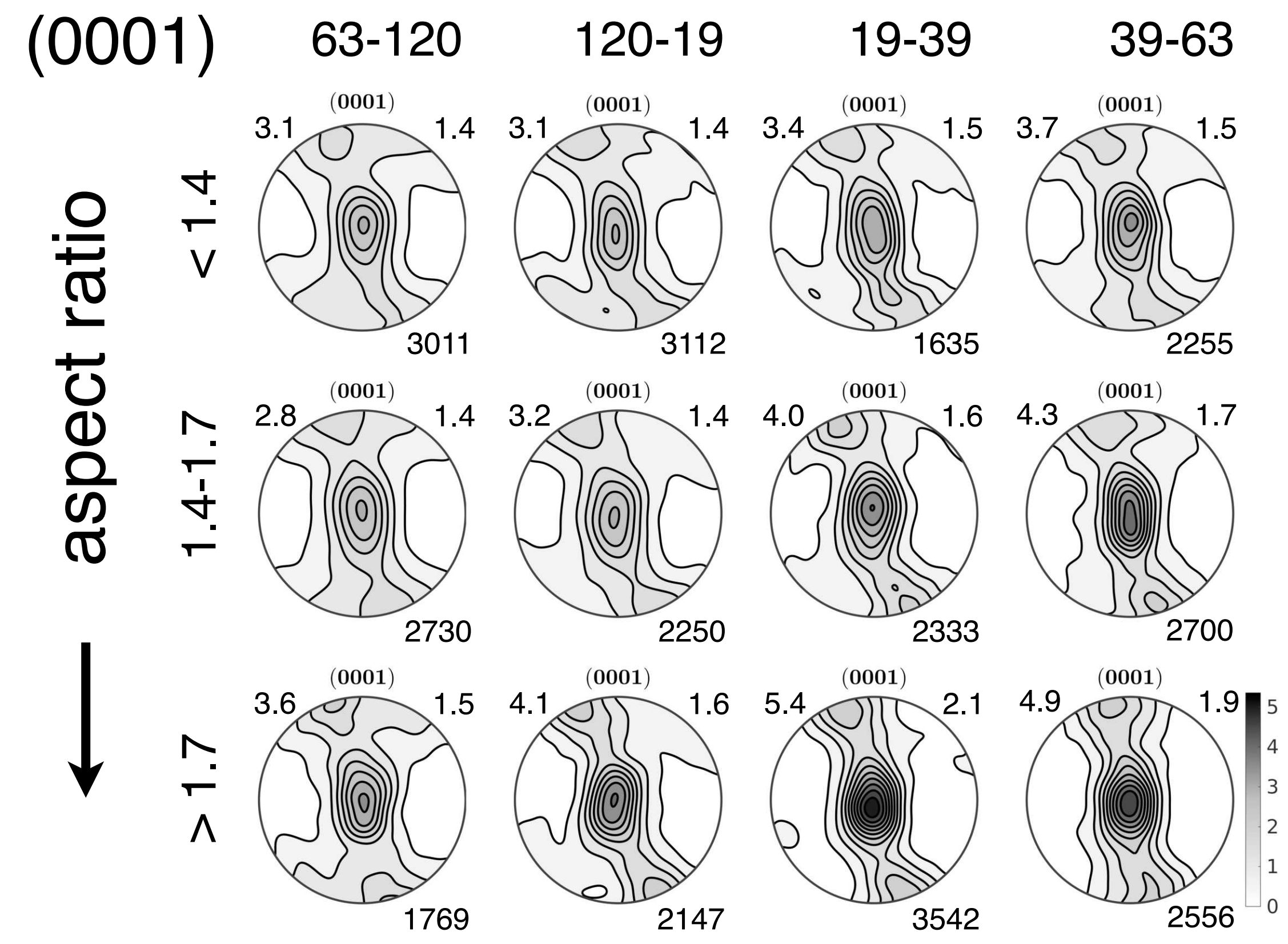
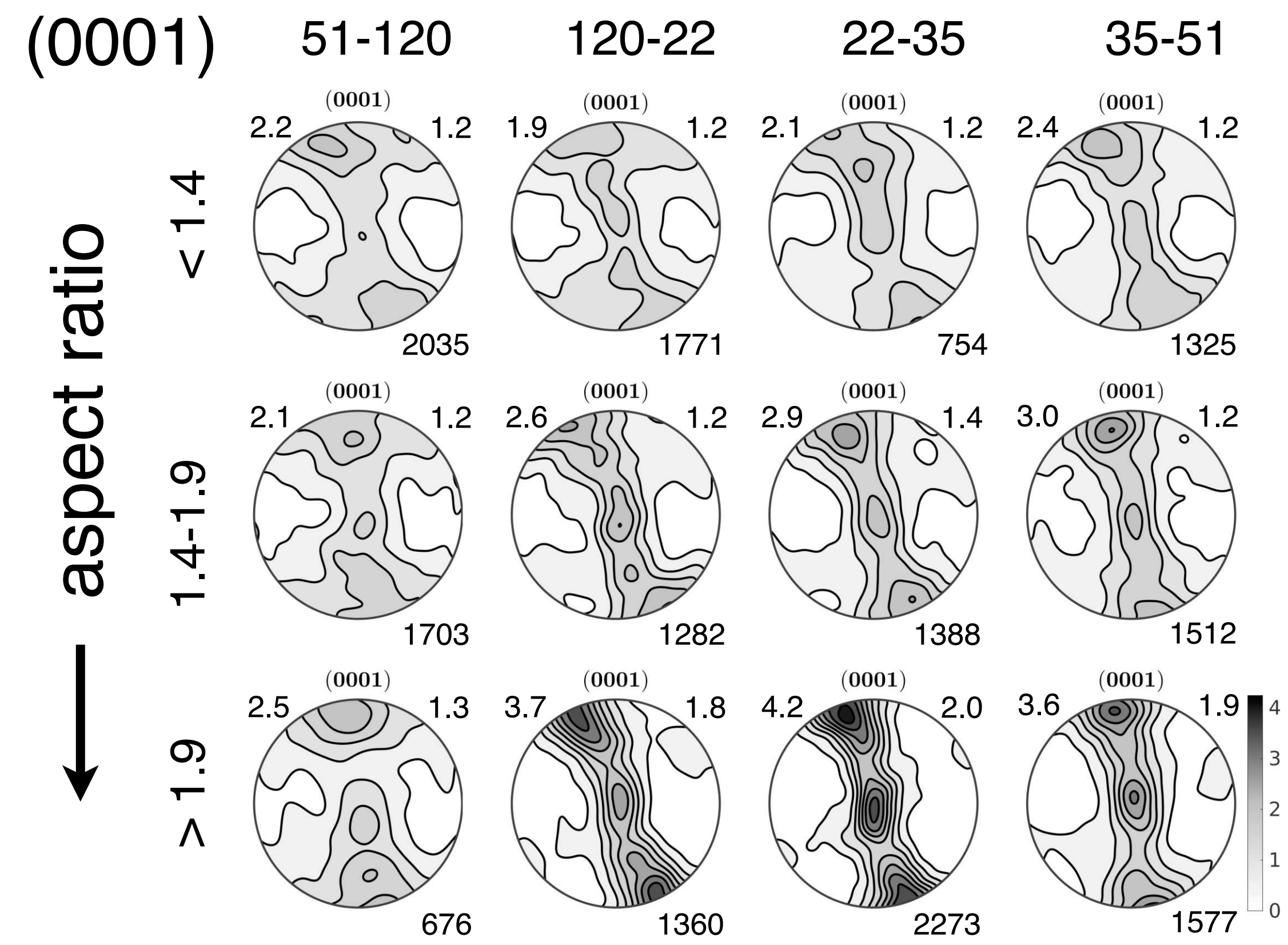
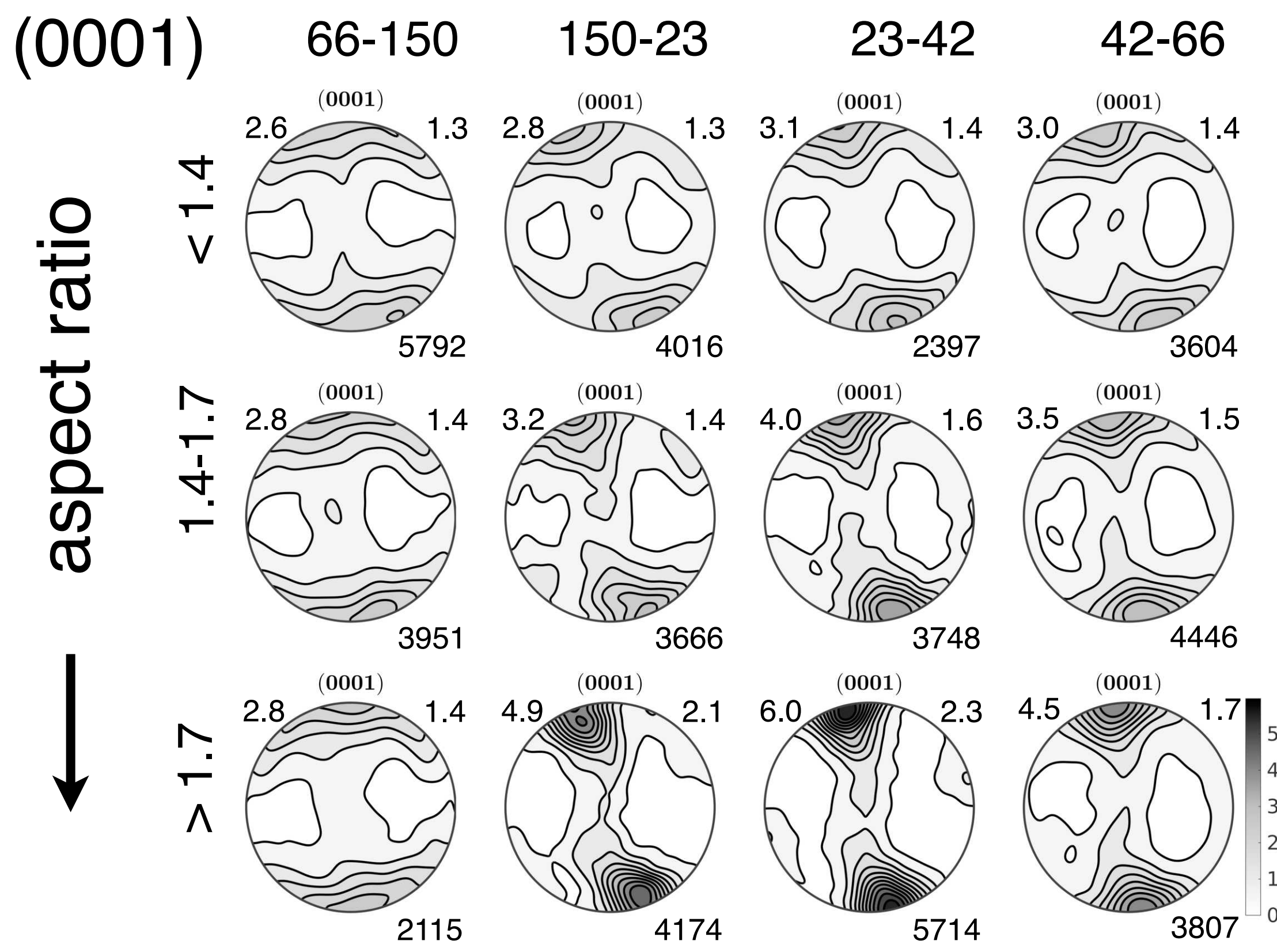
regime 2

regime 3

theta (°)

theta (°)

theta (°)



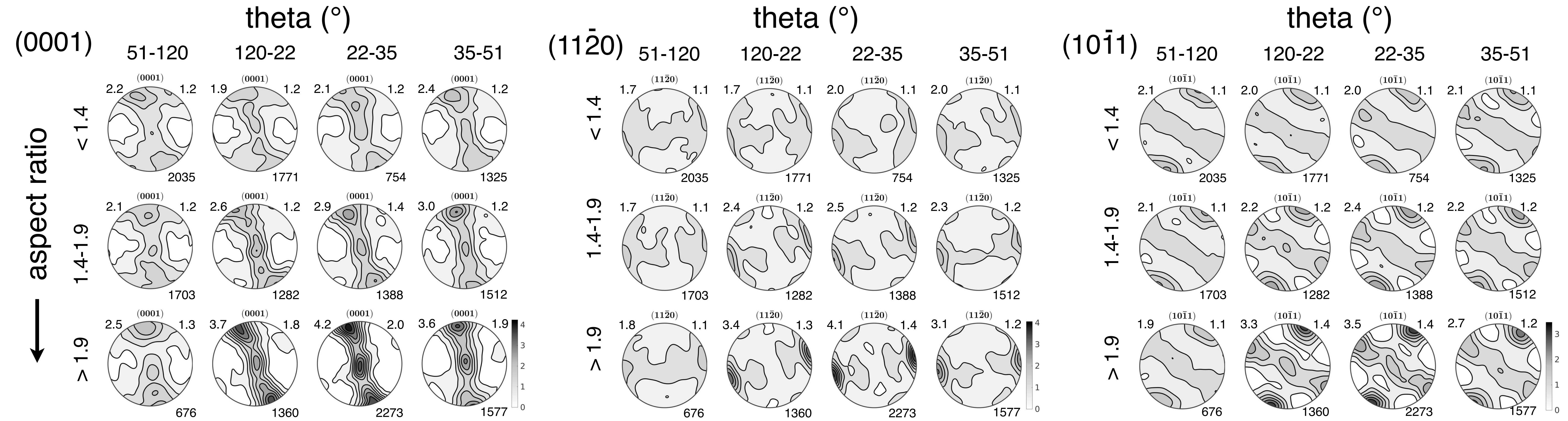
-> more deformation related grain shape - more girdle/center component
-> girdle rotation due to gbs (?)

C-axis pole figures for grain long axis trend (theta) - aspect ratio classes. Theta increases from W clockwise and within classes towards the right, aspect ratios towards the bottom of each 4-by-3 pole figure matrix. Maximum density and pole figure J-index given at left and right top of each pole figure, number of grains within each class at the bottom. Contours at 0.5 times uniform density. Theta classes are chosen for equally spaced circular quantiles centered around the minimum population. Theta classes shown in rose diagrams for long axis trend frequencies and number fraction histograms for 99% of all aspect ratios.

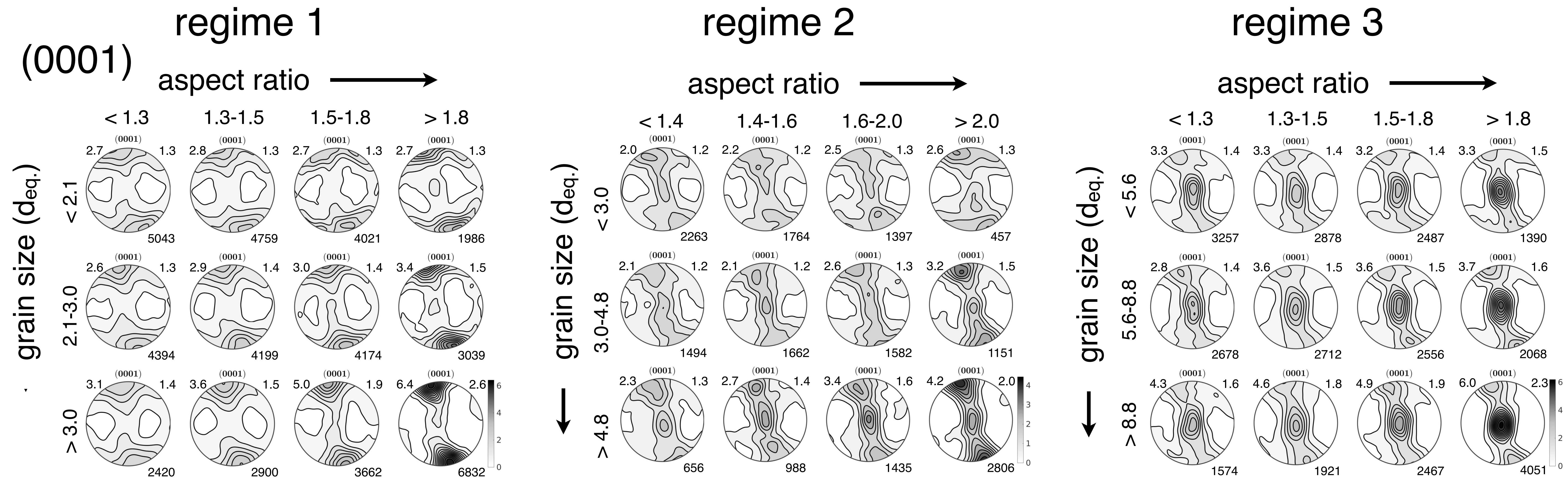
toc

<< >>

regime 2



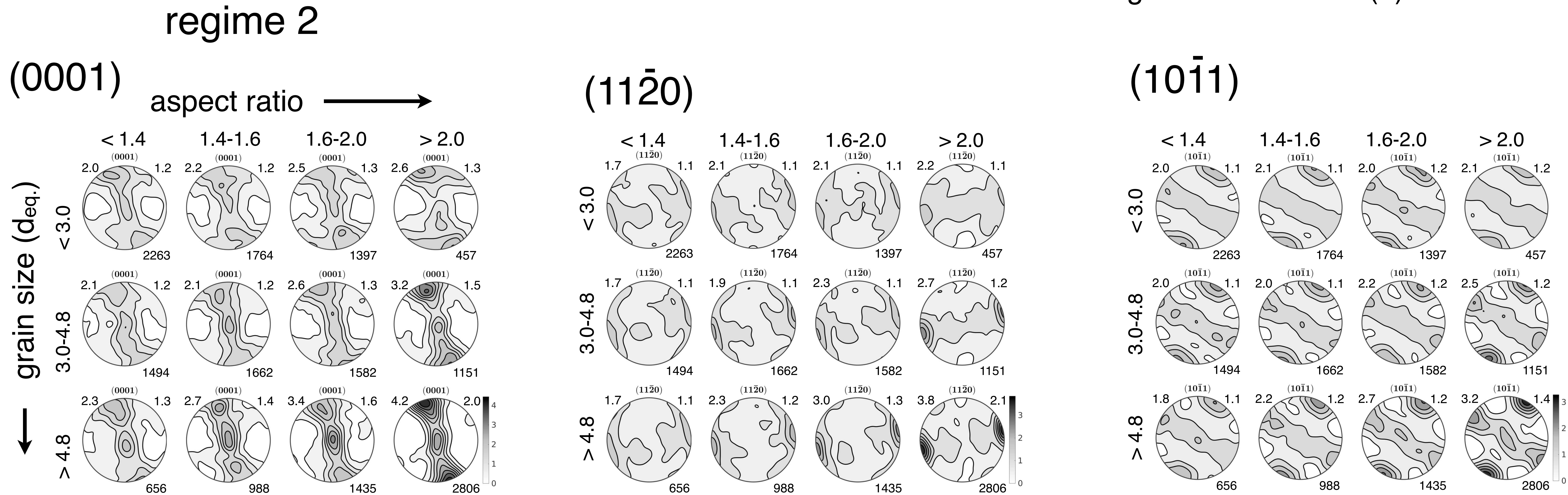
Pole figures for regime 2 sample for c,a,r planes for grain long axis trend (theta) - aspect ratio classes. Theta increases from W clockwise and within classes towards the right, aspect ratios towards the bottom of each 4-by-3 pole figure matrix. Maximum density and pole figure J-index given at left and right top of each pole figure, number of grains within each class at the bottom. Contours at 0.5 times uniform density.



C-axis pole figures for aspect ratio - grain size classes. Aspect ratio increases to the right, grain size towards the bottom of each 4-by-3 pole figure matrix. Classes for each property are chosen as equally spaced quantiles of the entire population. Textures calculated for grain modal orientations (one orientation per grain). Maximum density and pole figure J-index given at left and right top of each pole figure, number of grains within each class at the bottom. Contours at 0.5 times uniform density. Shear zone boundary horizontal and shear sense sinistral, upper hemisphere, equal area projections. Histograms show distribution of number fraction of area equivalent diameters and aspect ratios of 99% of all grains.

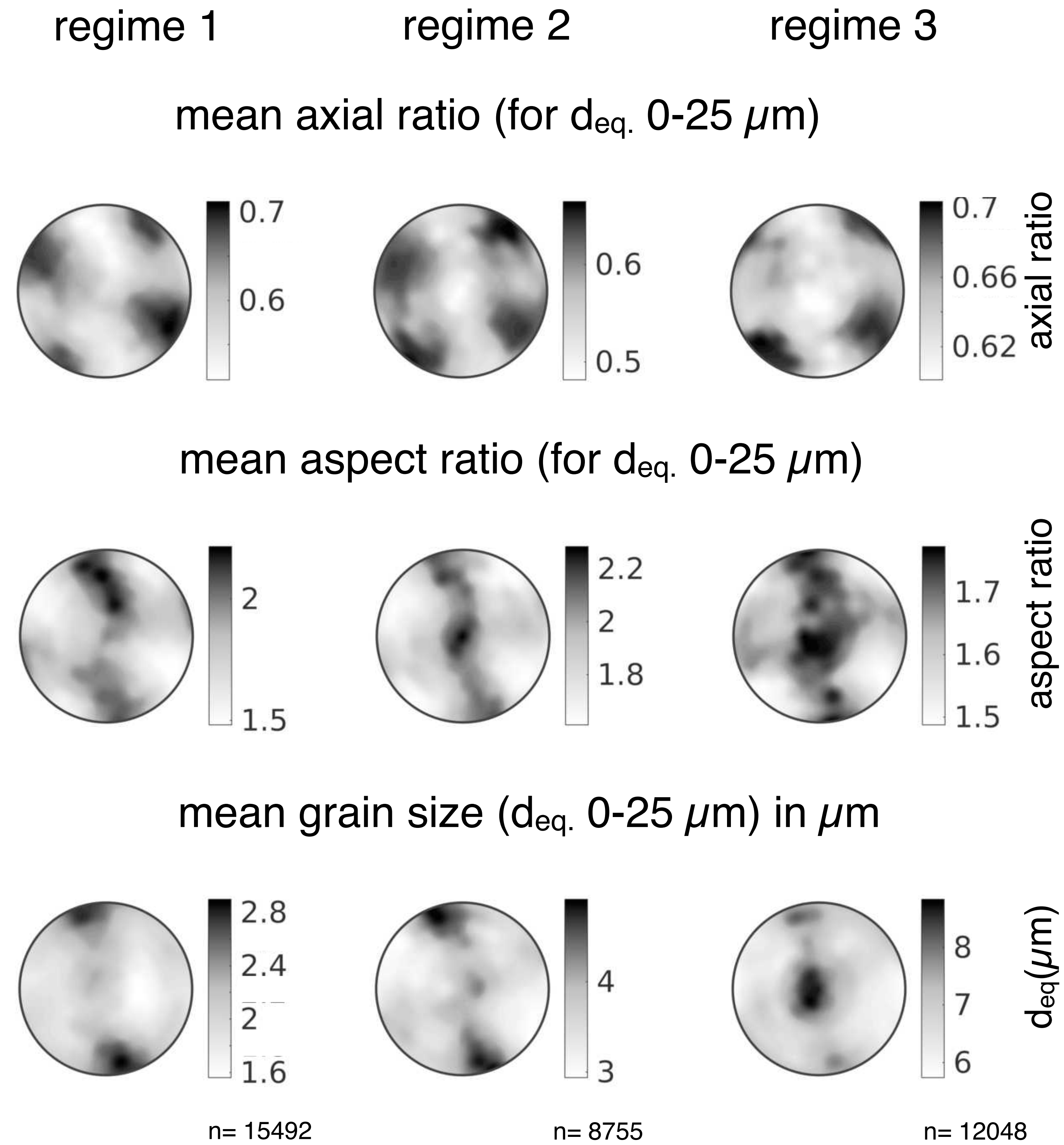
-> large, isometric grains, weak & broad peripheral c-axis distribution

- grain size relation (2)

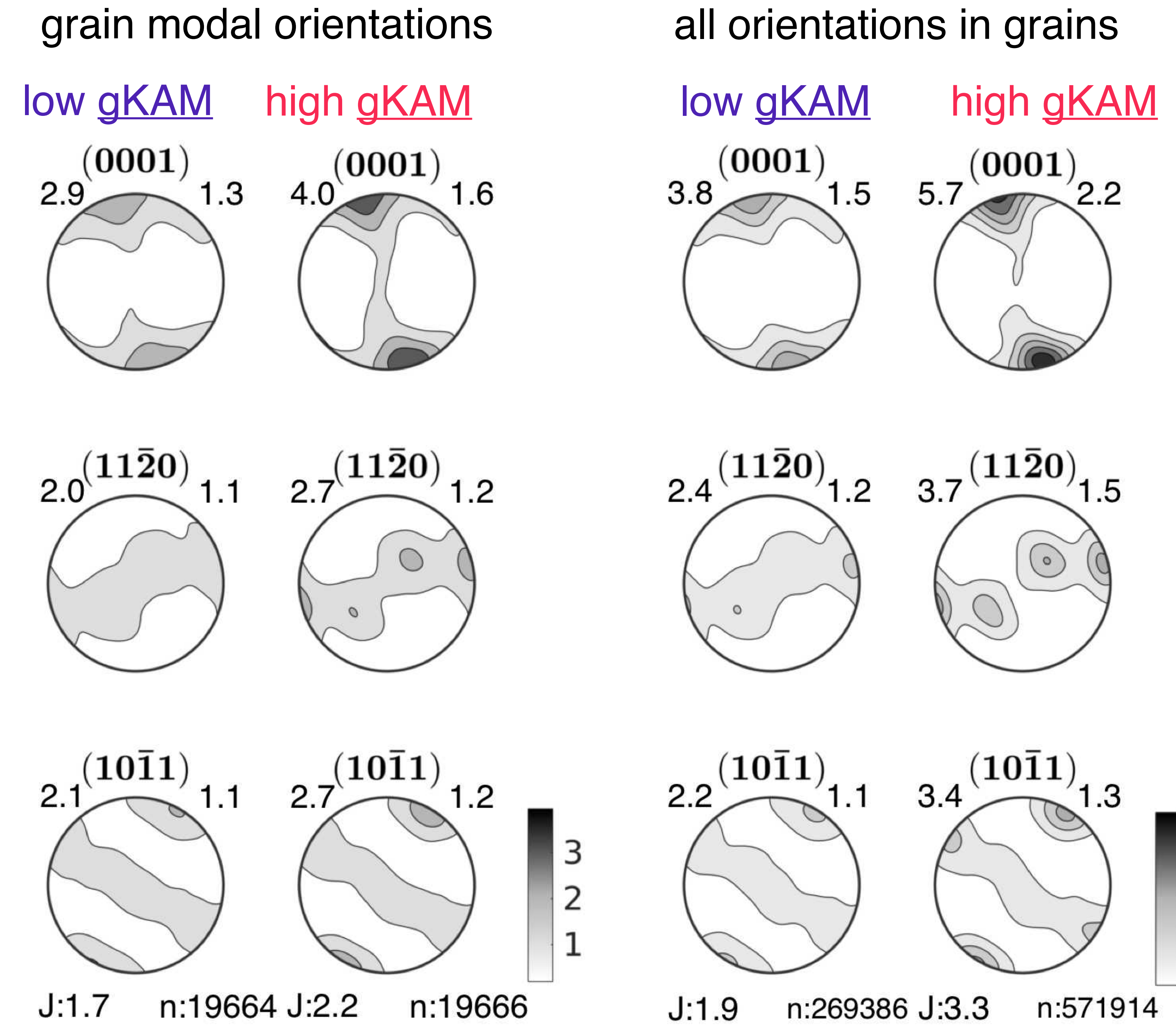
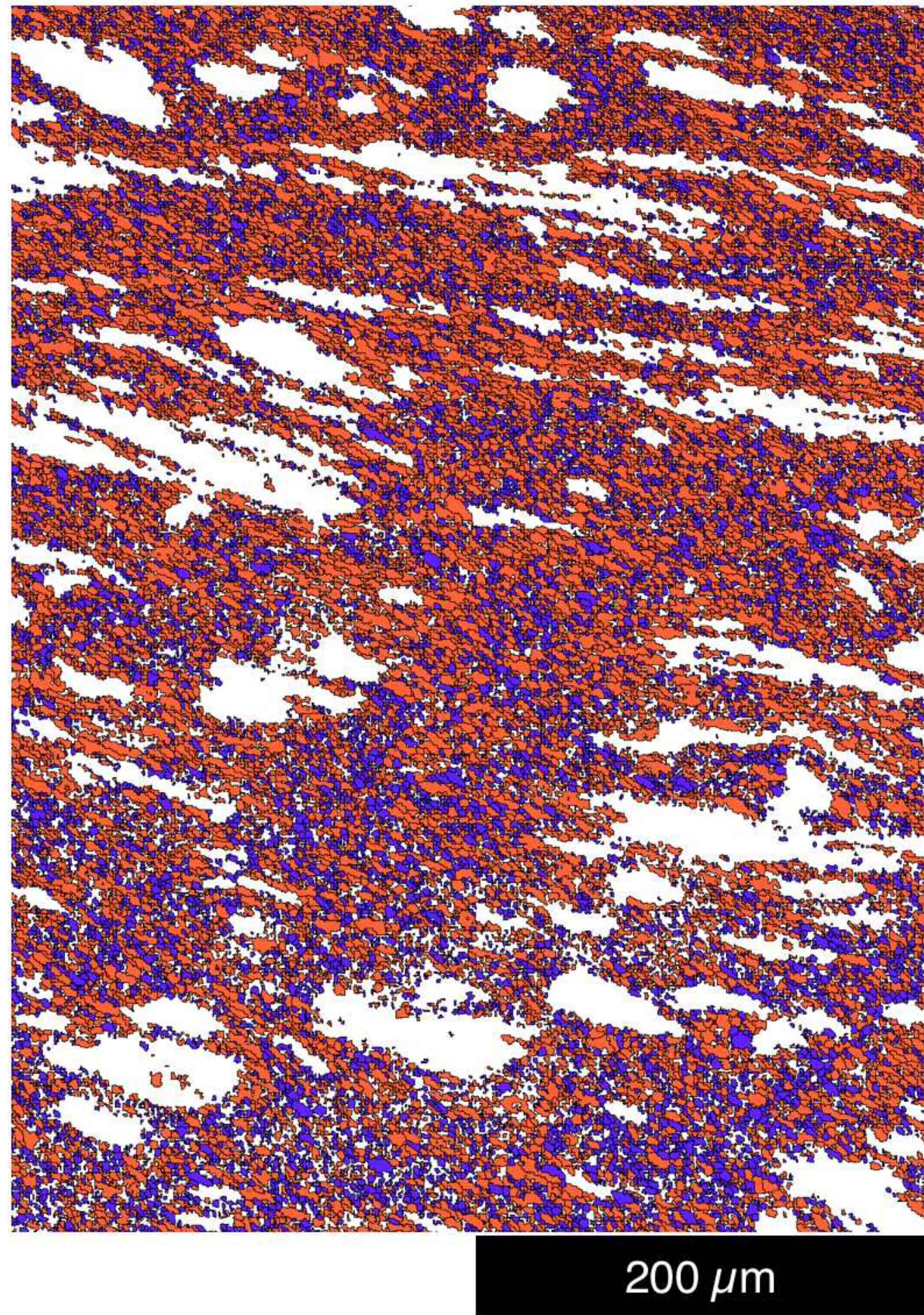


Pole figures for poles to c, a and r for aspect ratio - grain size classes only for regime 2. Aspect ratio increases to the right, grain size towards the bottom of each 4-by-3 pole figure matrix. Classes for each property are chosen as equally spaced quantiles of the entire population. Textures calculated for grain modal orientations (one orientation per grain). Maximum density and pole figure J-index given at left and right top of each pole figure, number of grains within each class at the bottom. Contours at 0.5 times uniform density. Shear zone boundary horizontal and shear sense sinistral, upper hemisphere, equal area projections. Histograms show distribution of number fraction of area equivalent diameters and aspect ratios of 99% of all grains.

Pole figures of axial ratio, aspect ratio and grain size: Average axial ratio, aspect ratio and grain size estimated in c-axis pole figure space for grains smaller 25 μm . Upper hemisphere, equal area projection, greyscale bar indicates the average axial ratio, aspect ratio and grain size to be expected for grains with a corresponding c-axis direction.

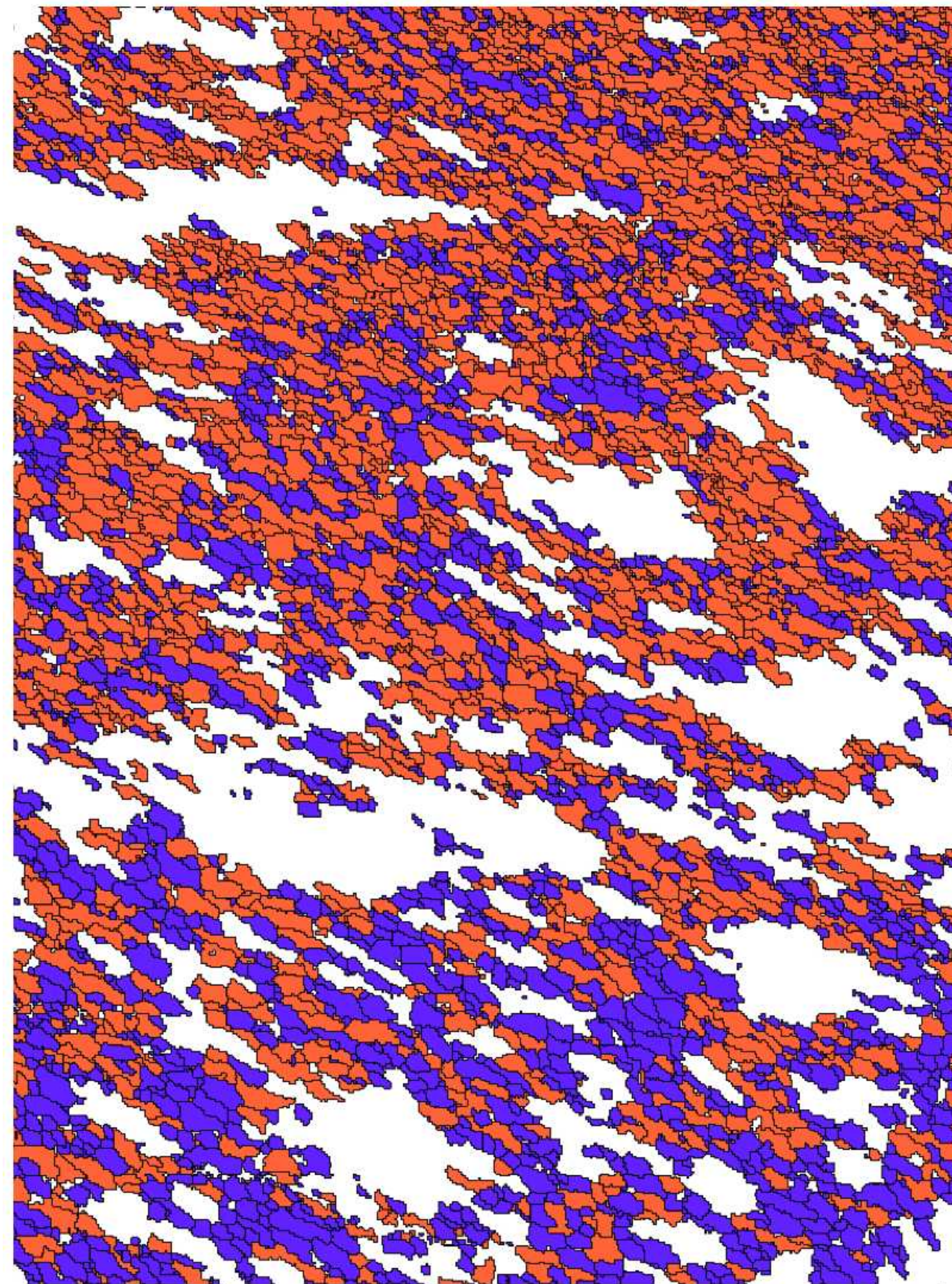


regime 1



Pole figures for low gKAM - high gKAM populations for grains (1 modal orientation per grain) and all the corresponding orientations of grains lower and higher than the median of all gKAMs in each sample and within a grain size range of 1-12 μm. Contours at 1 times uniform.

maximum of pole figure J-index
 J-index of odf number of orientations

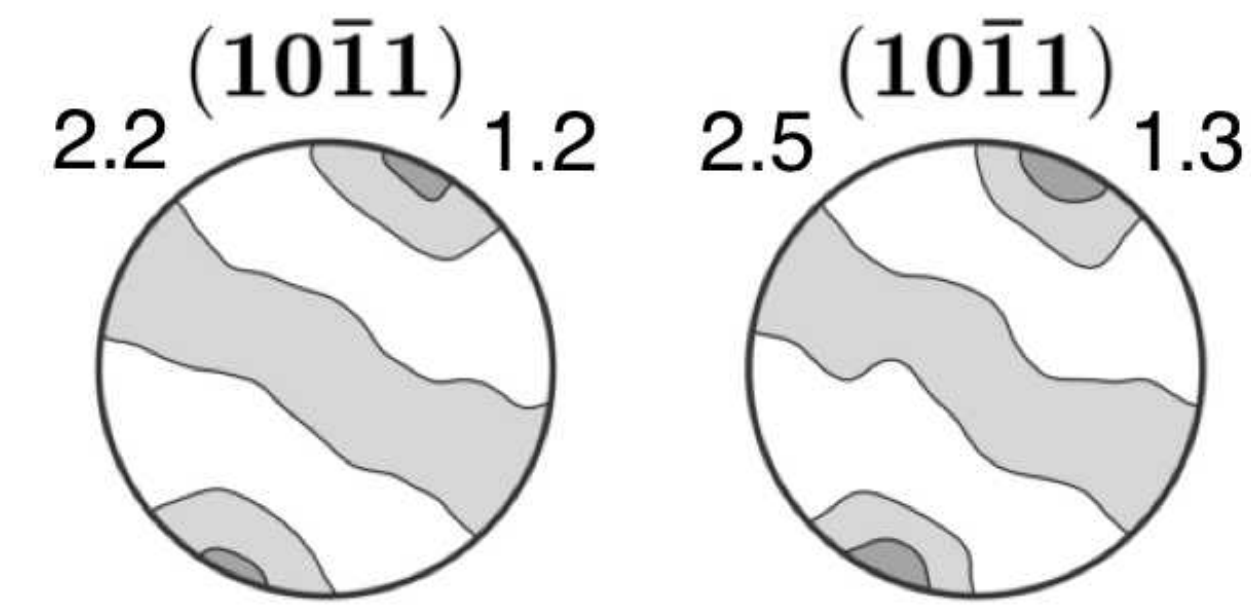
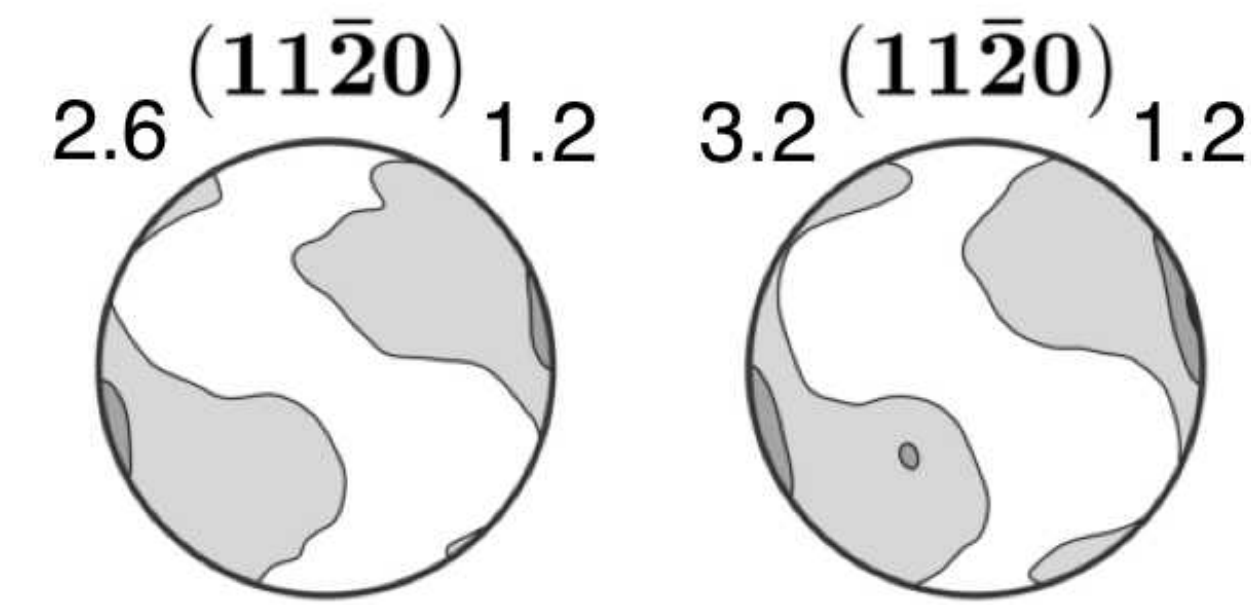
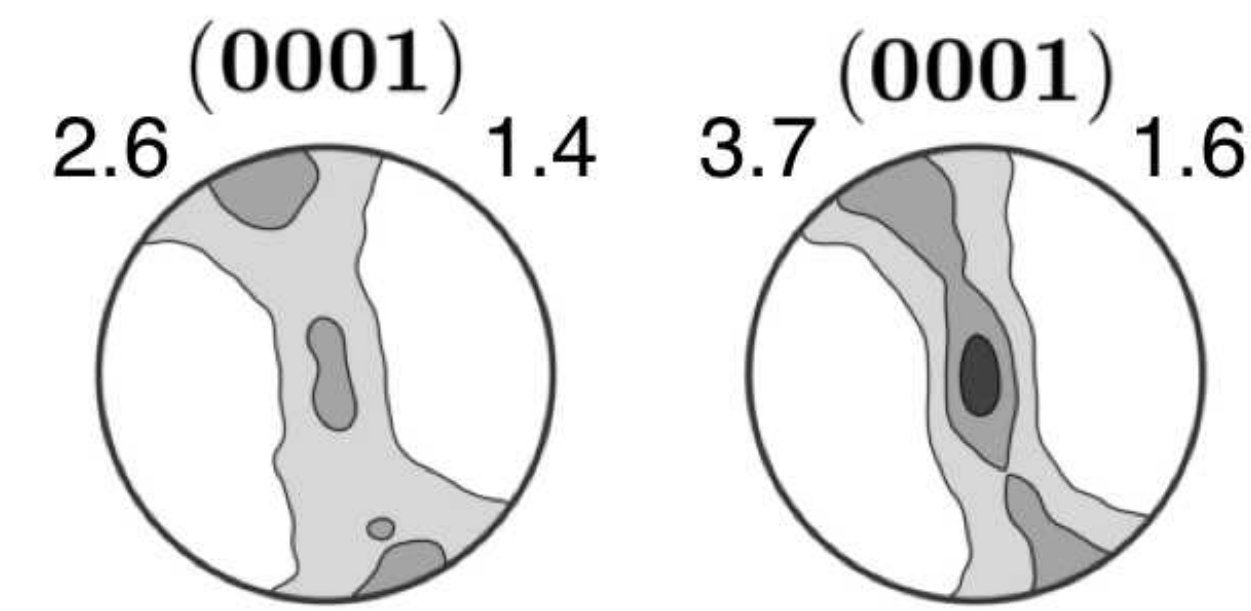


200 μm

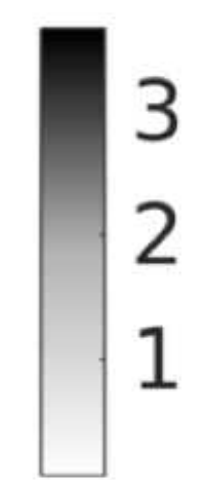
regime 2

grain modal orientations

low gKAM high gKAM

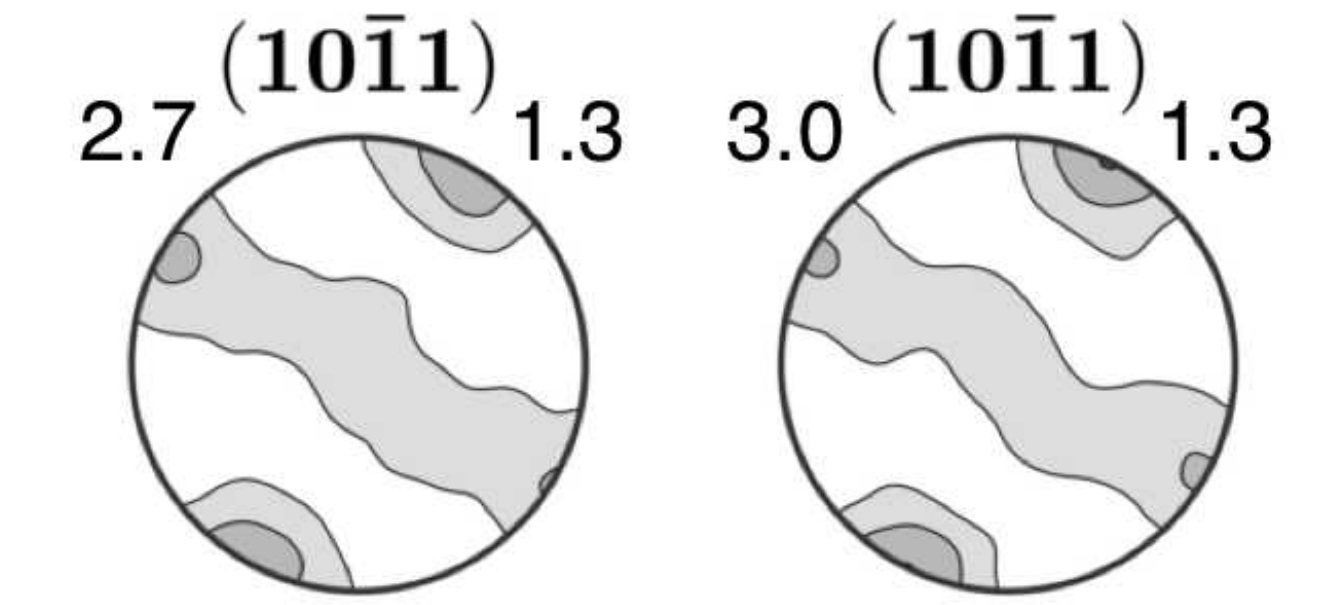
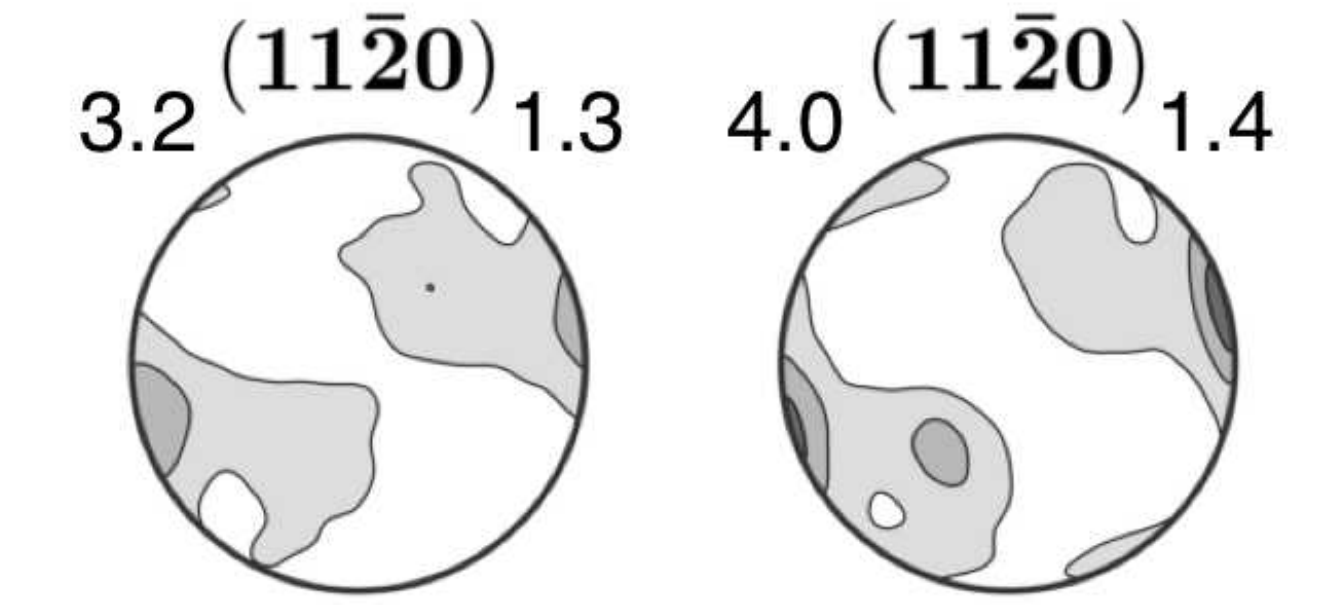
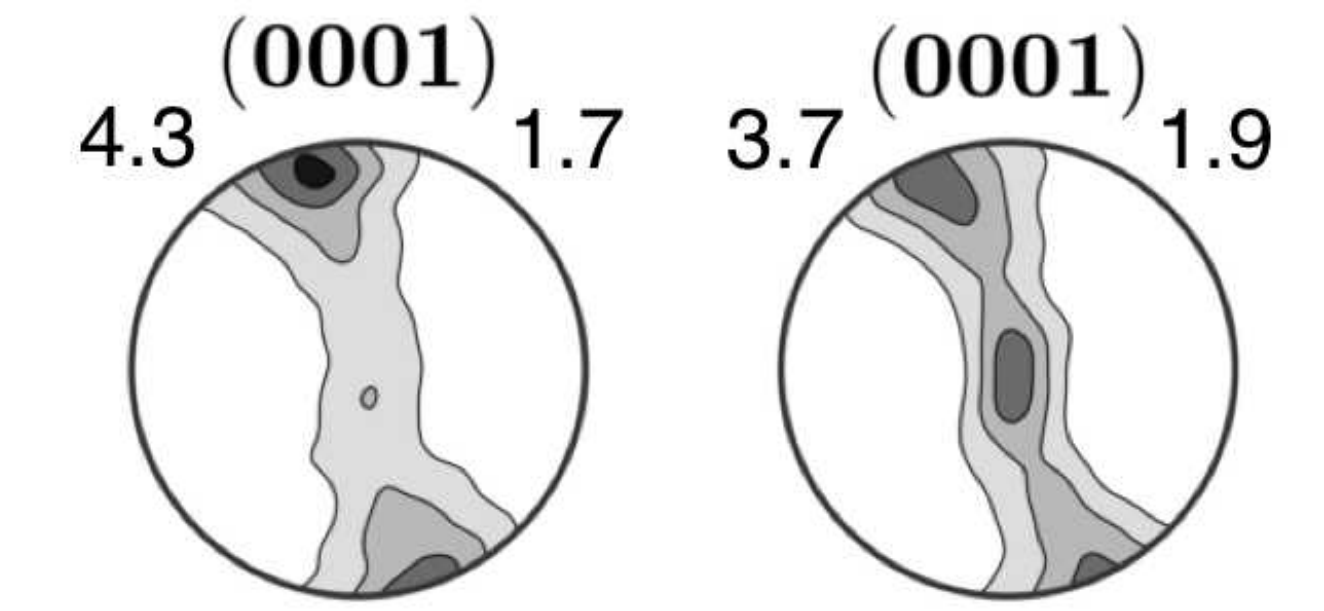


J:1.9 n:8371 J:2.3 n:8373



all orientations in grains

low gKAM high gKAM



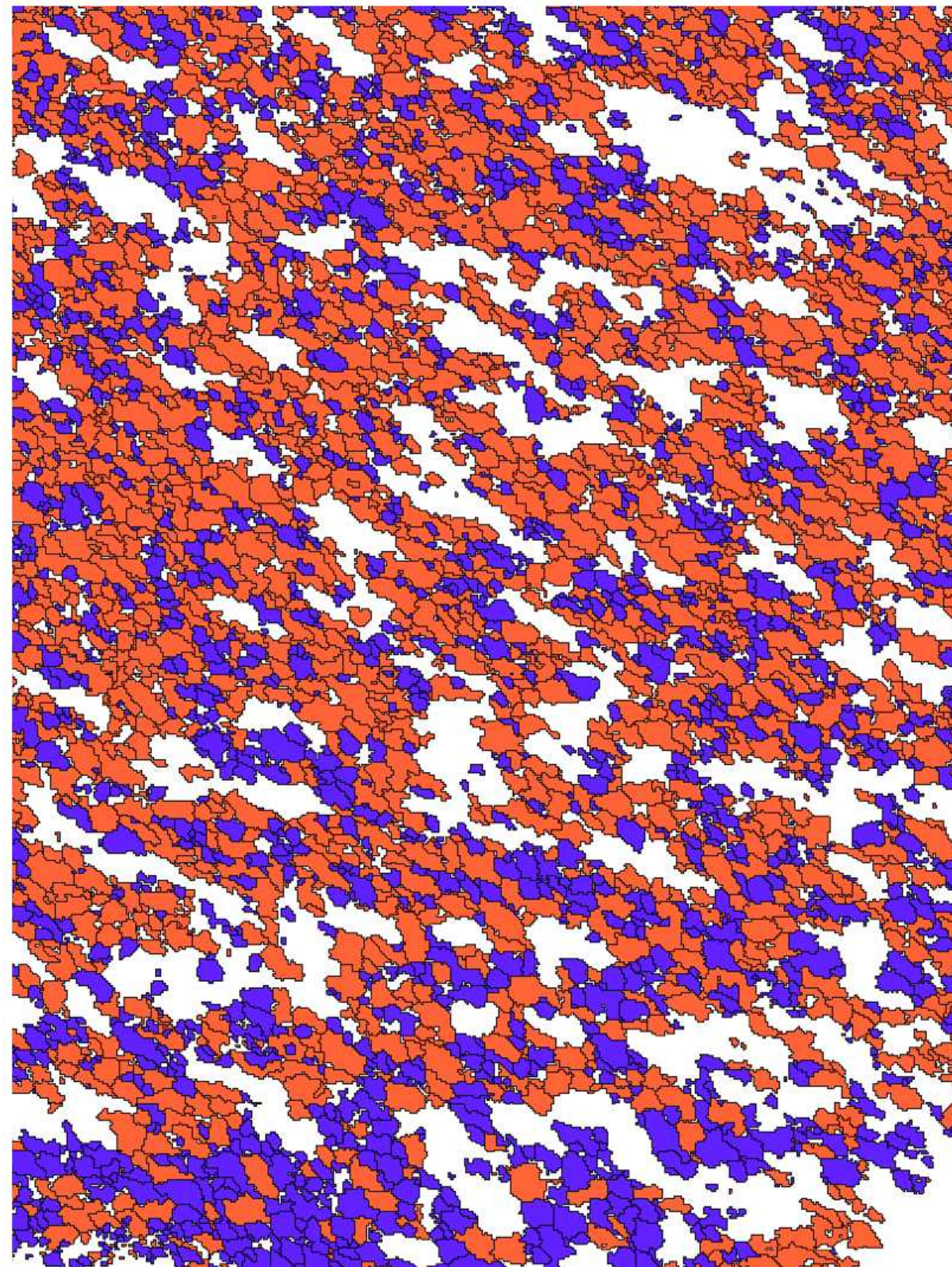
J:2.4 n:192057 J:2.9 n:336428



Pole figures for low gKAM - high gKAM populations for grains (1 modal orientation per grain) and all the corresponding orientations of grains lower and higher than the median of all gKAMs in each sample and within a grain size range of 1-12 μm. Contours at 1 times uniform.

toc

<< >>

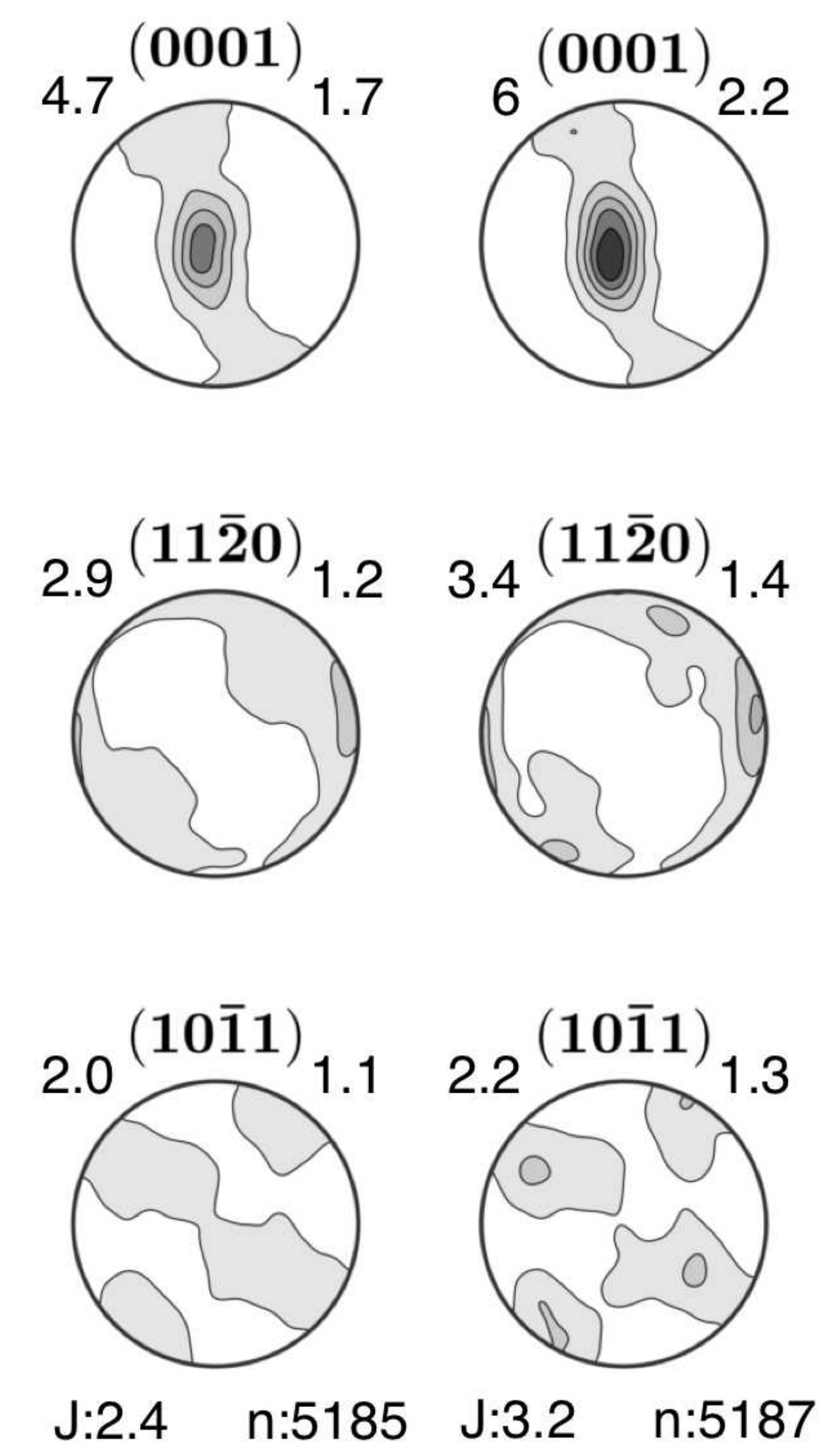


regime 3

250 μm

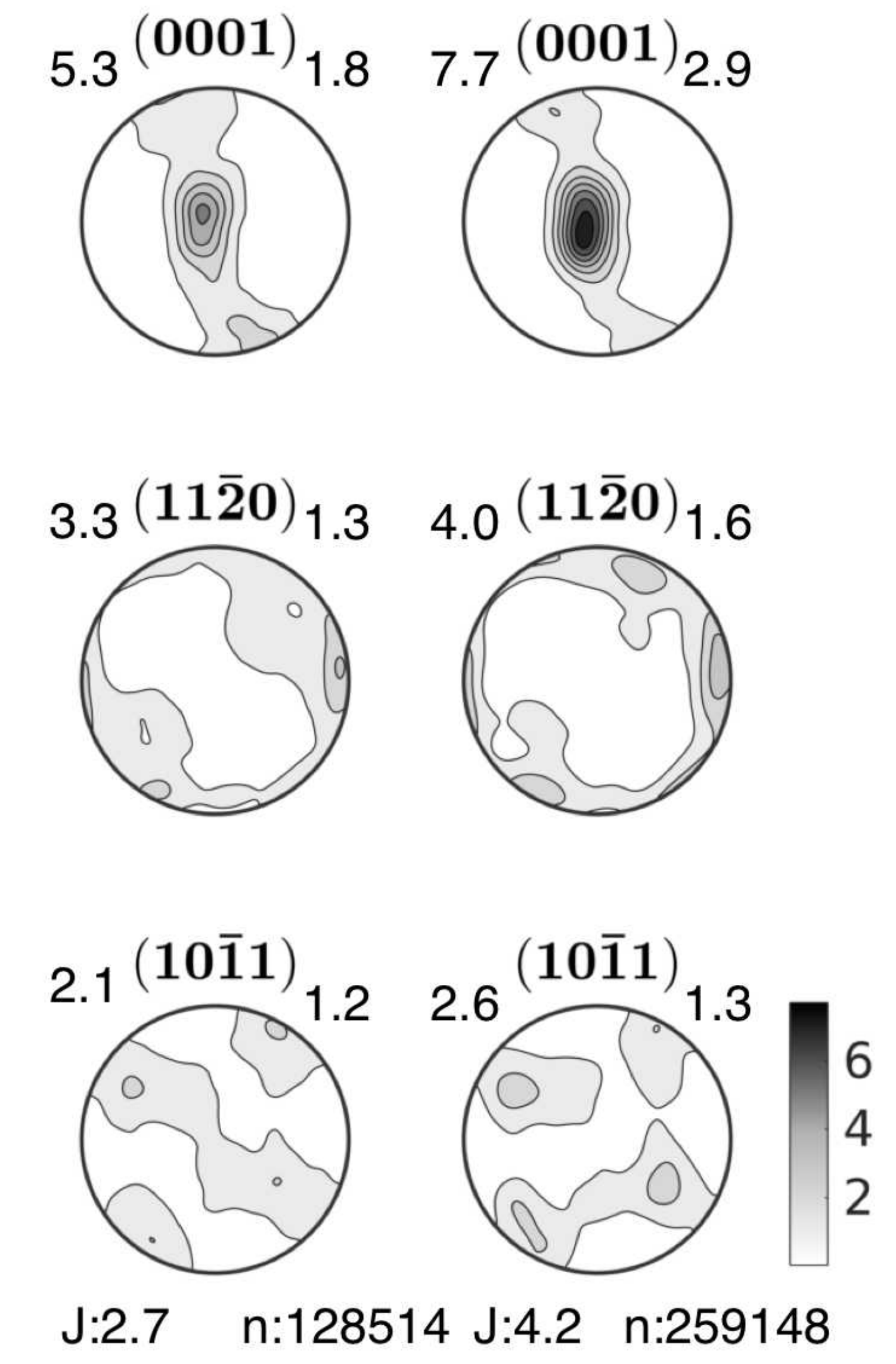
grain modal orientations

low gKAM high gKAM

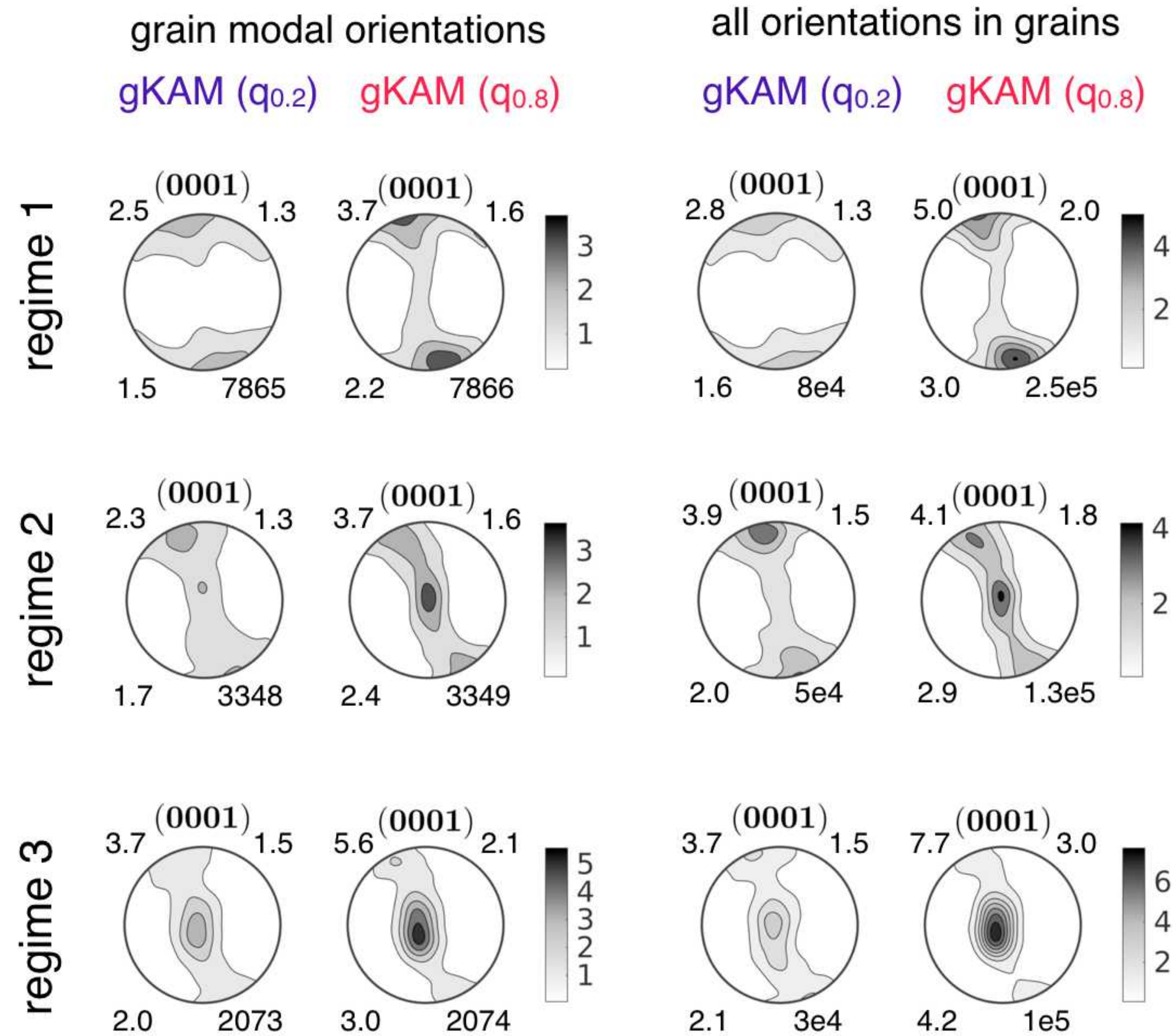


all orientations in grains

low gKAM high gKAM

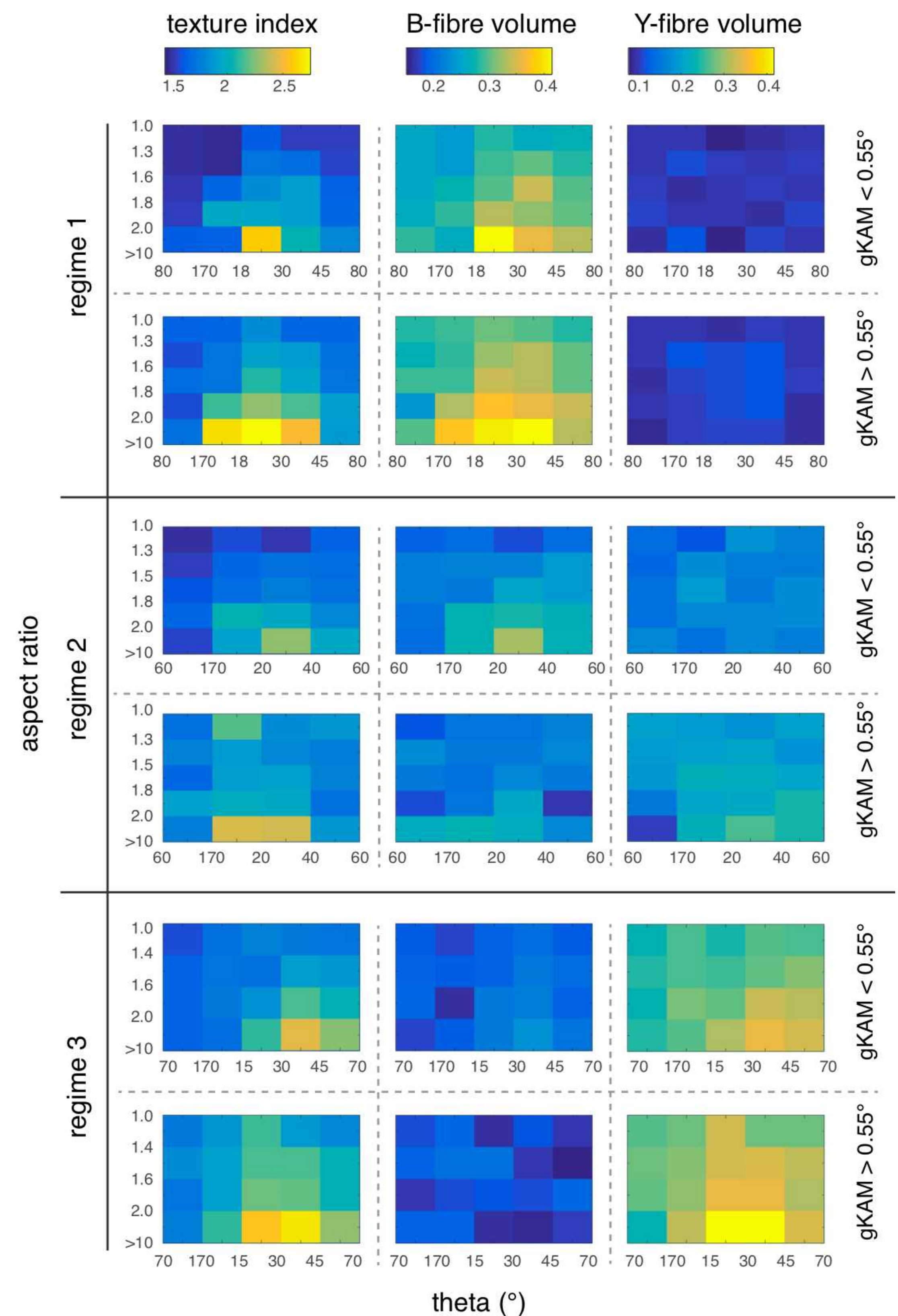
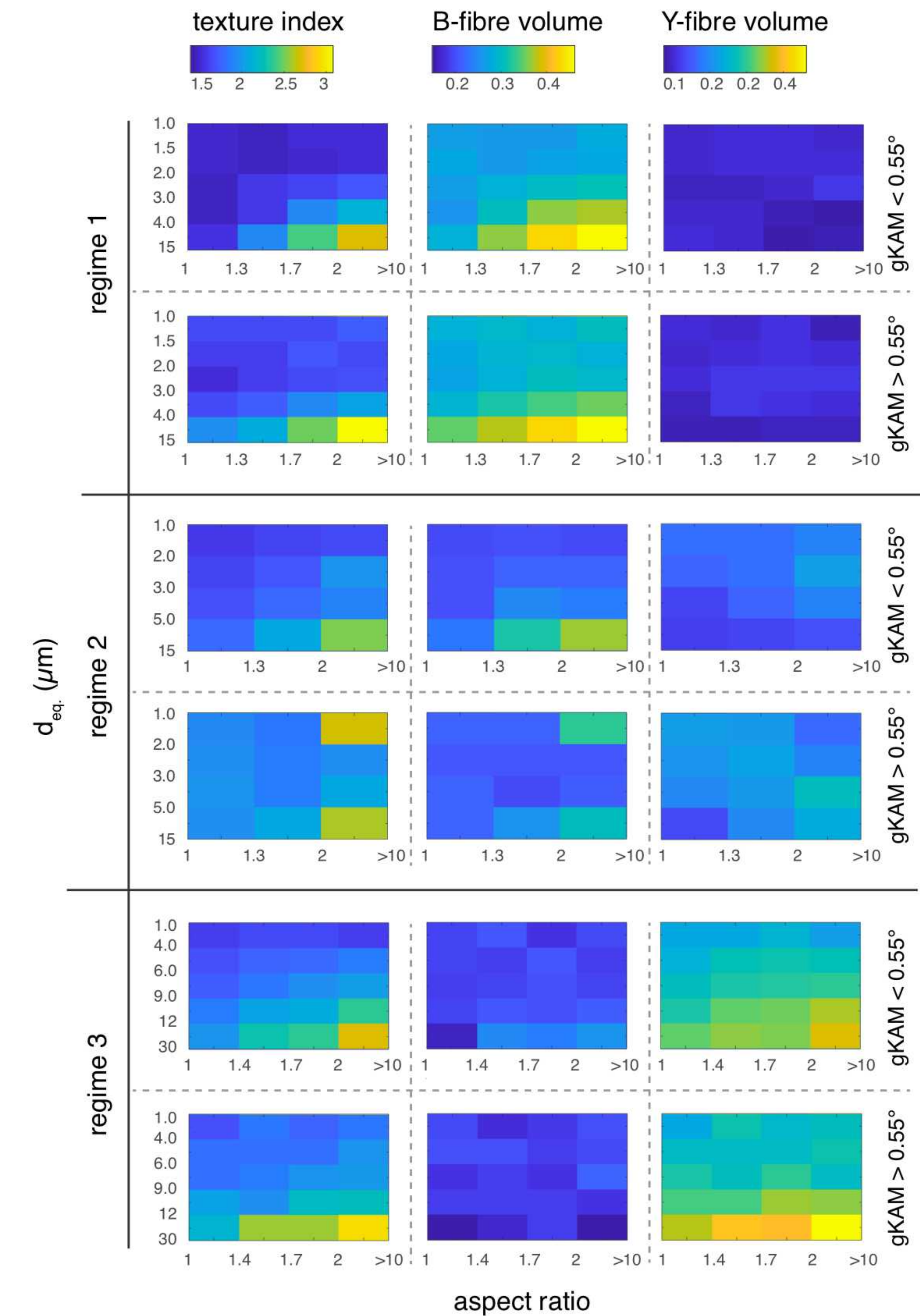


Pole figures for low gKAM - high gKAM populations for grains (1 modal orientation per grain) and all the corresponding orientations of grains lower and higher than the median of all gKAMs in each sample and within a grain size range of 1-25 μm . Contours at 1 times uniform.



-> high intragranular deformation intensity, higher girdle/center component

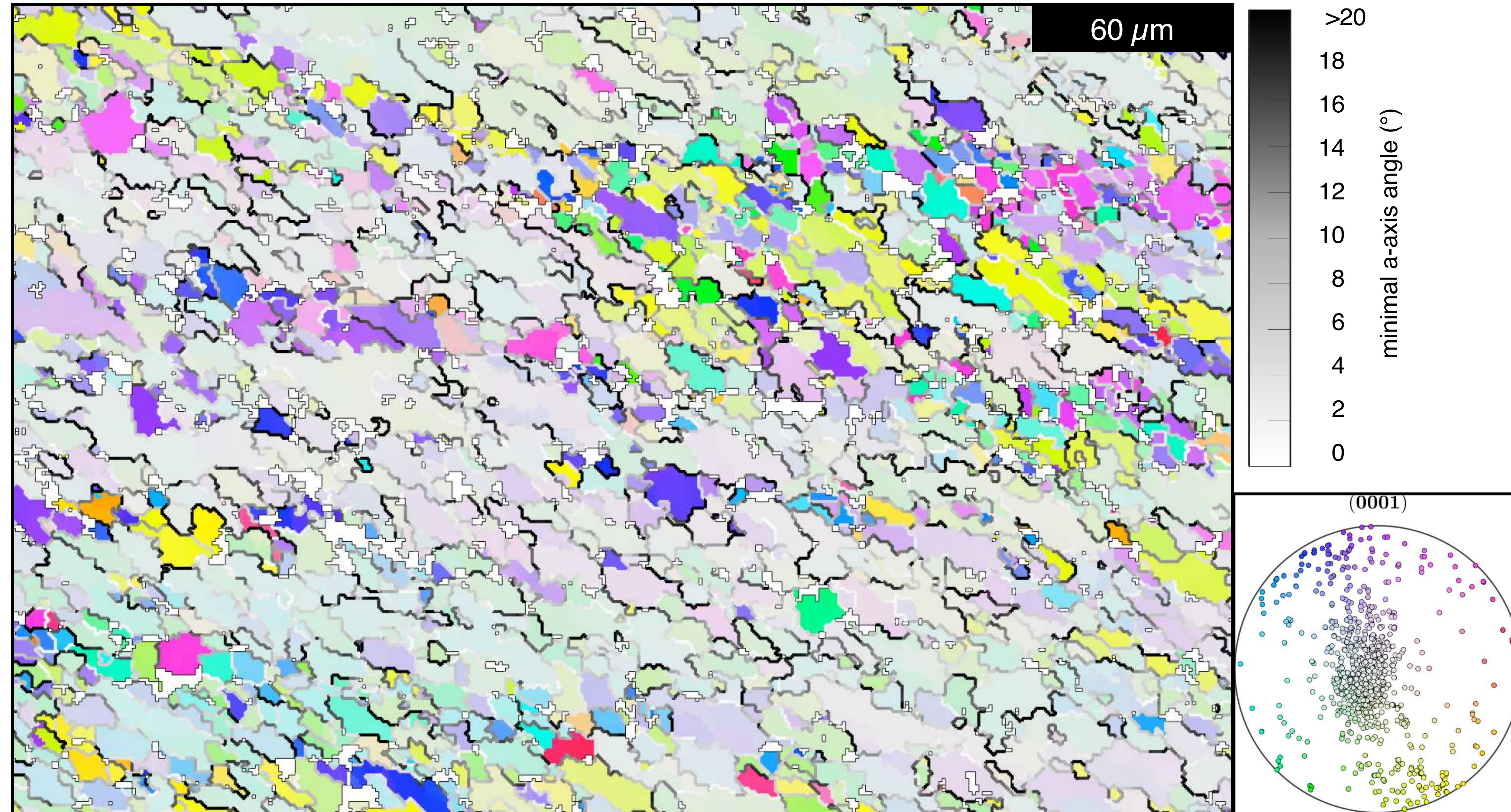
C-axis pole figures for grains (1 modal orientation per grain) and all the corresponding orientations of grains lower than the 0.2 quantile and higher than the 0.8 quantile of all gKAMs in each sample and within a grain size range of 1-12 μm (regime 1,2) and 1-25 μm (regime 3).



Quantitative comparison of texture index and volumes of texture components using color maps for texture index, B-fibre and Y-fibre volume in aspect ratio - grain size and grain long axis trend - aspect ratio space. Each parameter matrix exists for a low and a high gKAM population. Fibre volumes are calculated as the volume of the odf within a c-axis fibre within a radius of 30° directed towards the peripheral (B-fibre) and the central c-axis maximum (Y-fibre) known from the pole figures. Absolute values within each column are quantitatively comparable.

-> high intragranular deformation intensity or high grain lengthening and alignment, higher texture and more center (Y-fibre) component

c-axis map and a-axis angle across grains boundaries



Slip direction transparency of grain boundaries and low angle boundaries: EBSD map of a regime 3 sample with c-axis color-coding, mainly showing grains of a Y-domain (pastel colors) with a few grains with peripheral c-axis directions (saturated colors) and a grain boundary color coding as a function of the minimal angle between a-axes (ignoring polarity) of adjacent measurement points across a grain boundary. Since the a-direction is most likely the dominant slip direction, white boundaries are transparent to dislocation glide on a in case adjacent glide planes are favorably oriented as well. Note that within the Y-domain large angles are quite frequent and gradual a-axis misorientations can be observed. Additionally, noteworthy is the occurrence of <a>-transparent boundaries between grains of the Y-domain and grain with less inclined or peripheral c-axes. Upper hemisphere, equal area c-axis polefigure of 1000 randomly selected orientations out of the displayed area. Color coding identical to map.

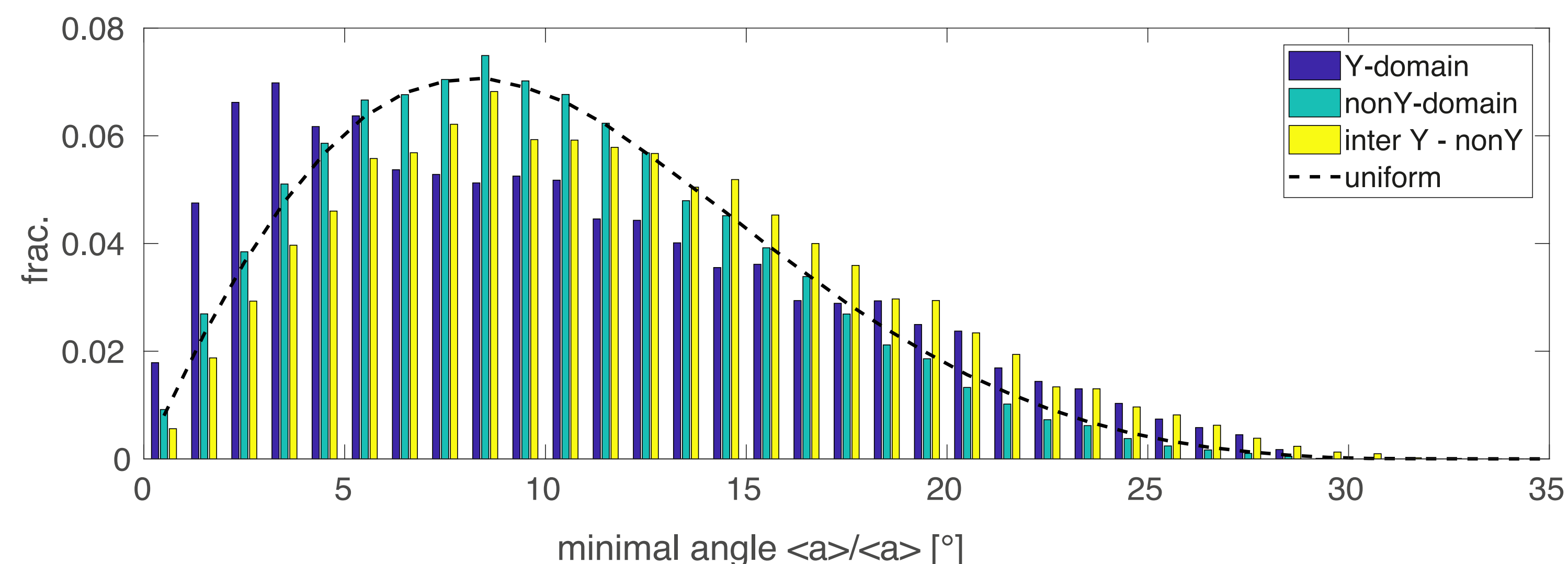
-> (mis-)alignment of <a> due to crystal plasticity
 -> internal rotation of grains in y-domains (requires gbs)

toc

<< >>

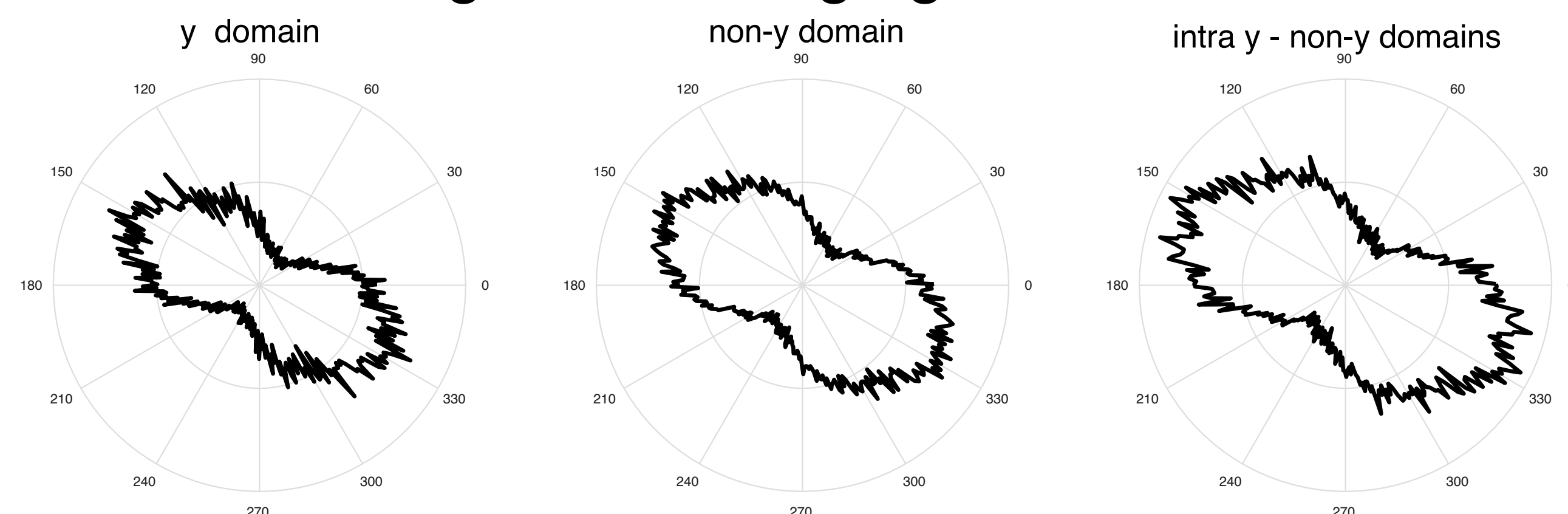
Inter $\langle a \rangle / \langle a \rangle$ angle distribution for different texture domains

$\langle a \rangle$ - transparency - (2)



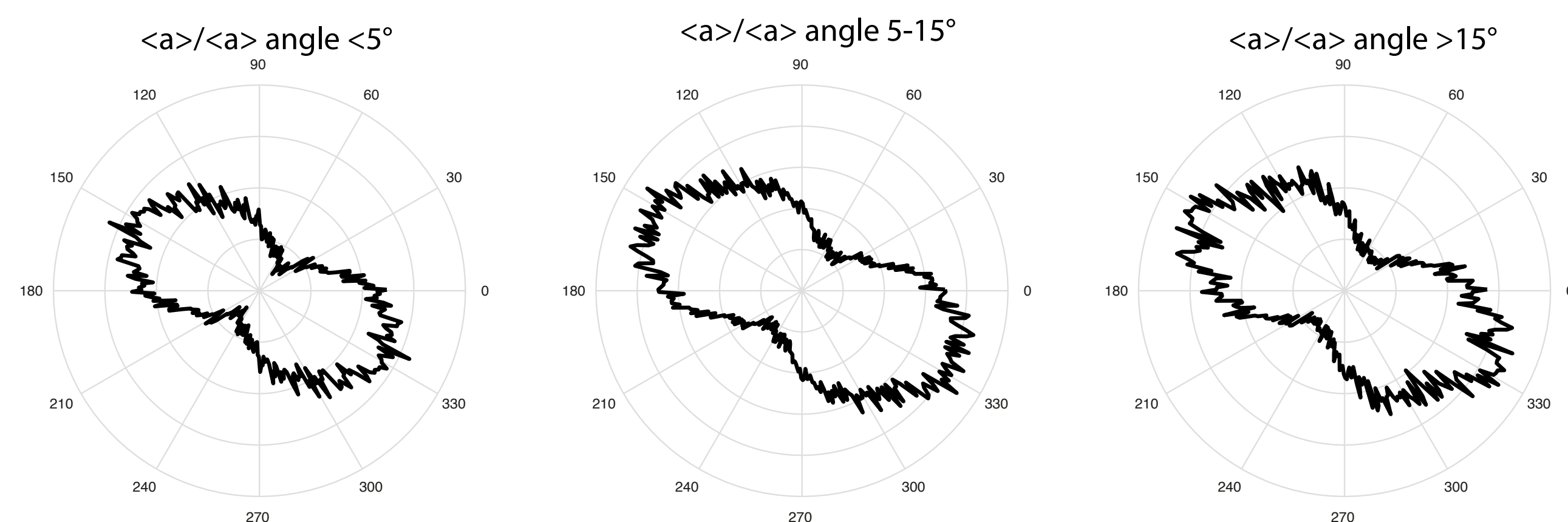
Distribution of angles between adjacent $\langle a \rangle$ directions across a grain boundaries in regime 3. Histogram for grains within the Y-domains (contained within a 40° cone for the c-axis directions), outside this domain and for interdomainal boundaries. Stippled line shows the distribution expected for a uniformly textured aggregate.

surface ODF of grains belonging to different texture domains



The surface ODF of boundaries in the y-domain is closest to orthorhombic while the surface ODF of boundaries between domains shows the most monoclinic fabric which may indicate that those boundaries in the y domain are most related to a strain fabric.

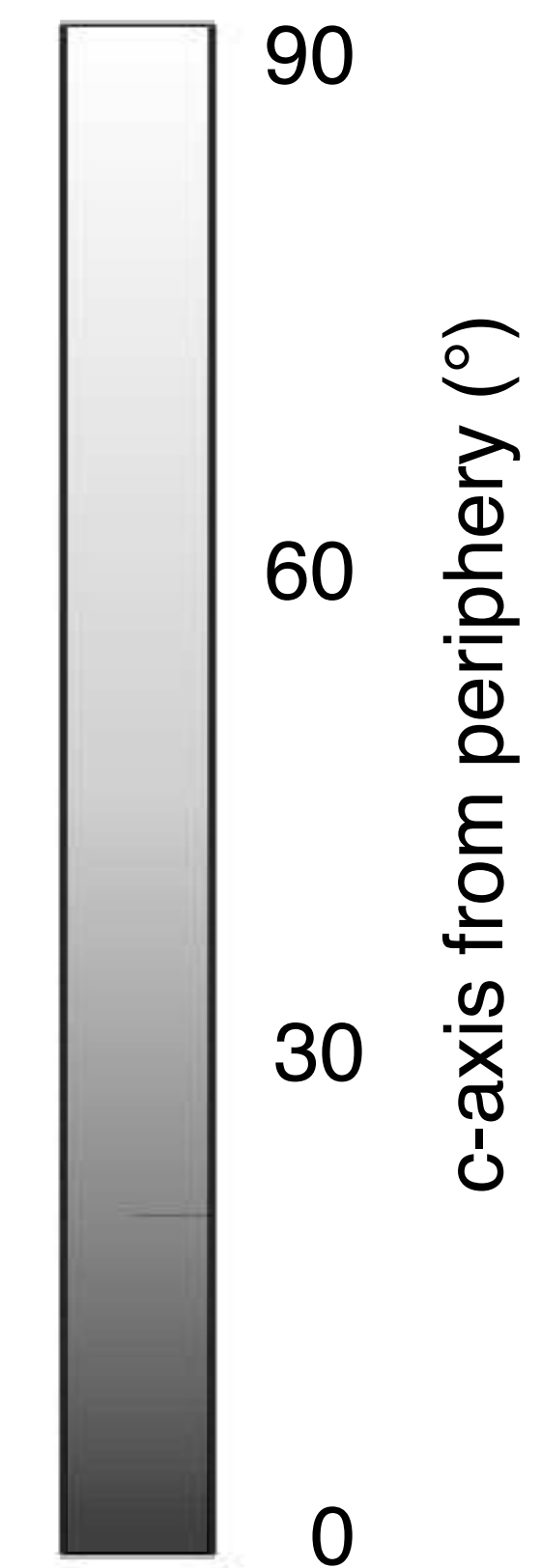
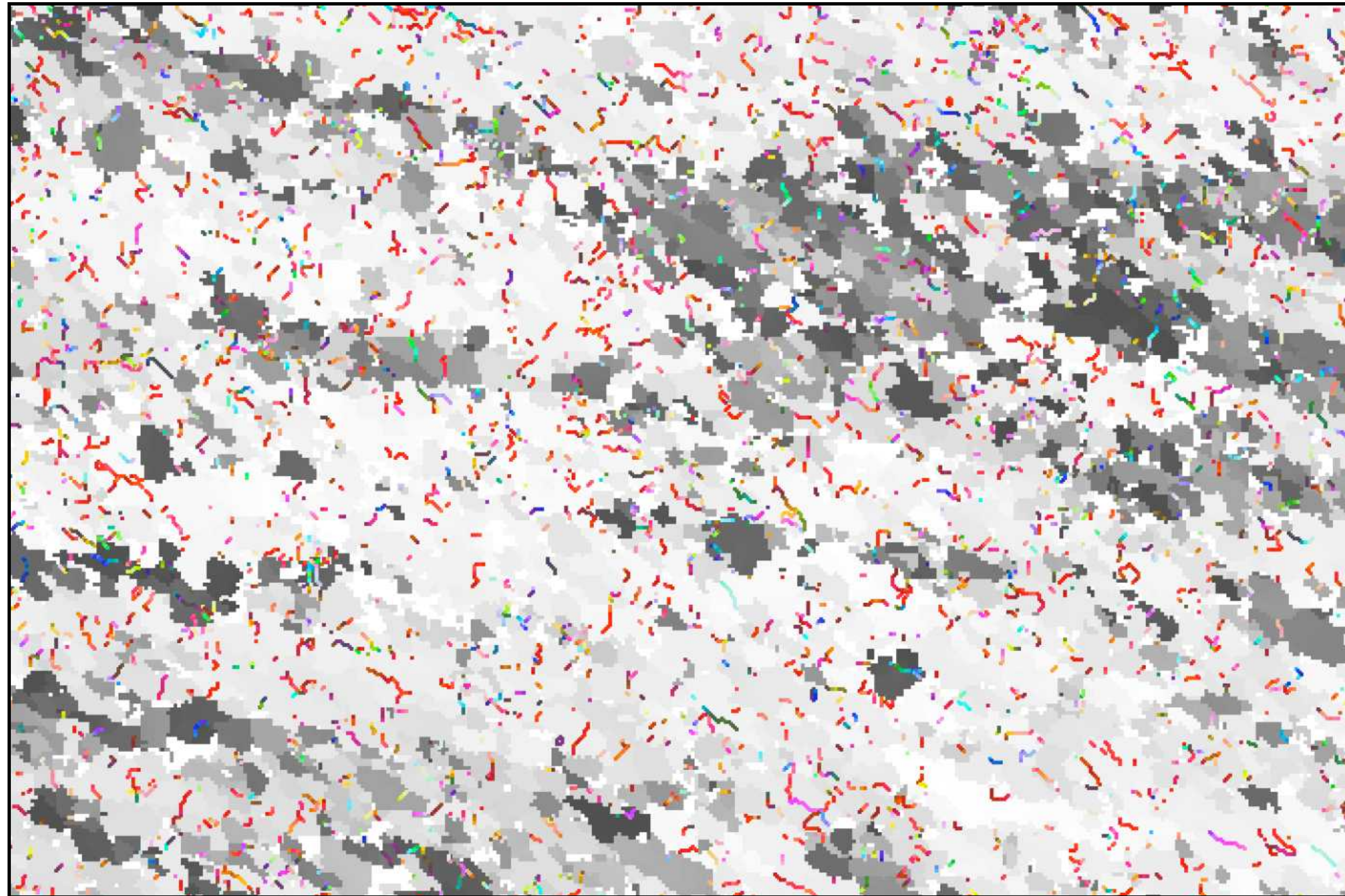
surface ODF of grains with low/high $\langle a \rangle$ -transparency



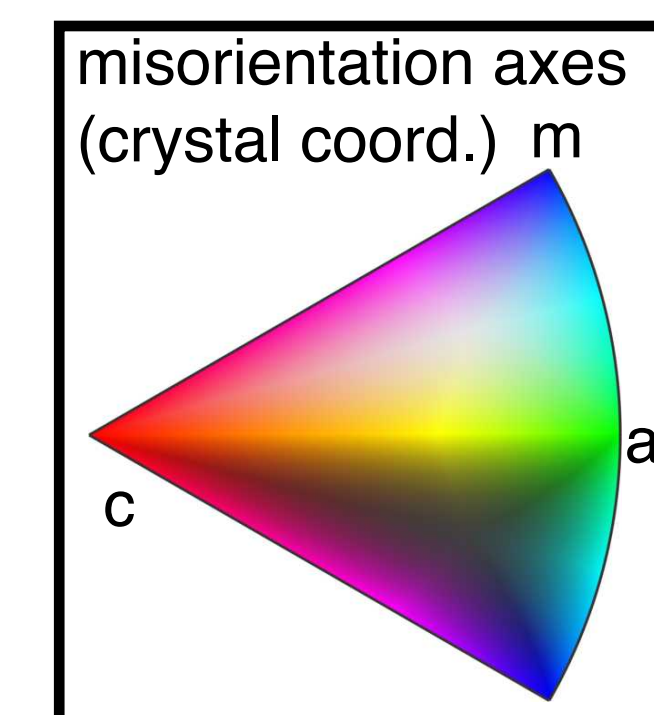
The surface ODF of obtained from boundaries which have a very low $\langle a \rangle / \langle a \rangle$ angle are closest to an orthorhombic fabric.

c-axis inclination and misorientation axes of low angle boundaries (2-9°)

Misorientation analysis (1)

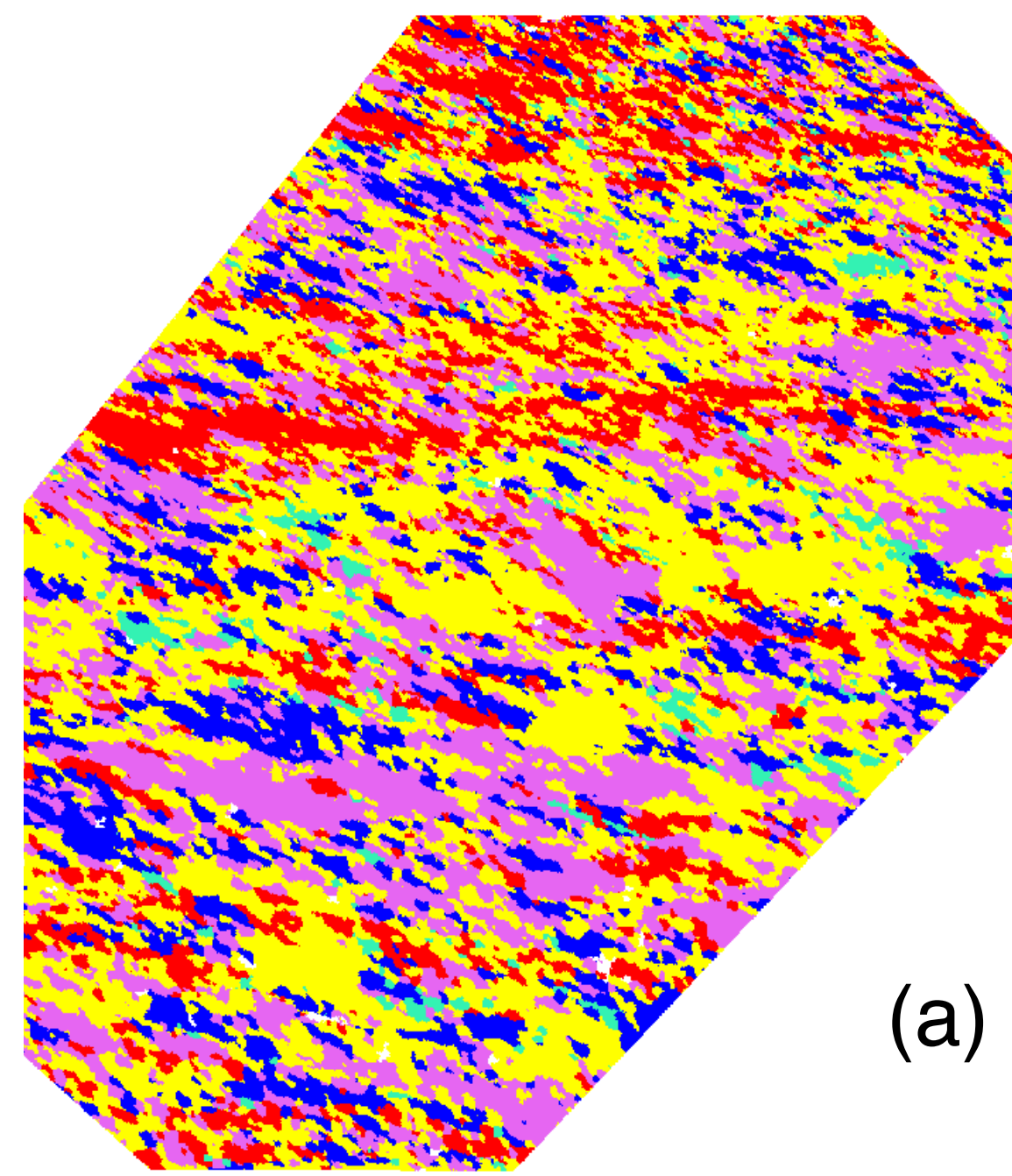


EBSD map with grey value displaying the angular distance of the c-axis from the periphery (inverse inclination) and low angle boundaries (2-9° misorientation angle) color-coded for the misorientation axis in crystal coordinates. For clarity, grain boundaries are not shown.

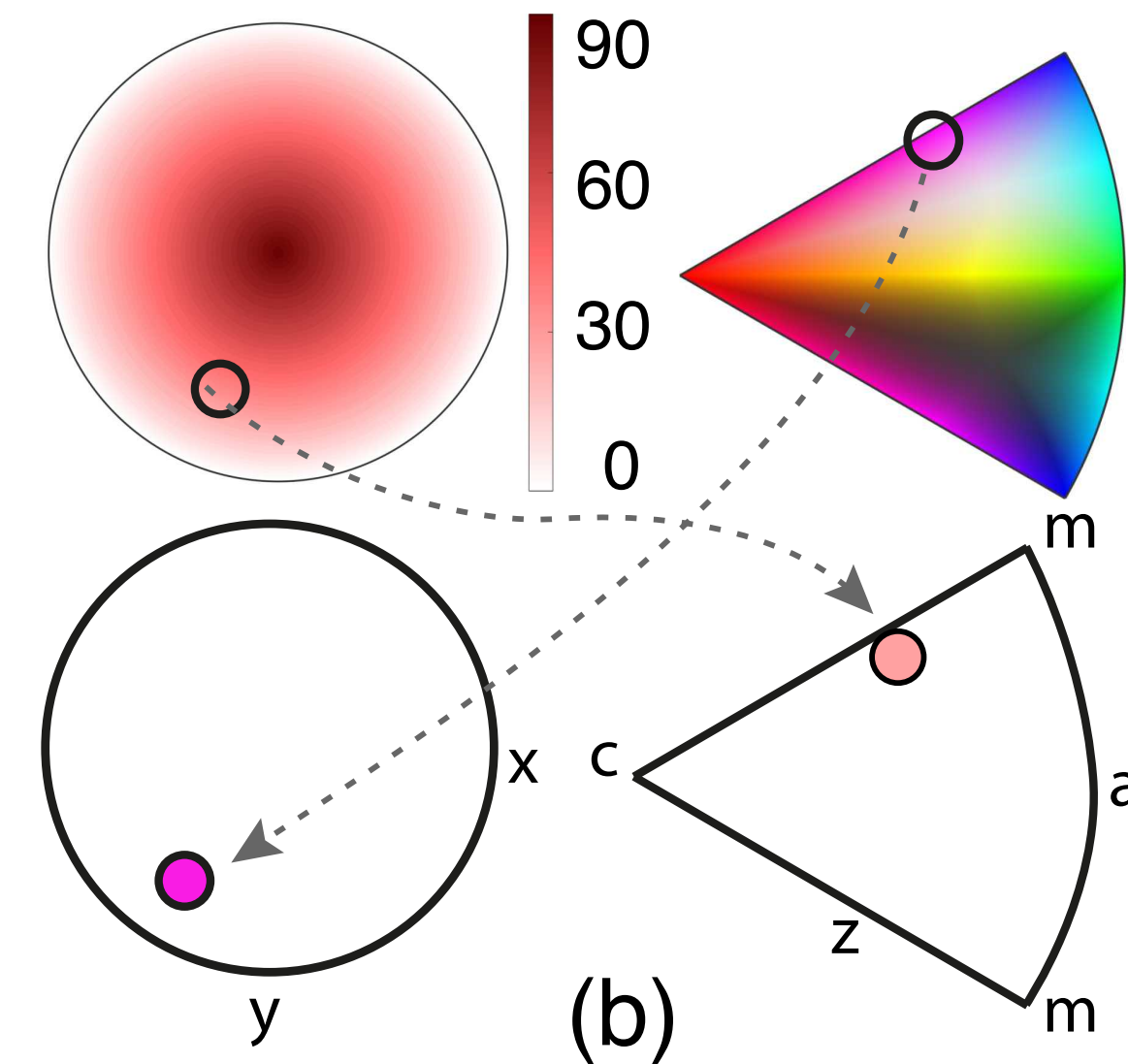
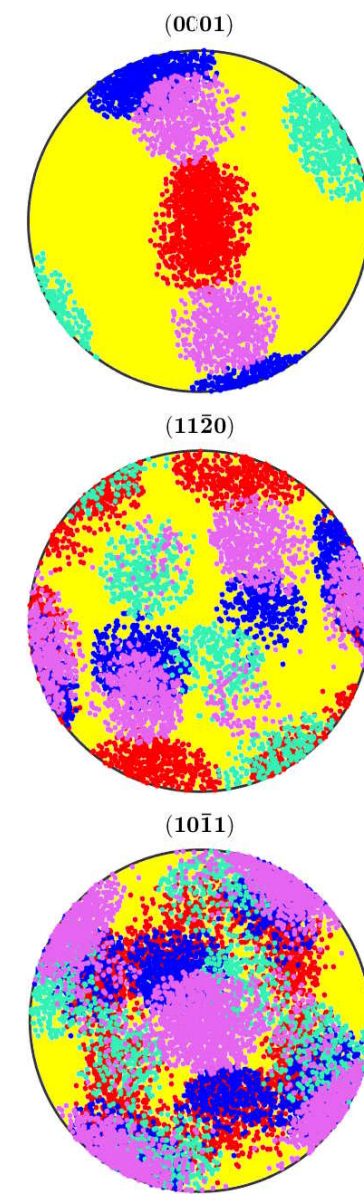


-> LAB with dominantly misor. axes close to [c in y-domain]

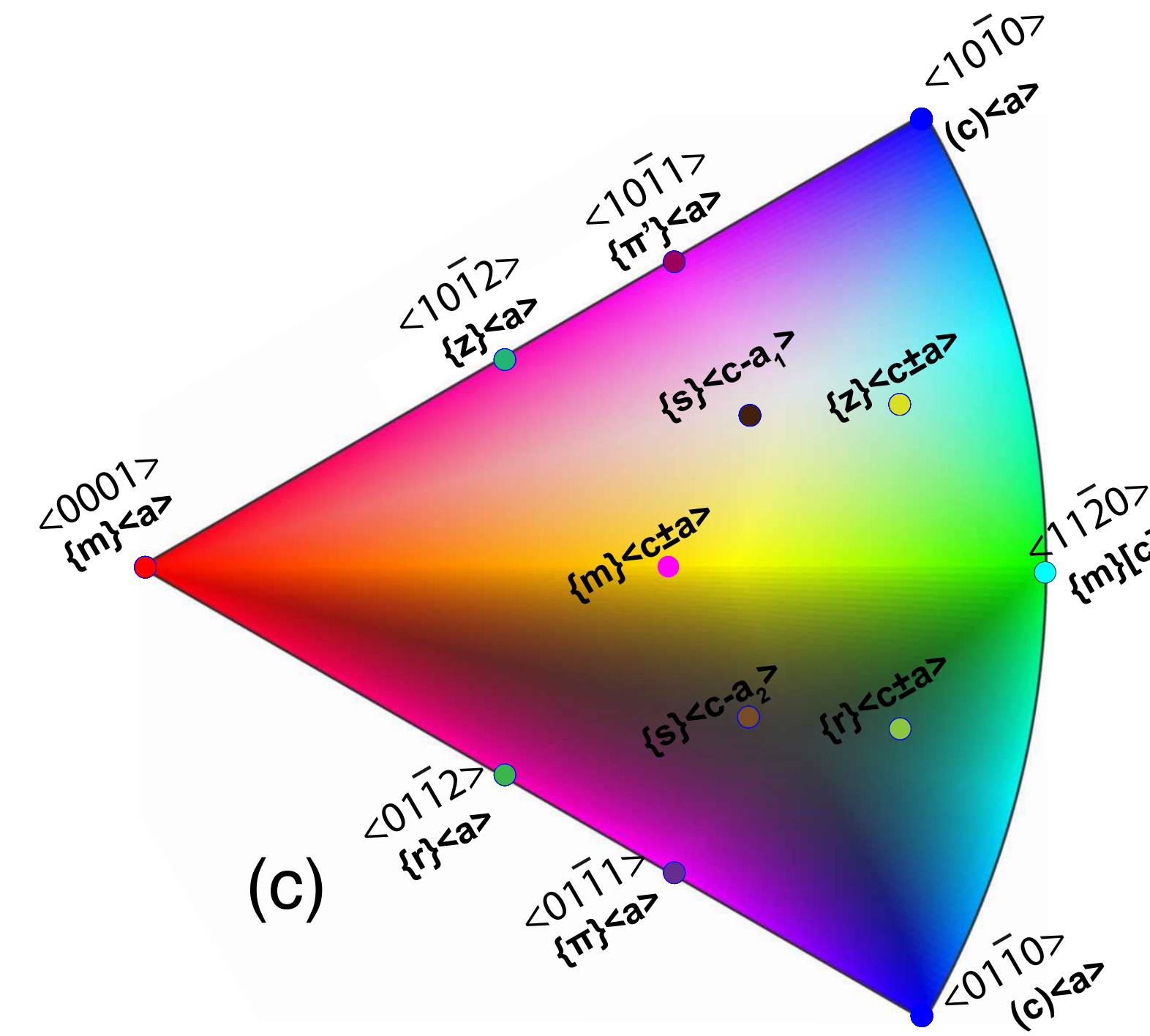
Misorientation analysis (2)



(a)



(b)



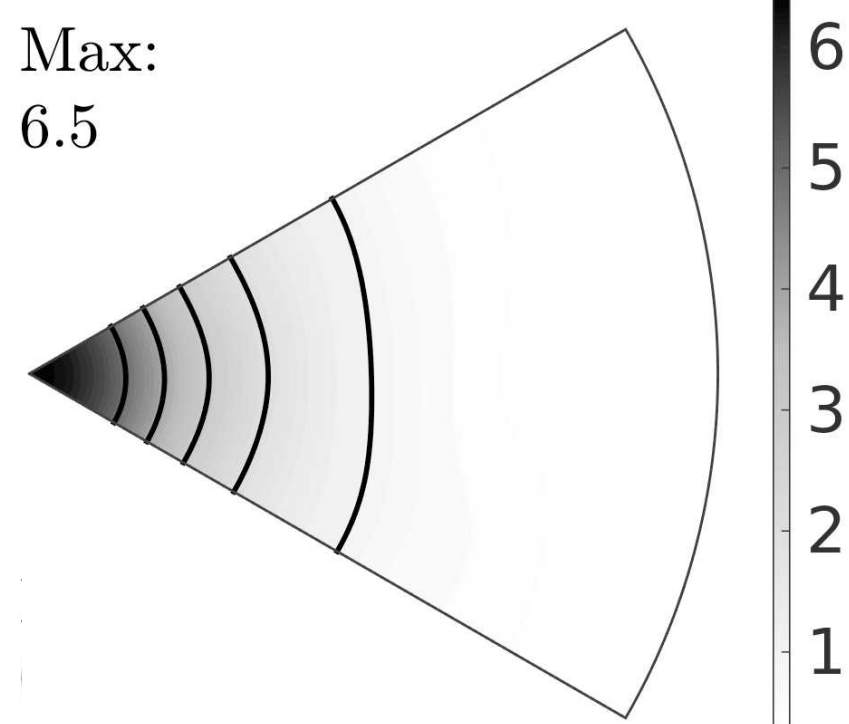
(c)

Misorientation axes for texture domains: (a) Texture domains determined within an angle of 25° around the orientation modes color-coded in red (Y-grains), blue (B-grains), pink (R-grains) and green (σ-grains). All other other orientations from grains not with that range are yellow. Pole figures for a,m,r showing a subset of poles. Color-coding of directions (b) is such that misorientation axes in crystal coordinates are color-coded by the inclination of the same axis in specimen coordinates. Analogously, misorientation axes in specimen coordinates are color-coded to the corresponding direction in crystal coordinates. (c) Color key used for crystal directions and annotations for rotation axes formed by pure tilt boundaries of indicated slip systems. (d) Misorientation axes obtained for low angle boundaries with misorientation angles of 2-9° from within grains falling into each texture component. Misorientation axes are plotted with density contours at steps of 1 times uniform and as a subset of individual directions.

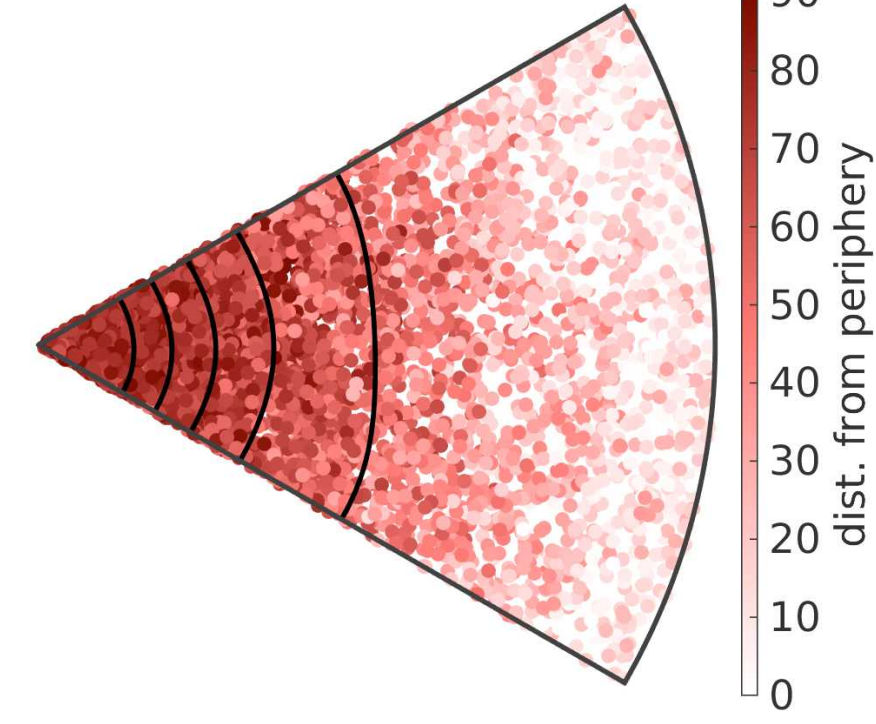
(d)

v-grains

Max:
6.5

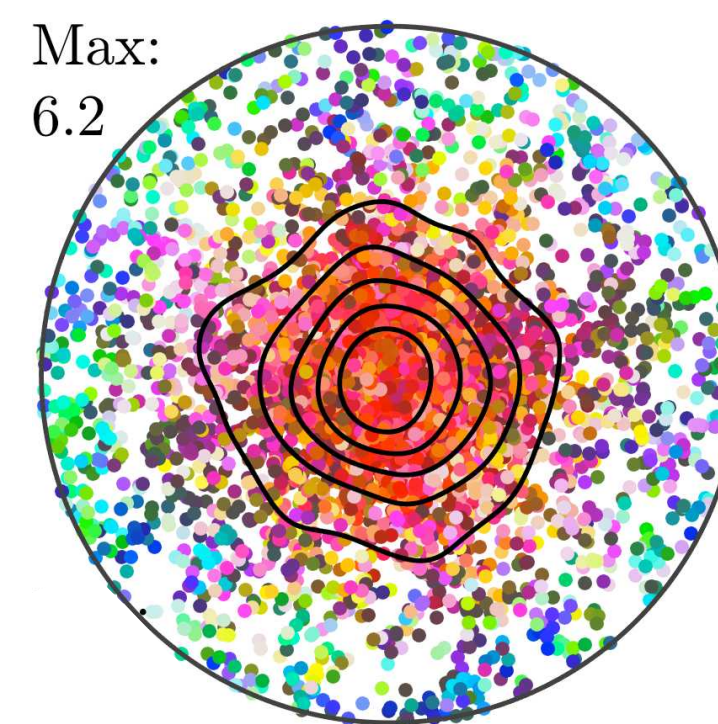


misorientation axes
crystal ref. frame

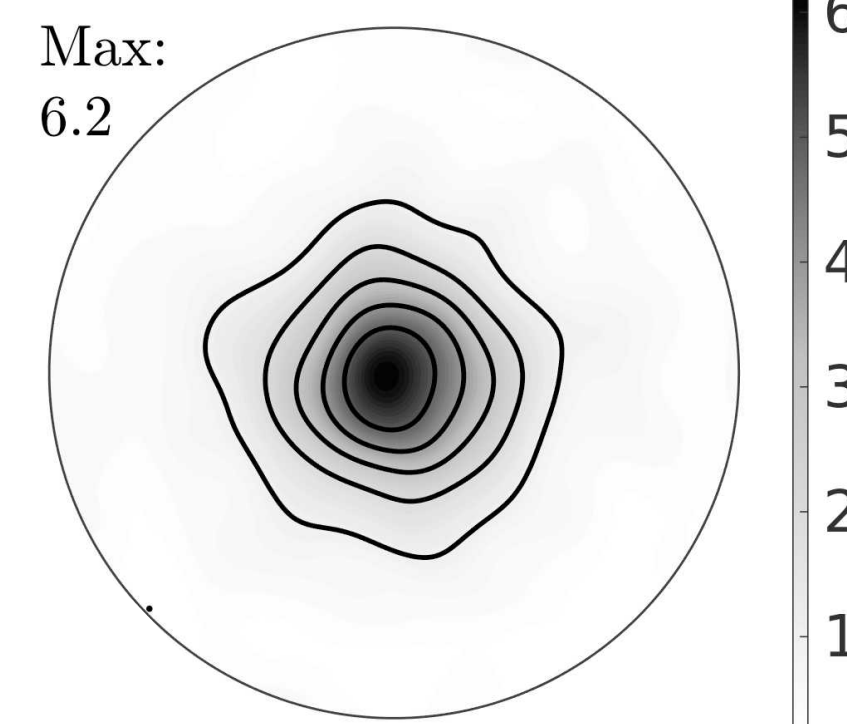


misorientation axes
specimen ref. frame

Max:
6.2



Max:
6.2



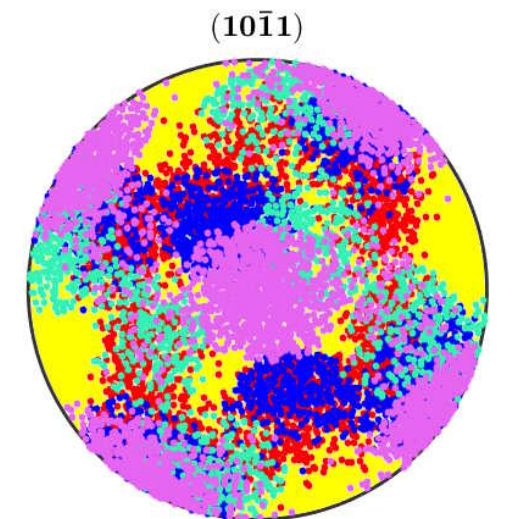
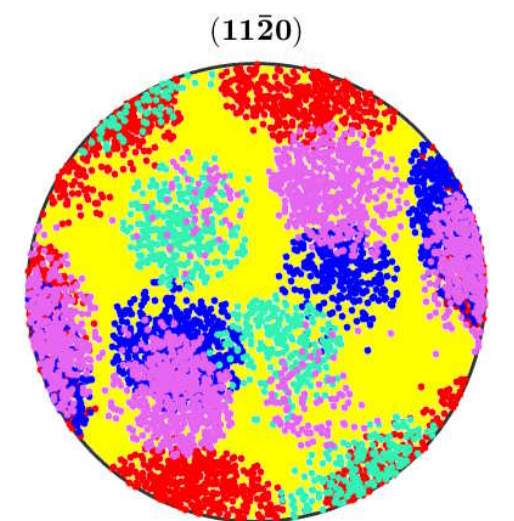
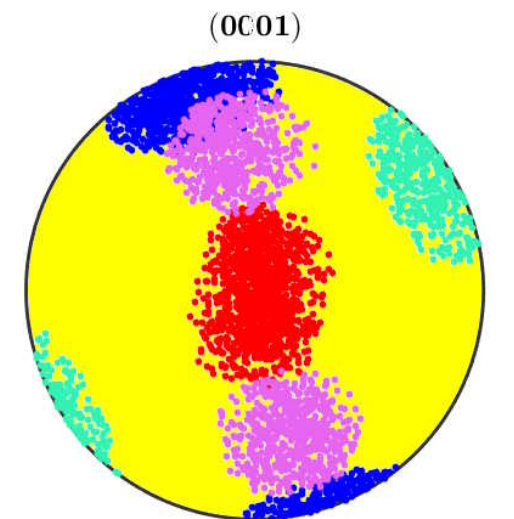
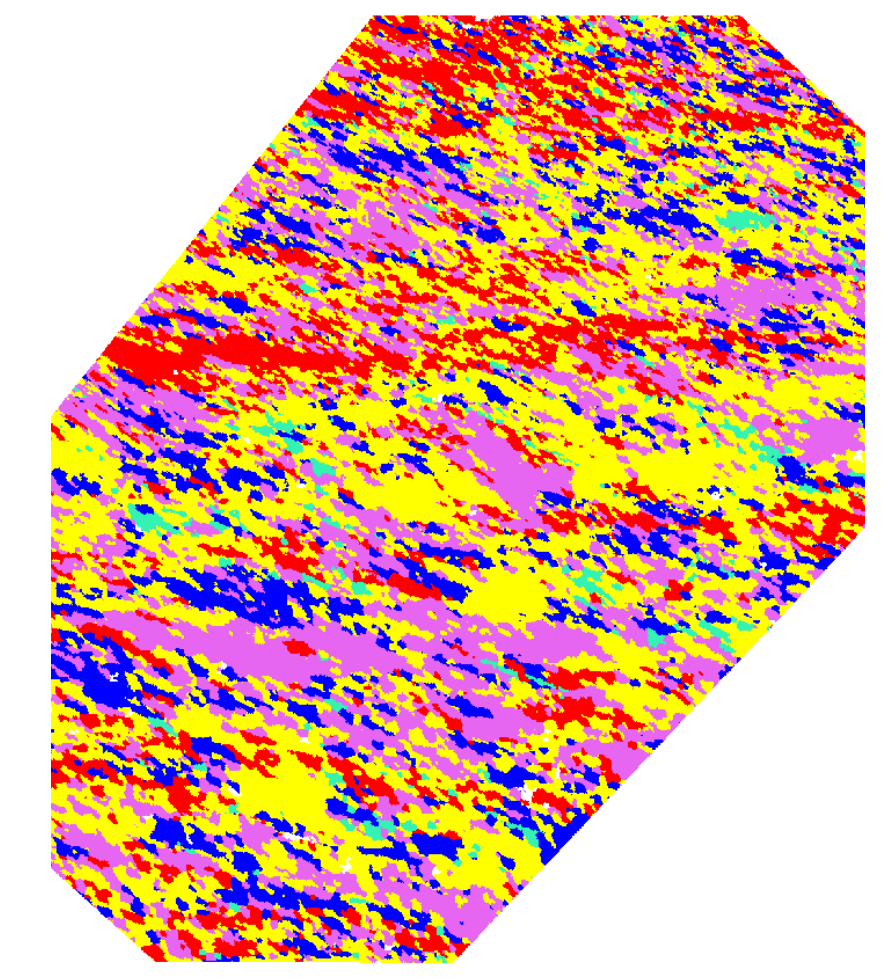
toc

<< >>

regime 2

misorientations axes
crystal ref. frame

misorientation axes
specimen ref. frame

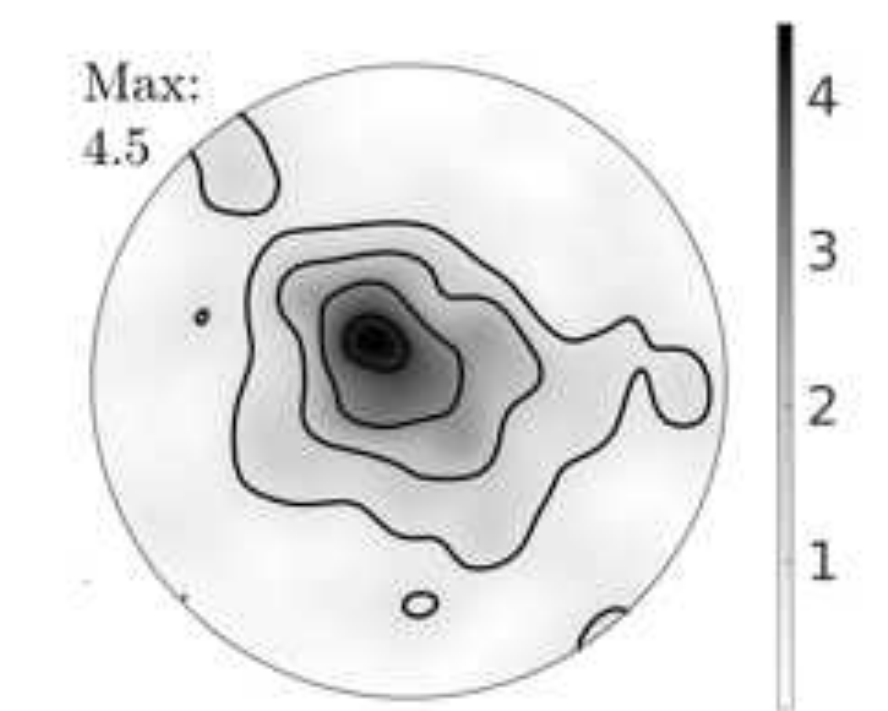
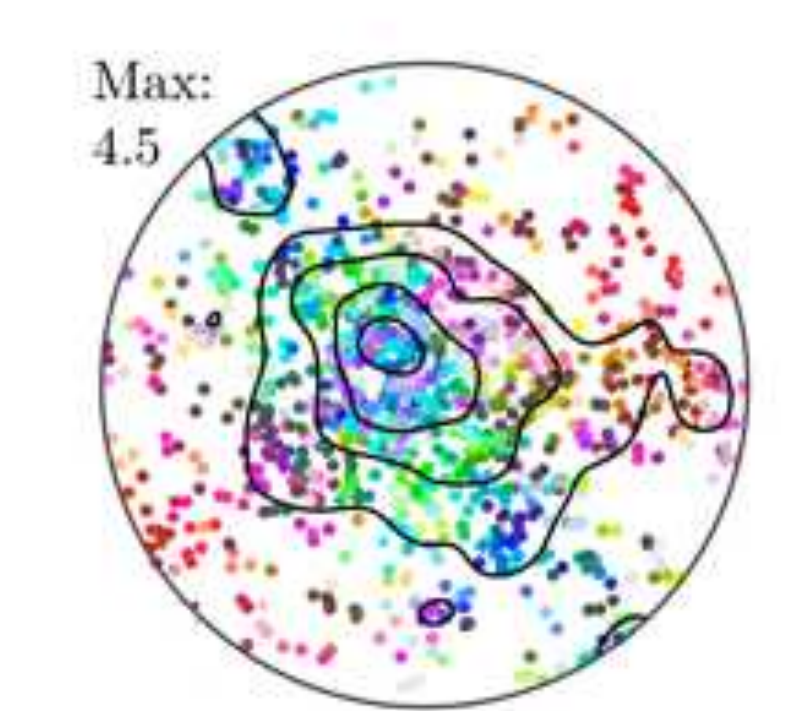
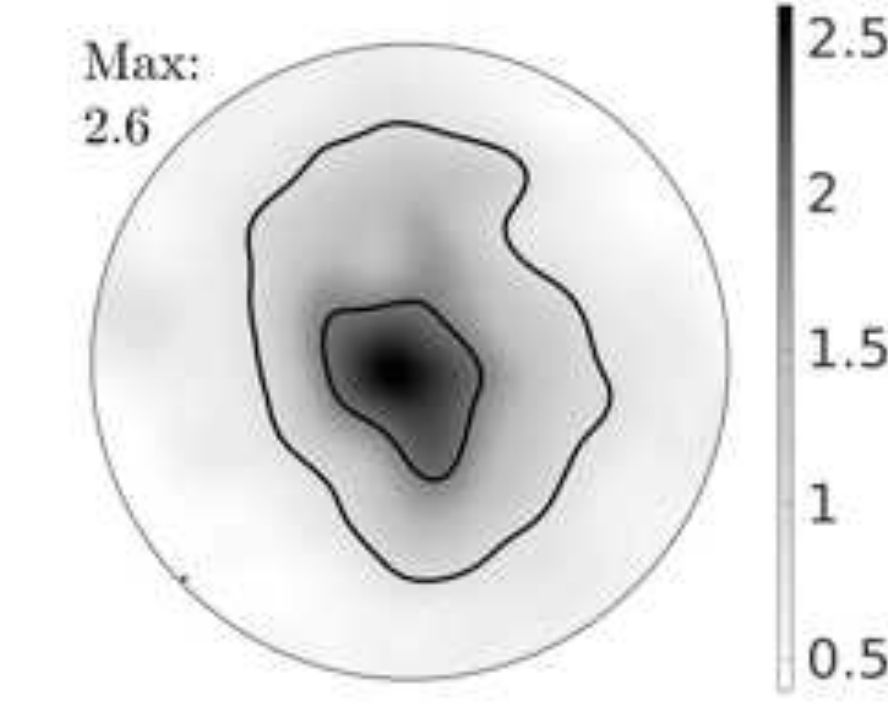
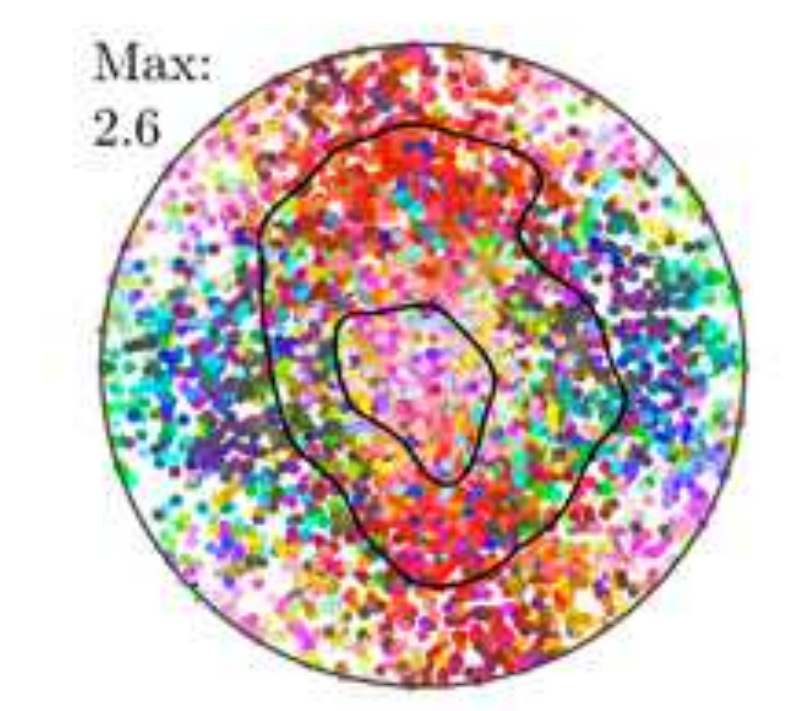
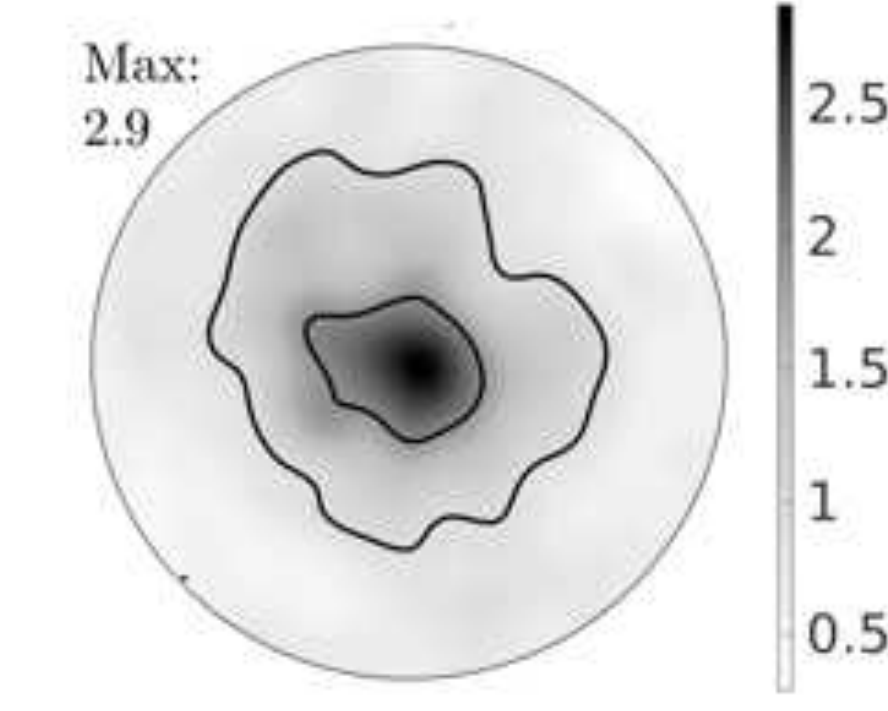
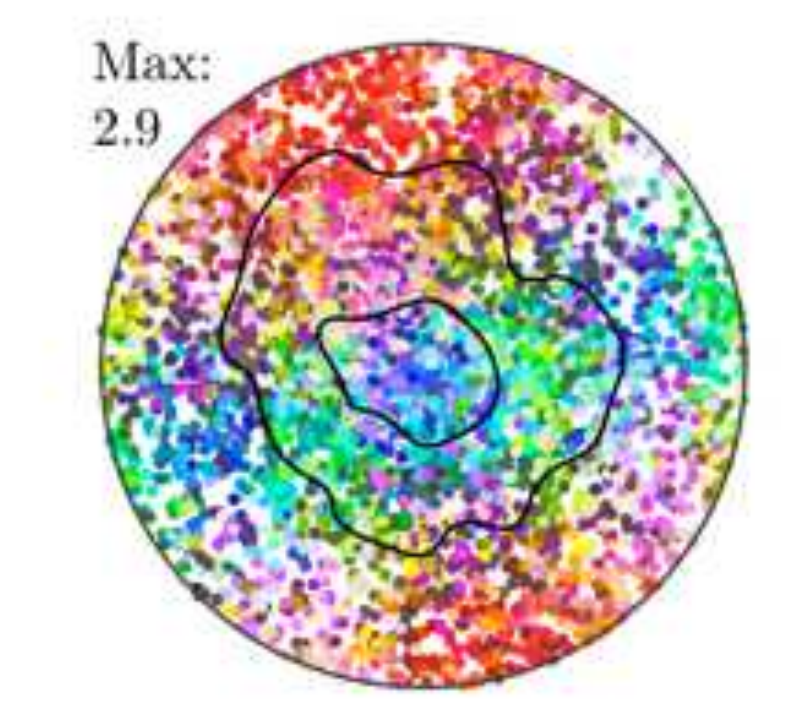
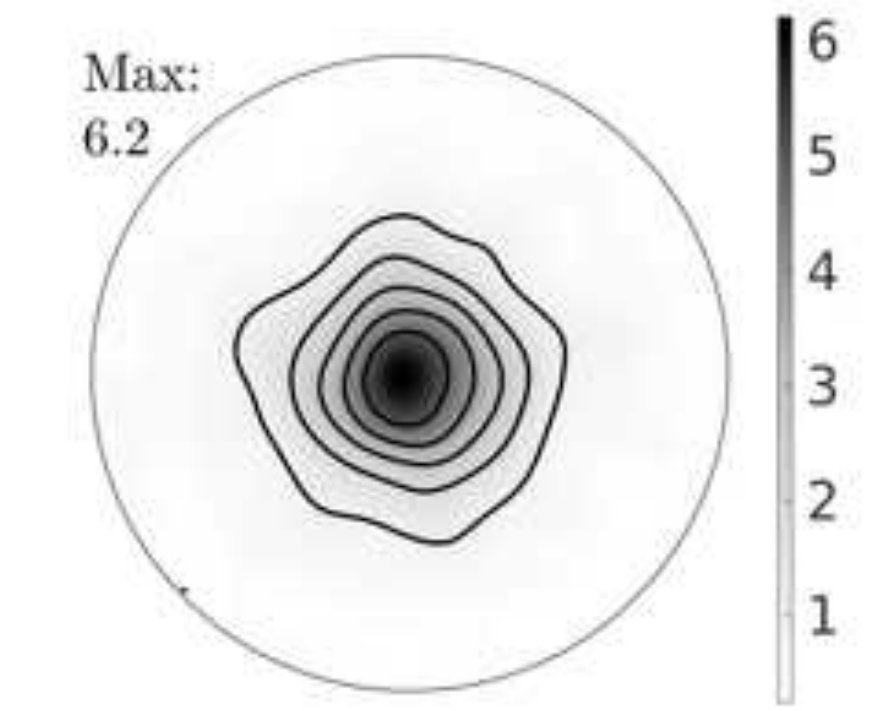
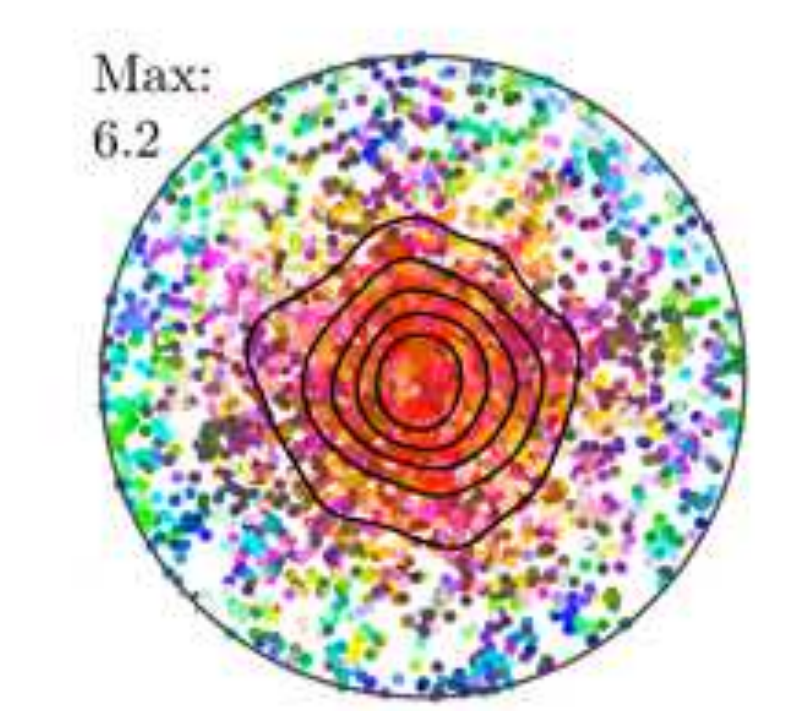
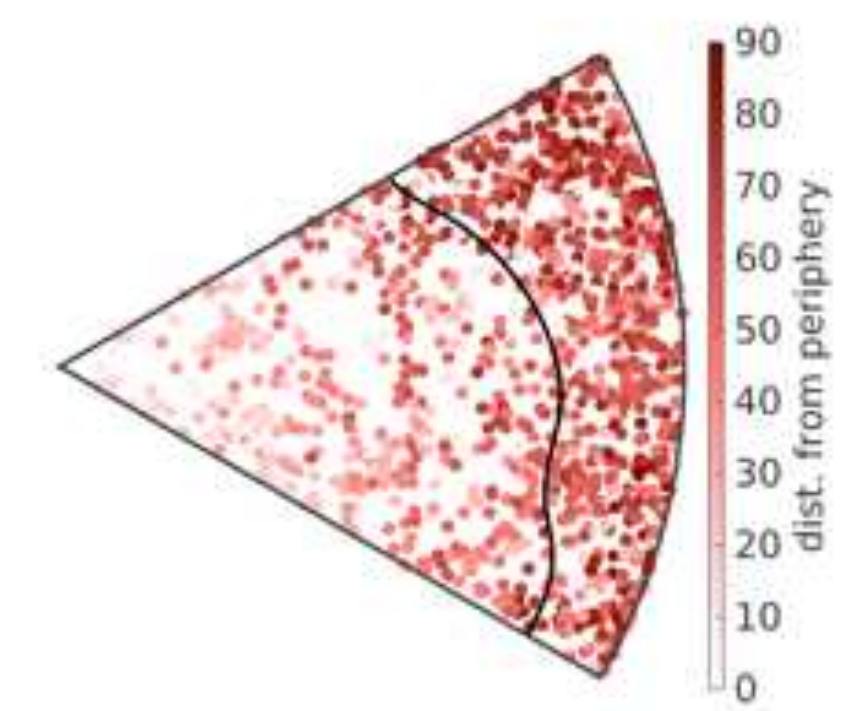
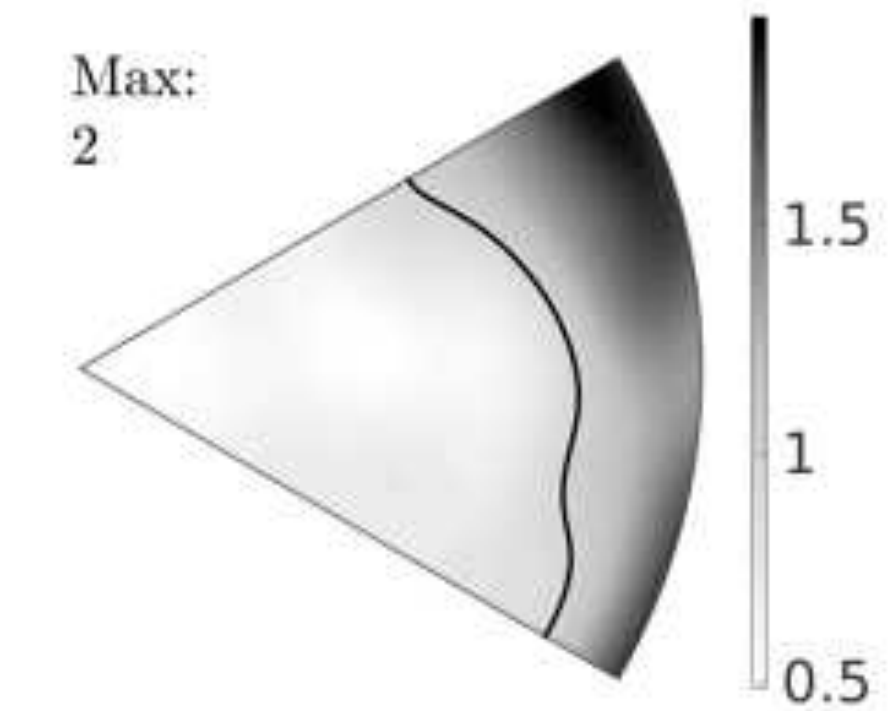
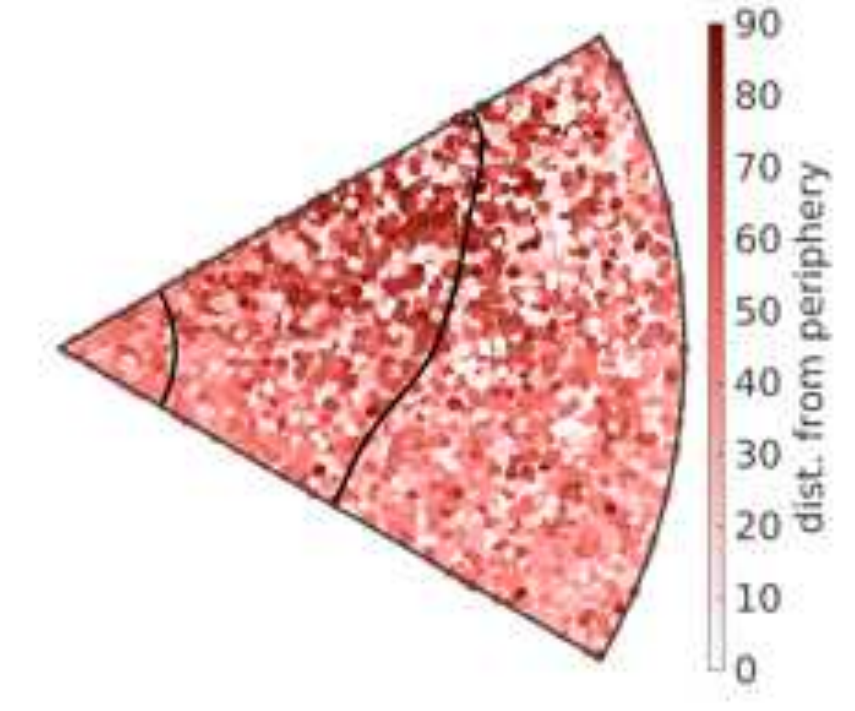
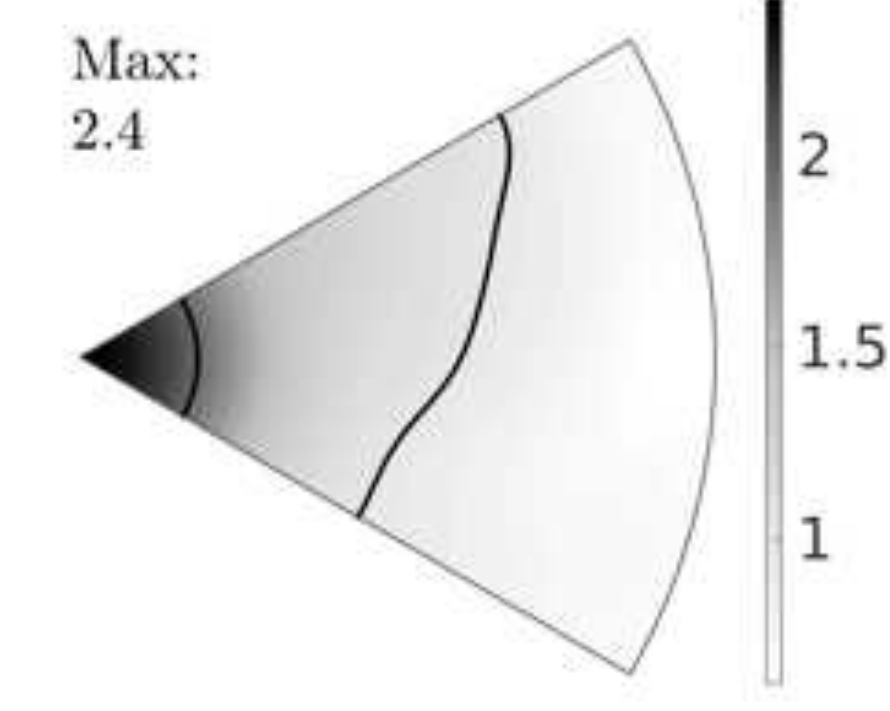
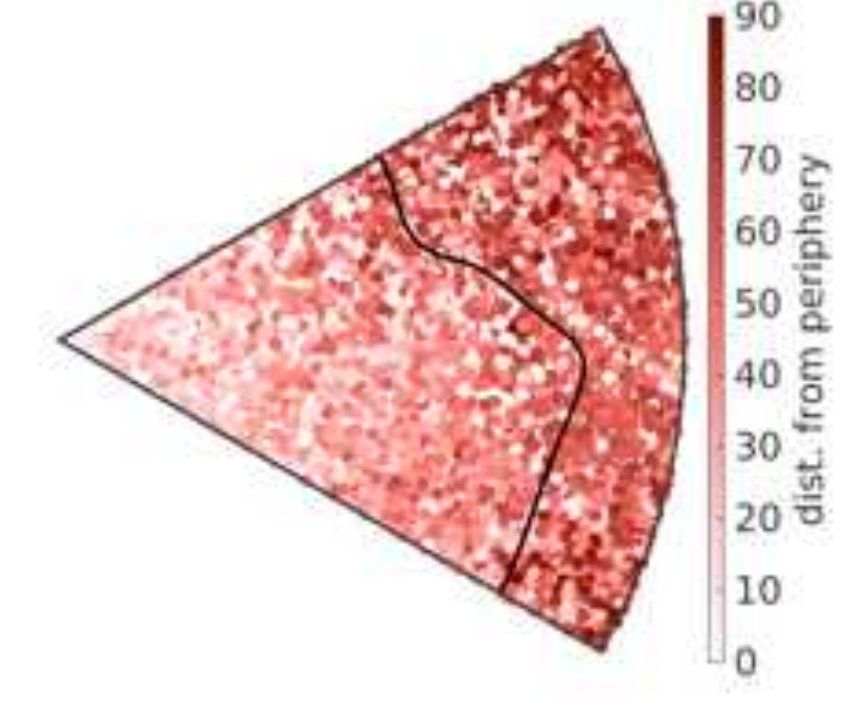
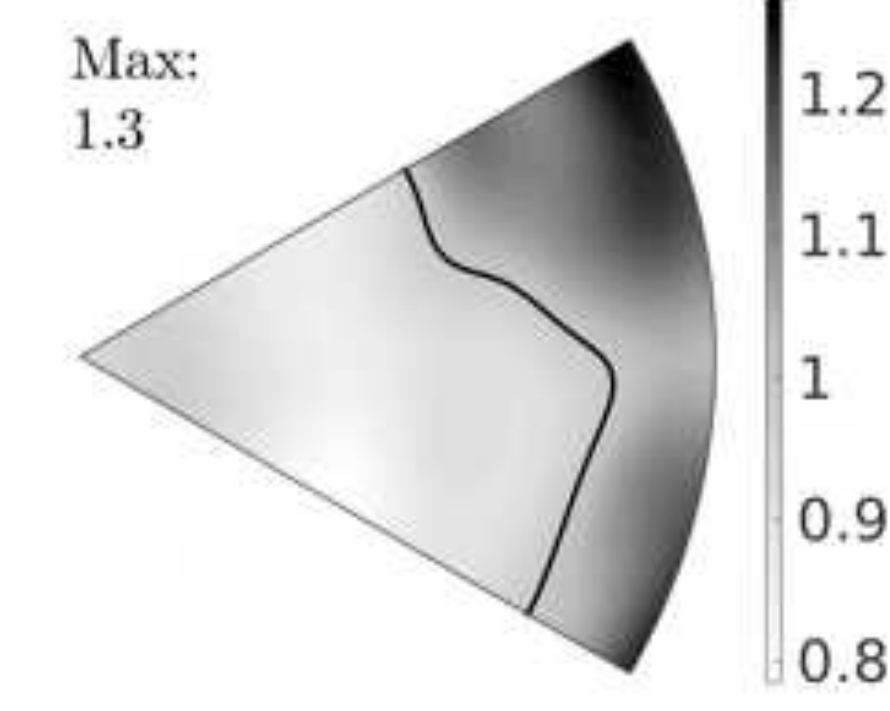
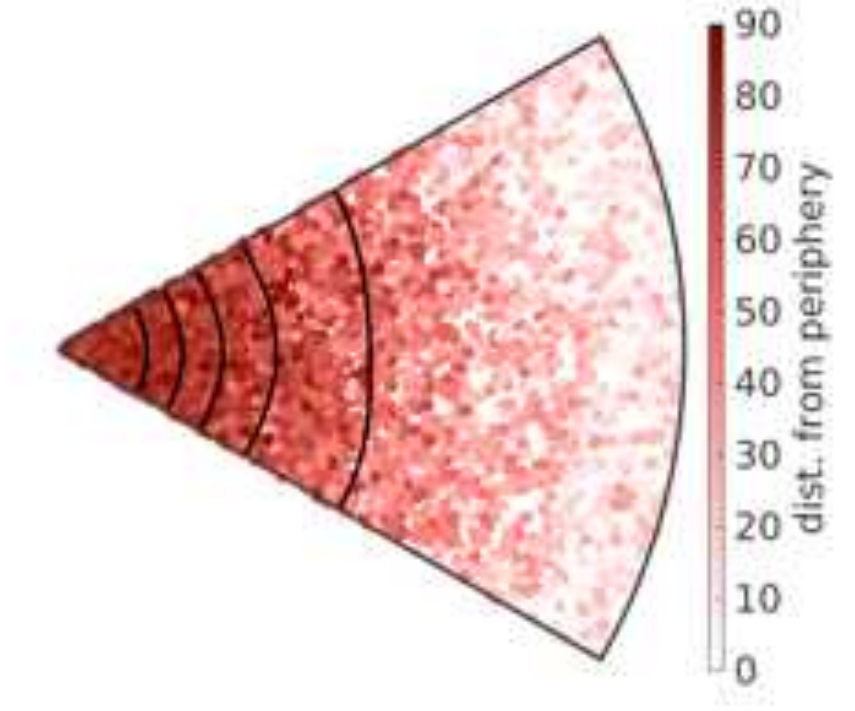
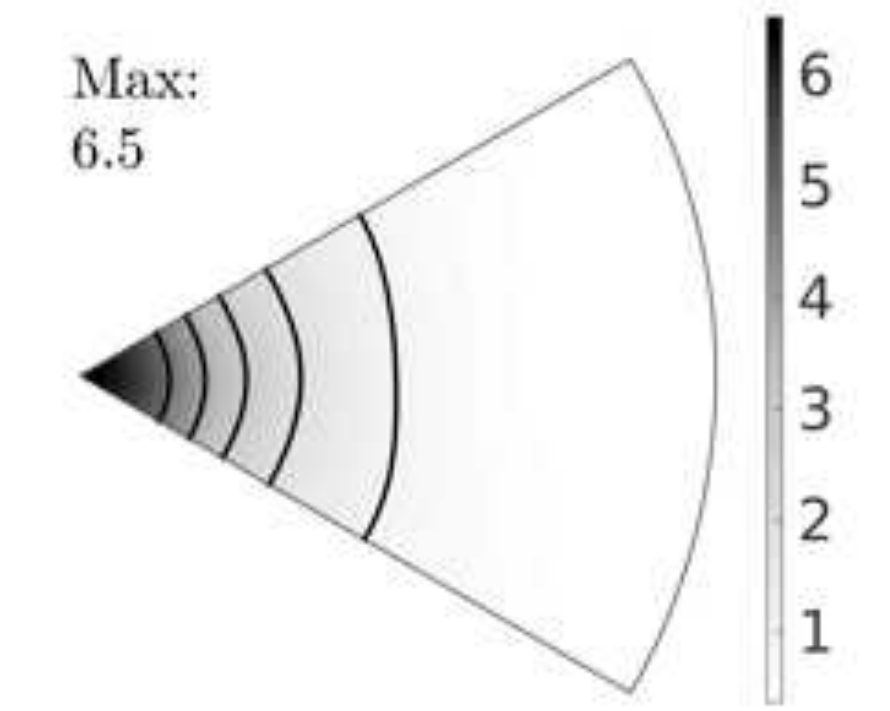


y-grains

b-grains

r-grains

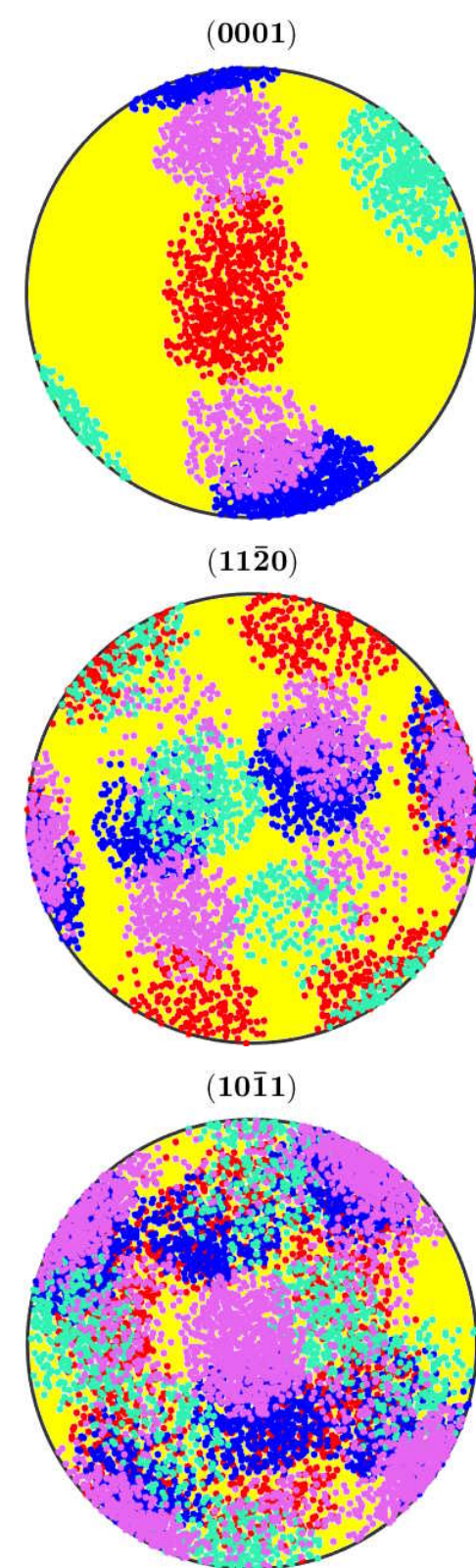
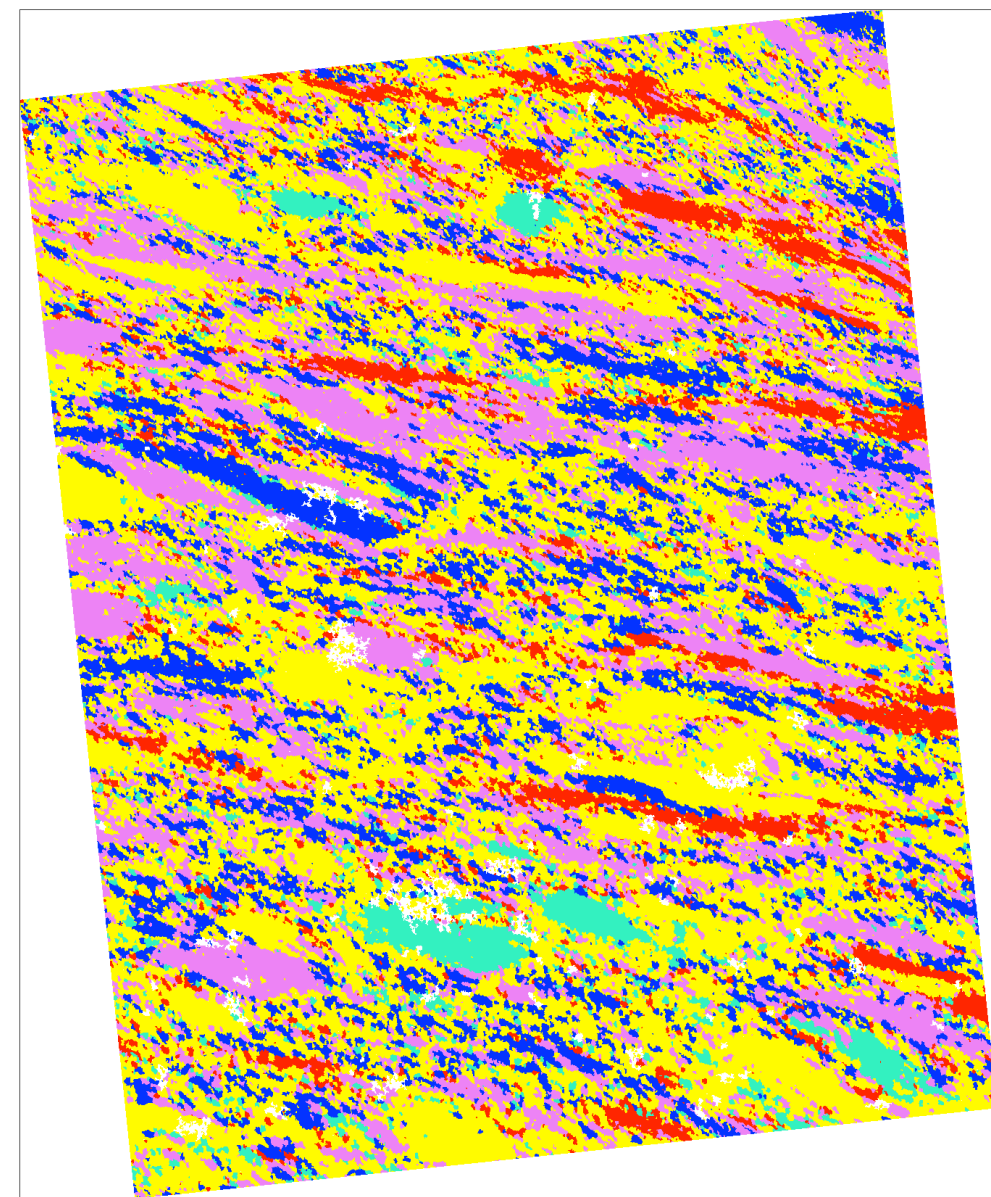
σ-grains



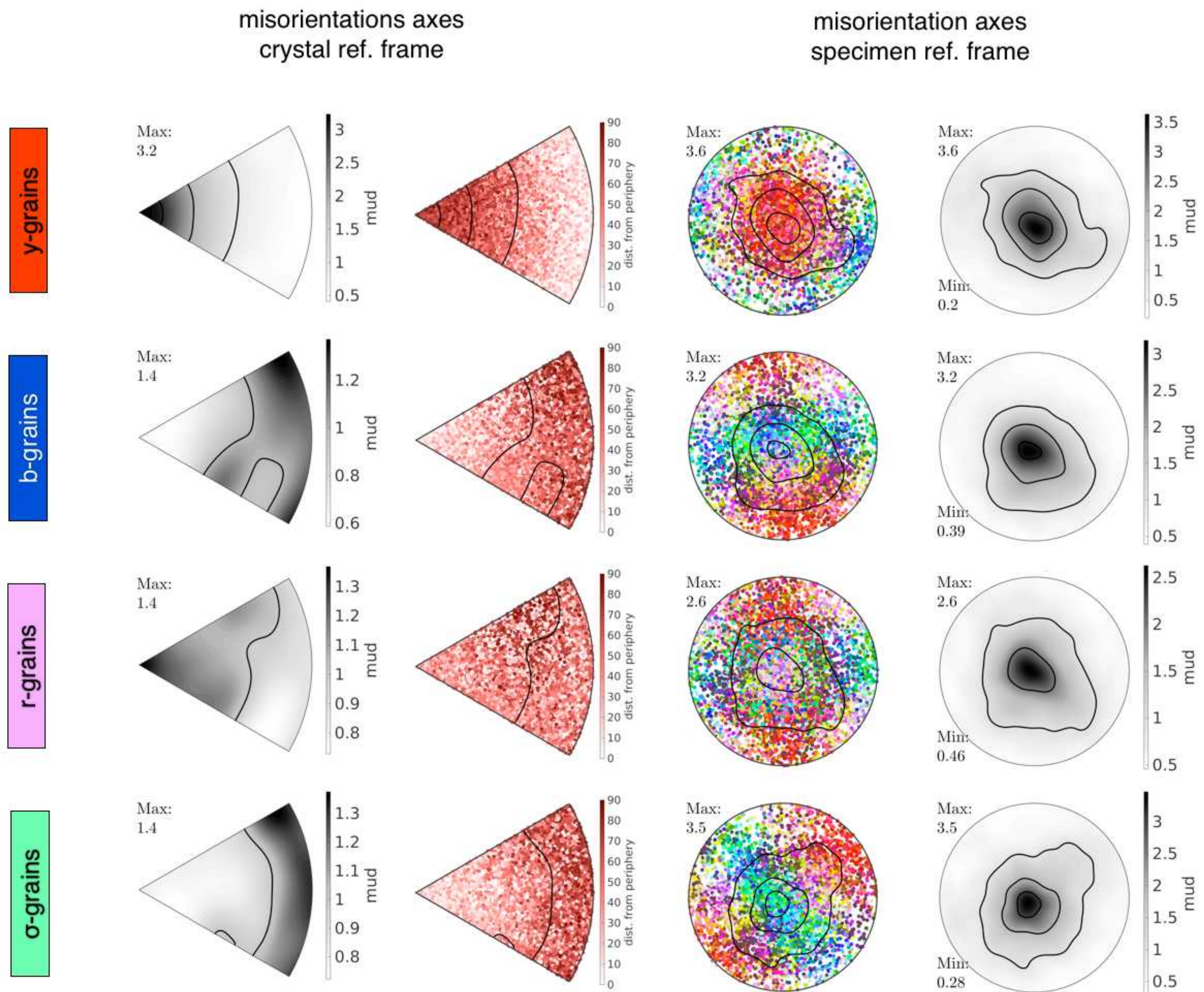
>>explain color-coding

<< toc >>

regime 1

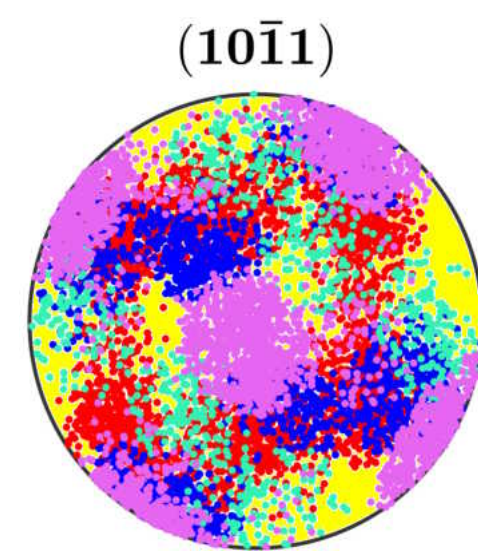
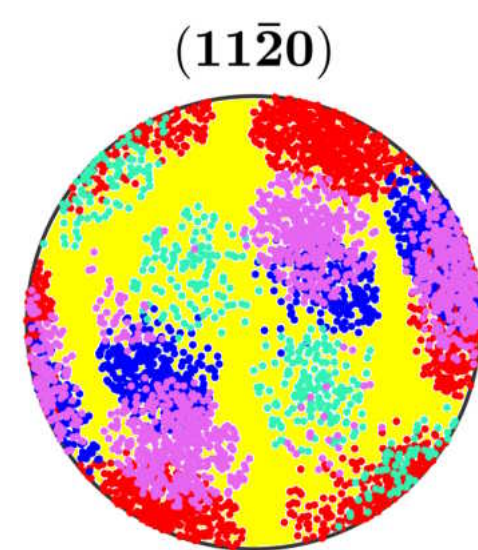
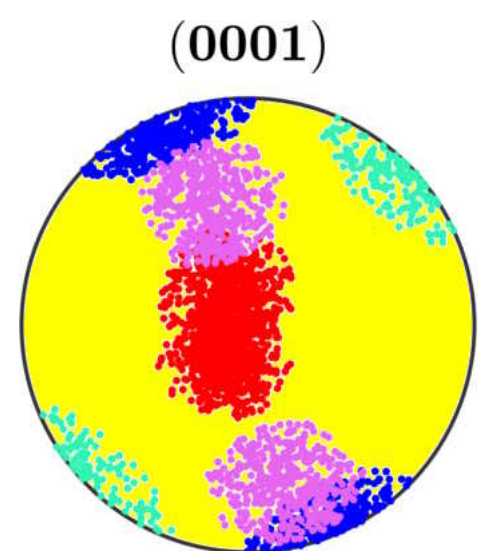
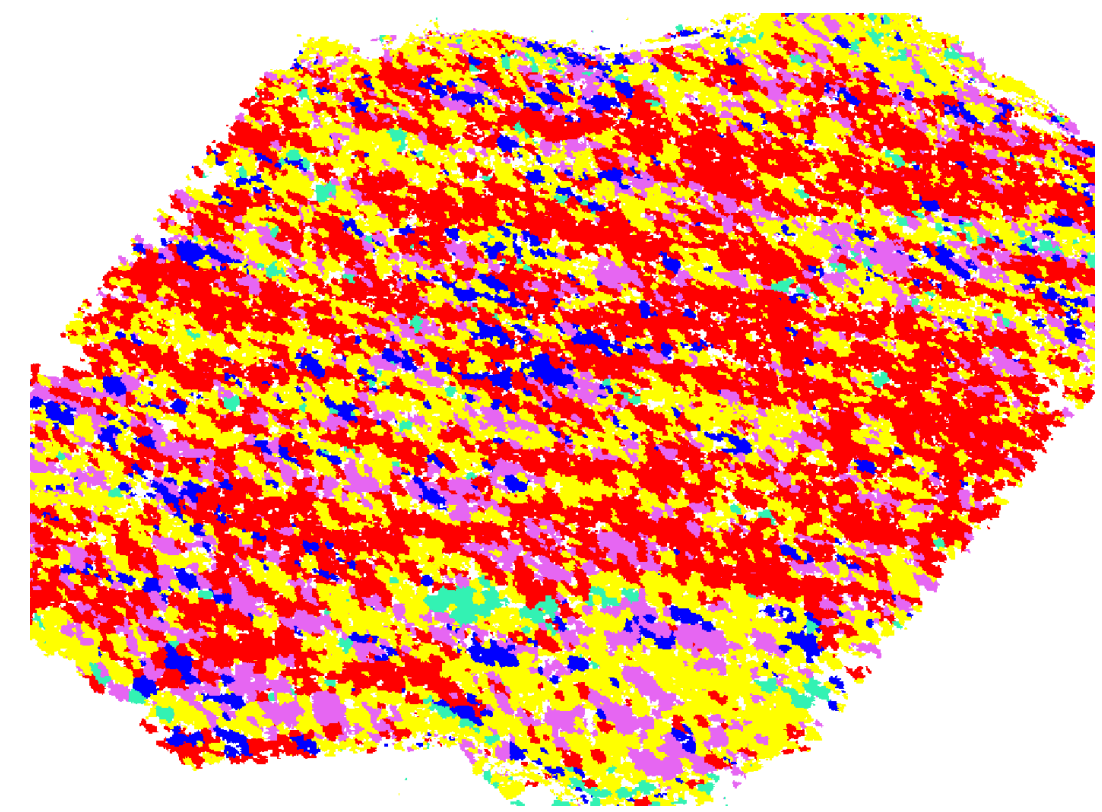


>>explain color-coding



<< toc >>

regime 3



y-grains

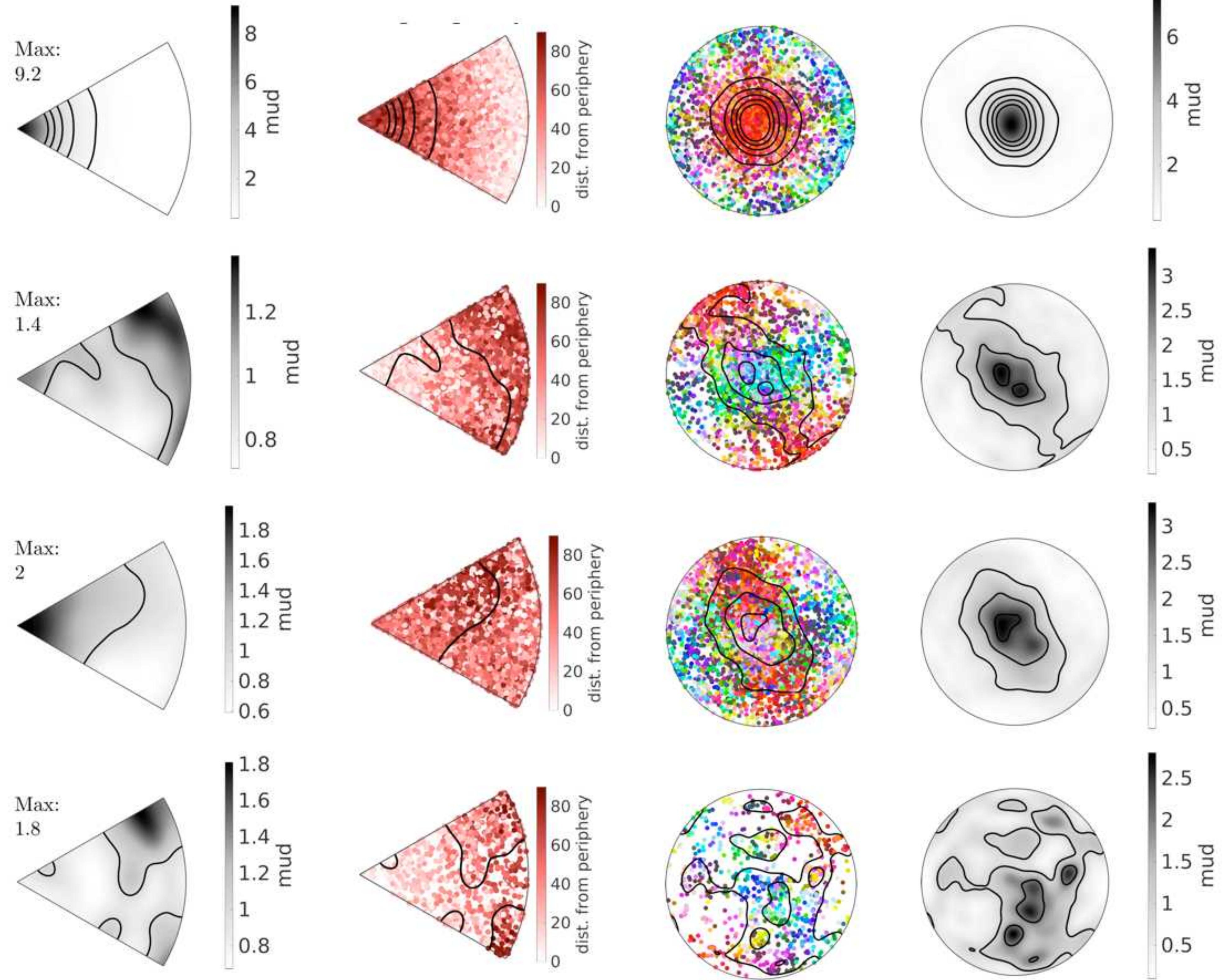
b-grains

r-grains

σ-grains

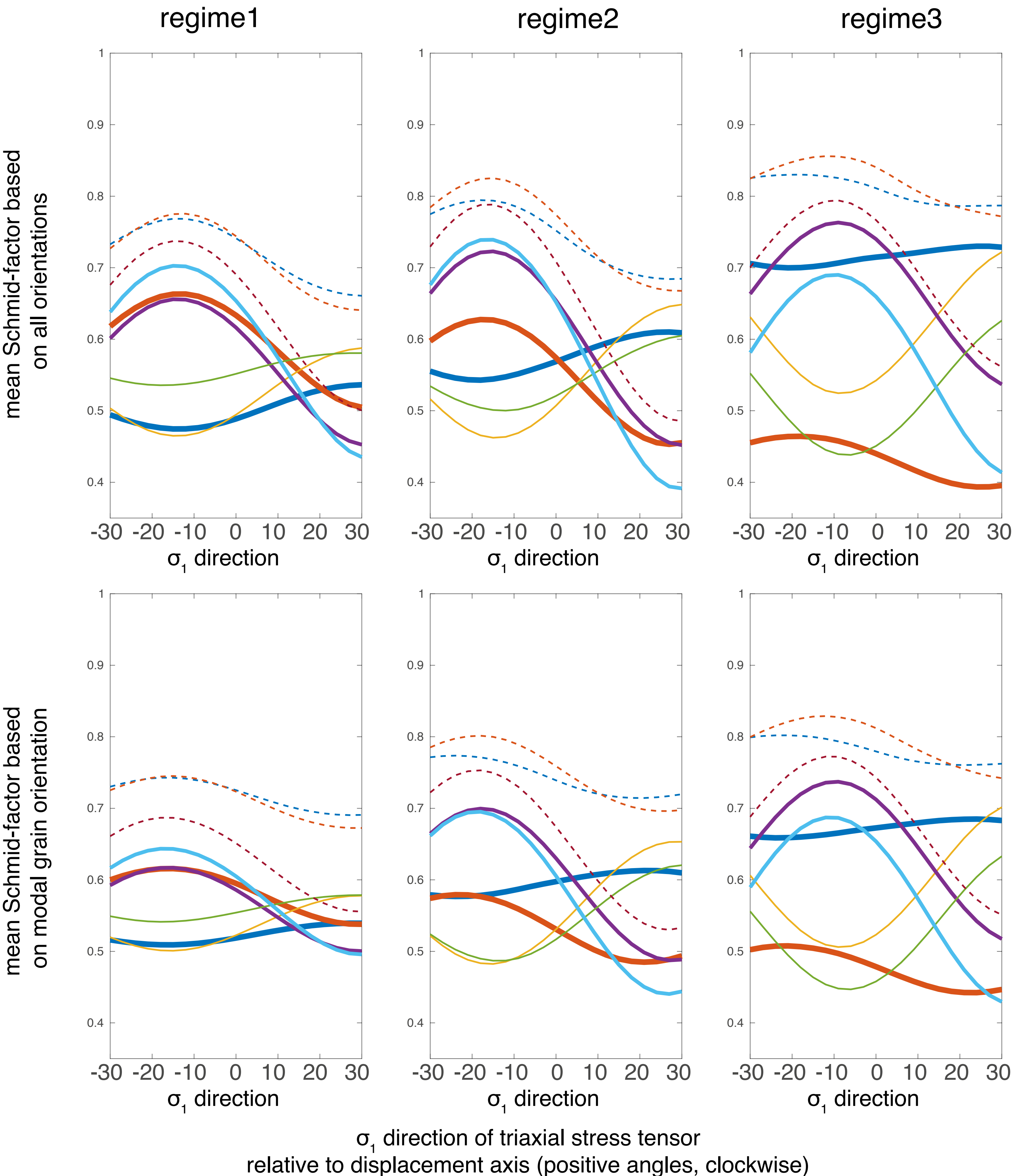
misorientations axes
crystal ref. frame

misorientation axes
specimen ref. frame



>>explain color-coding

<< toc >>

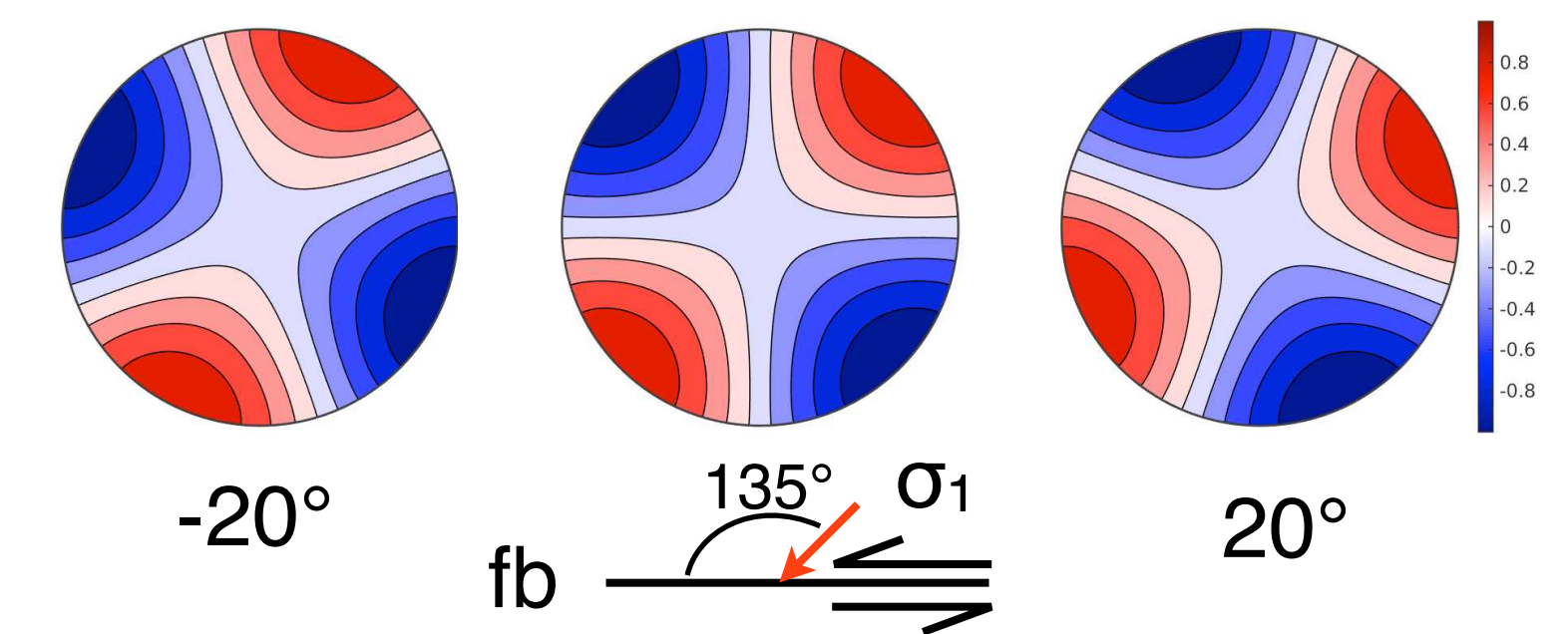


The generalized Schmid factor Sf (Reid, 1973) is calculated from a given slip system and a stress tensor, and presents the ratio between the shear stress on a slip system and the norm of the macroscopic stress tensor. Since the general shear experiments are plane strain and displacement is resolved parallel to the dip of the forcing block, we use a triaxial, normalized stress tensor. A Sf is calculated for the modal orientation of all grains and for every orientation within a map, the average giving the mean Sf. The mean Sf is plotted as a function of the direction of σ_1 , centered around the direction of the load axis (45° with respect to the shear plane)

-> Schmid factors basal-a are considerably lower than for {pi'/z}-a

generalized Schmid factor

$$S = \frac{\tau_{res}}{\|\sigma\|} = \frac{m_{ij}\sigma_{ij}}{\|\sigma\|}$$



Observation: Texture transition without a change in temperature (but flow stress)

Model:

Two texture forming mechanisms compete:

- (1) at high stress- directed growth of new grains with c-axes at the periphery (dominant in regime 1_{*})
- 2) attraction of [c]-axes along the girdle towards the center of the polefigure during dislocation glide on {m}-, {z}- and {pi'}-<a> (dominant in regime 3)

Supporting indication:

Misorientation axes

Schmid factors

round, 'undeformed', small grains in conjugate positions with [c] at the periphery

increasing texture strength towards regime 3 indicates less gbs and more crystal plasticity

[c]-grains in shear band orientations in high stress samples

-> fracturing, nucleation and growth well known feature (in the Griggs rig)

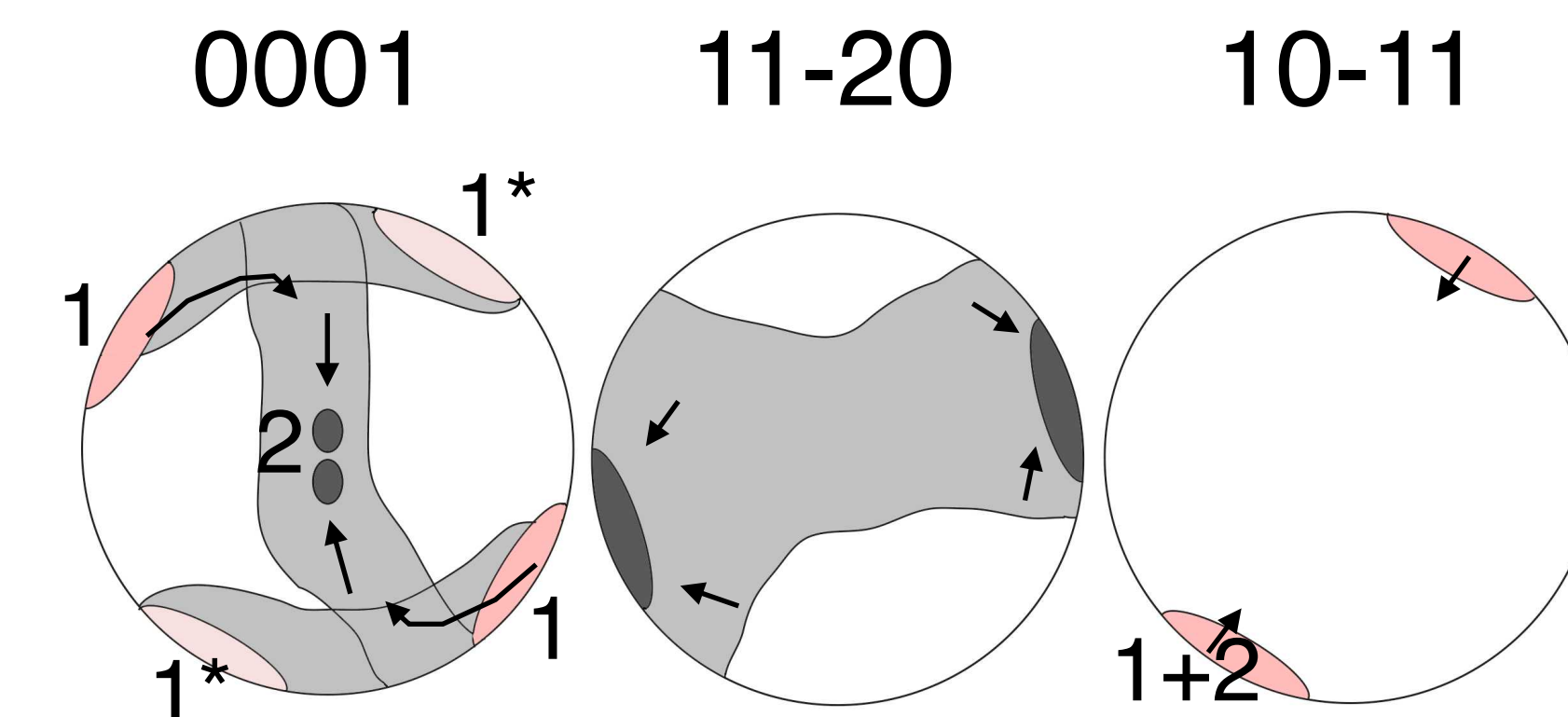
-> (c)-<a> never been demonstrated as an efficient, strain accommodating slip system

Implications:

Peripheral [c]-axes are not indicative of efficient (c)-<a>

Y-domains not an indicator of high temperature but high strain (realized by dislocation glide, mechanisms

2) at stresses low enough to suppress oriented growth (mechanism 2)

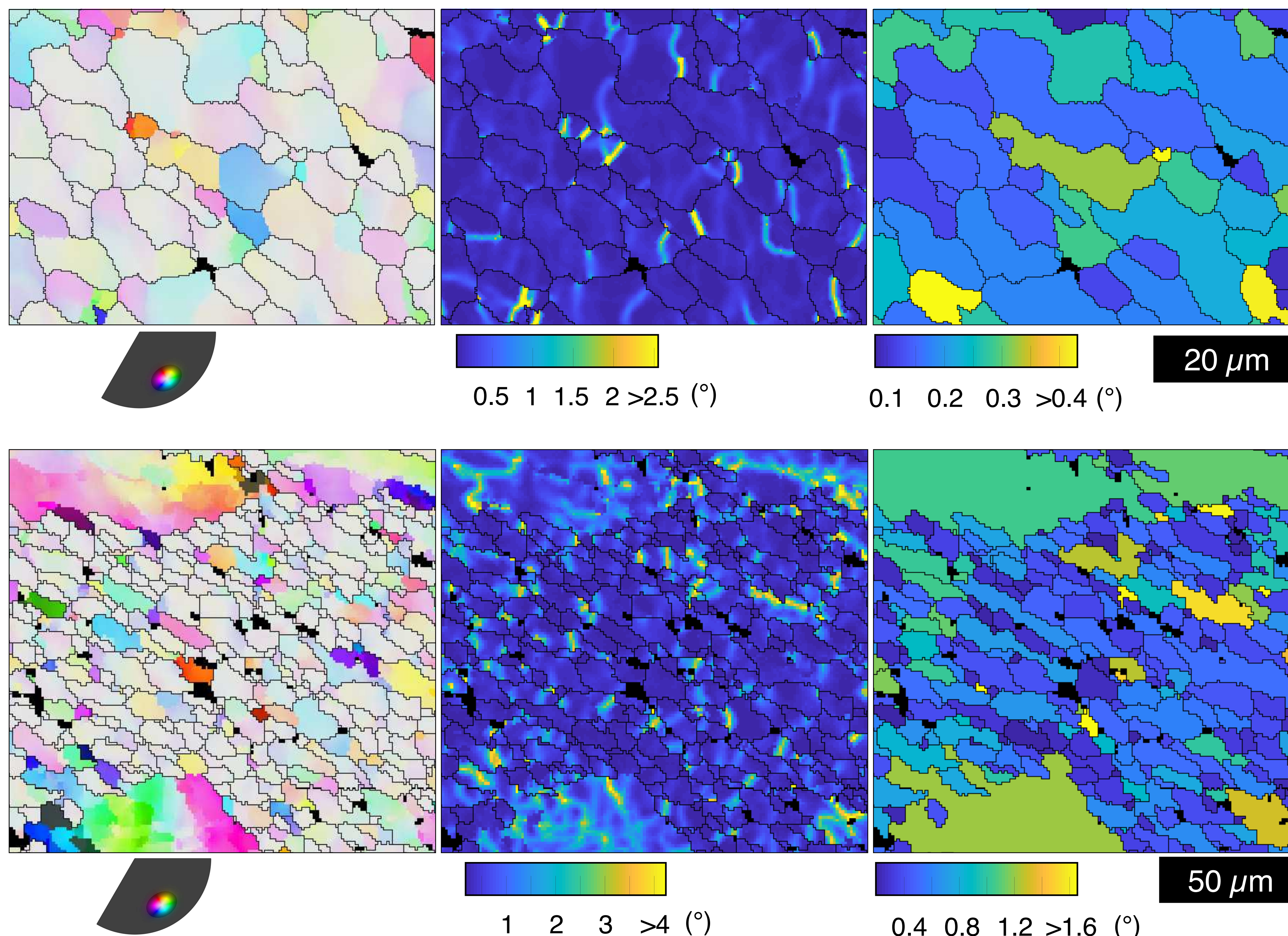


Definition of the gKAM with intragranular misorientations

Misorientation
to mean orientation

kernel average
misorientation (KAM)

grain averaged
KAM (gKAM)



Parts of EBSD maps of 0.25 and 1 μm step size showing the misorientation to the mean orientation within a tightly confined color range after noise removal, the Kernel average misorientation (KAM) of 3rd order (24 pixel neighborhood) of boundaries below 8° misorientation angle and the grain averaged KAM (gKAM) is defined by the sum of the KAM of all pixels within a grain divided by the number of pixels.

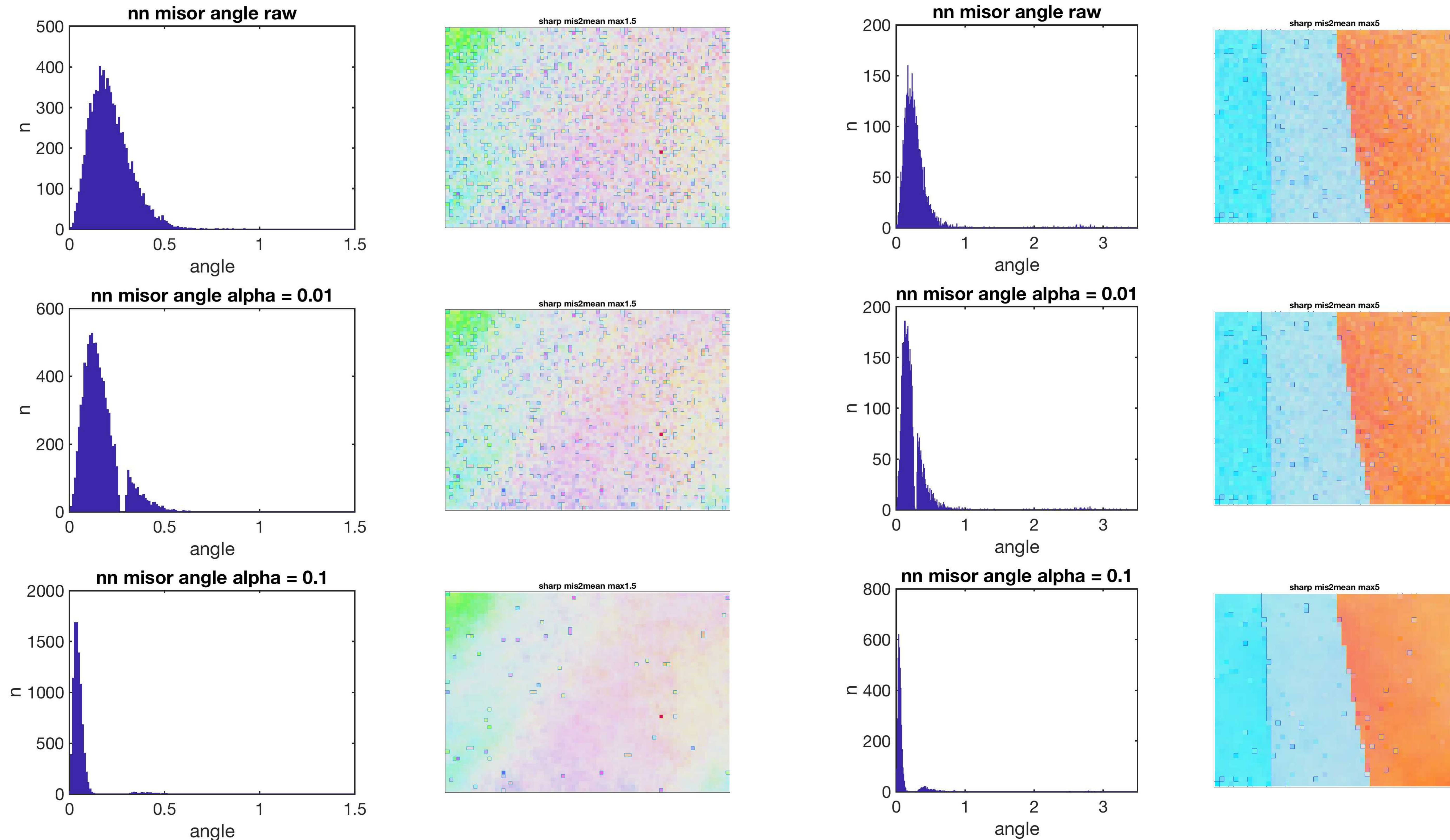
The gKAM is a measure of misorientation density within a grain, imposed by the frequency and the angle of low angle boundaries. The absolute magnitude of the gKAM will depend on the order of the KAM and the step size and the noise level.

A relevant gKAM can only be calculated for sufficiently noise free data.

toc

<< >>

Noise filtering of ebsd data using a half-quadratic filter*



* Bergmann, R., R. H. Chan, R. Hielscher, J. Persch, and G. Steidl (2016), Restoration of Manifold-Valued Images by Half-Quadratic Minimization, Inverse Problems and Imaging, 10 (2), 281–304, Doi:10.3934/ipi.2016001.

Oriented formation (nucleation/growth/...) or newgrains in fractures, highly stressed crystals

in experiments:

e.g.

Hobbs, B. E. (1968), Recrystallization of Single Crystals of Quartz, *Tectonophysics*, 6(5), 353-

Gleason, G. C., J. Tullis, and F. Heidelbach (1993), The Role of Dynamic Recrystallization in the Development of Lattice Preferred Orientations in Experimentally Deformed Quartz Aggregates, *J. Struct. Geol.*, 15(9-10), 1145–1168.

Vernooij, M. G. C., B. Den Brok, and K. Kunze (2006b), Development of Crystallographic Preferred Orientations by Nucleation and Growth of New Grains in Experimentally Deformed Quartz Single Crystals, *Tectonophysics*, 427(1-4), 35–53, Doi: 10.1016/J.Tecto.2006.06.008.

Trepmann, C. a., B. Stockhert, D. Dorner, R. H. Moghadam, M. Kuester, and K. Roeller (2007), Simulating Coseismic Deformation of Quartz in The Middle Crust and Fabric Evolution during Postseismic Stress Relaxation - An Experimental Study, *Tectonophysics*, 442(1-4), 83–104, Doi:10.1016/J.Tecto.2007.05.005.

Trepmann, C. a., and B. Stoeckhert (2013), Short-Wavelength Undulatory Extinction in Quartz Recording Coseismic Deformation in The Middle Crust - An Experimental Study, *Solid Earth*, 4(2), 263–276, Doi:10.5194/Se-4-263-2013.

and nature:

e.g.

Hippertt, J. (1994), Microstructures and C-Axis Fabrics Indicative of Quartz Dissolution in Sheared Quartzites and Phyllonites, *Tectonophysics*, 229(3-4), 141–163.

Hippertt, J., and M. Egydiosilva (1996), New Polygonal Grains Formed by Dissolution-Redeposition in Quartz Mylonite, *J. Struct. Geol.*, 18(11), 1345–1352.

Menegon, L., G. Pennacchioni, R. Heilbronner, and L. Pittarello (2008), Evolution of Quartz Microstructure and C-Axis Crystallographic Preferred Orientation Within Ductilely Deformed Granitoids (Arolla Unit, Western Alps), *J. Struct. Geol.*, 30(11), 1332–1347, Doi:10.1016/J.Jsg.2008.07.007.

Kjoll, H. J., G. Viola, L. Menegon, and B. E. Sorensen (2015), Brittle-Viscous Deformation of Vein Quartz Under Fluid-Rich Lower Greenschist Facies Conditions, *Solid Earth*, 6(2), 681–699, Doi: 10.5194/Se-6-681-2015.

References:

Bouchez, J. L., and a. Pecher (1981), The Himalayan Main Central Thrust Pile and its Quartz-Rich Tectonites in Central Nepal, *Tectonophysics*, 78(1-4), 23–50.

Heilbronner, R., and J. Tullis (2002), The Effect of Static Annealing On Microstructures and Crystallographic Preferred Orientations of Quartzites Experimentally Deformed in Axial Compression and Shear, Doi:10.1144/Gsl.Sp.2001.200.01.12

Heilbronner, R., and J. Tullis (2006), Evolution of C Axis Pole Figures and Grain Size During Dynamic Recrystallization: Results From Experimentally Sheared Quartzite, *Journal of Geophysical Research-Solid Earth*, 111(B10), B10,202, Doi:Doi 10.1029/2005jb004194.

Schmid, S., and M. Casey (1986), Complete Fabric Analysis of Some Commonly Observed Quartz C-Axis Patterns, *Geophysical Monograph*, Vol. 36, Pp. 263–286, American Geophysical Union.

Stipp, M., H. Stunitz, R. Heilbronner, and S. Schmid (2002), The Eastern Tonale Fault Zone: a 'natural Laboratory' for Crystal Plastic Deformation of Quartz Over a Temperature Range From 250 to 700 Degrees C, *Journal of Structural Geology*, 24(12), 1861–1884.